Development and Characterisation of a Tunable Laser Source in the Vacuum Ultraviolet

by

Christine Margarete Steinmann

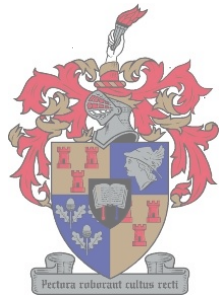

Thesis presented in partial fulfilment of the requirements for the degree of Master of Science at the University of Stellenbosch

Supervisors: **Dr. E.G. Rohwer**
Prof. P.E. Walters

December 1999

Declaration

I, the undersigned, hereby declare that the work contained in this thesis is my own original work and that I have not previously in its entirety or in part submitted it at any university for a degree.

22/11/1999
Date

Development and Characterisation of a Tunable Laser Source in the Vacuum Ultraviolet

Christine Margarete Steinmann
University of Stellenbosch
December 1999

Abstract

Four-wave frequency mixing in a metal vapour medium is a technique that is used to generate small bandwidth, frequency tunable coherent vacuum ultraviolet radiation for spectroscopic applications. The theory of nonlinear optics, applied to sum-frequency generation in a magnesium vapour medium at moderate input laser intensity, describes the requirements for optimal conversion efficiency accurately. The microscopic requirement - a sufficiently large third order susceptibility - is met by employing the $3s^2$-3s3d two-photon resonance of atomic magnesium to enhance the susceptibility for sum-frequency generation. The macroscopic requirement for the constructive interference of the sum-frequency contributions generated in different volume elements (termed the phase matching condition) can be met by using a two-component gaseous medium of magnesium vapour and krypton gas. In an experimental setup phase matching requires high homogeneity of the medium, very stable temperature conditions and the ability to fine tune the krypton magnesium pressure ratio. These conditions can be met in a crossed concentric heat pipe oven by relying on the properties of a dynamic liquid-vapour phase equilibrium. Results obtained with two similar experimental setups for four-wave frequency mixing in magnesium vapour confirm the theoretical predictions and show that the technically simple setup functions as an efficient laser source of tunable vacuum ultraviolet radiation.

Ontwikkeling en Karakterisering van 'n Frekwensie-afstembare Laserbron in die Vakuum Ultraviolet

Christine Margarete Steinmann
Universiteit van Stellenbosch
Desember 1999

Opsomming

Vier-foton frekwensie-vermenging in 'n metaaldamp medium is 'n tegniek wat gebruik word om 'n frekwensie afstembare laserbundel met 'n smal frekwensie bandwydte in die vakuum ultraviolet spektraalgebied te genereer. Die teoretiese beskrywing van nie-lineêre optika, toegepas op die spesiale geval van somfrekwensie-opwekking in 'n magnesiumdamp medium, lewer 'n goeie beskrywing van die vereistes vir optimale omsetting. Daar word aan die mikroskopiese vereiste - dat die derde orde suseptibiliteit 'n toereikende waarde moet hê - voldoen deur die $3s^2$-3s3d twee-foton resonans van die magnesium atome te benut. Aan die makroskopiese vereiste - dat die bydraes tot die som-frekwensie veld wat in verskillende volume-elemente van die medium opgewek is, konstruktief moet interfereer - word voldoen deur 'n twee-komponent medium bestaande uit magnesiumdamp en kriptongas te gebruik. In die eksperimentele opstelling vereis hierdie sogenaamde fase-aanpassingskondisie 'n baie homogene mengsel, 'n stabiele temperatuur en die vermoë om die kripton-magnesium drukverhouding fyn te kan instel. In 'n kruisvormige konsentriese hittepyp-oond kan daar, deur van die eienskappe van 'n dinamiese vloeistof-damp ewewig gebruik te maak, aan hierdie vereistes voldoen word. Eksperimentele resultate verkry met twee soortgelyke eksperimentele opstellings vir vier-foton frekwensie-vermenging in magnesiumdamp, bevestig die teoretiese voorspellings en bewys dat die tegnies eenvoudige opstelling as 'n doeltreffende frekwensie afstembare laserbron in die vakuum ultraviolet funksioneer.

Dedicated to Prof. P.J.G. de Vos,
the physicist whom I knew as a nature lover
and a true gentleman.

Acknowledgements

I wish to express my sincere gratitude to

Dr. E.G. Rohwer for excellent supervision of the project and many helpful and encouraging discussions on the experimental work.
Prof. P.E. Walters for advice and help in many ways.
Mr. U.G.K. Deutschländer and Mr. R.T. Gordon for indispensable help with all technical problems.
The personnel of the mechanical workshop of the Physics Department who manufactured the parts of the apparatus with great precision.

Prof. Dr. C.R. Vidal of the Max Planck Institut für extraterrestrische Physik in Garching, Germany for the opportunity to visit this institute and to do experimental work in his laboratory; also for his lectures and valuable comments and advice during his visit to Stellenbosch.
Herr B. Steffes and Frau G. Steffes for their hospitality and Dr. T. Sykora for his kind help in the laboratory during my visit in Garching. Herr B. Steffes for his advice on the operation of a heat pipe system.

Prof. J.M. Brown of Oxford University for kindly sending me a copy of his publication "An Atlas of Optogalvanic Transitions in Neon."

All the personnel and fellow students of the Physics Department of the University of Stellenbosch for two years of pleasant collaboration and help in numerous ways.

My grandmother, Mrs. C.M. Hattingh, for her much appreciated help with the editing of the manuscript.
My parents, sister and brother and all my friends for their invaluable support.

God, the Creator of all things and Giver of all talents and abilities.

My studies were supported financially by the National Research Foundation (NRF) and my study visit to Germany has been made possible by the support of the Hans Merensky Stipendien Stiftung.

The excimer laser used in this project was made available by the National Laser Facility.

Contents

Chapter 1

Problem statement and overview

1.1 Introduction and problem statement

In 1960 the first successful laser was built. Since then lasers have brought great advances in spectroscopic techniques - especially in the infrared and visible regions of the spectrum. In this spectral range the development of lasers as sources of frequency tunable coherent radiation with a small frequency bandwidth set new boundaries on high resolution spectroscopy. In the ultraviolet and vacuum ultraviolet sources of coherent radiation like H_2, F_2, CO and inert gas halogen excimer lasers exist. Of these sources, however, only the excimer lasers are to some extent tunable over a limited range of frequencies, but their large linewidth, typically 10 cm^{-1} [48], makes excimer lasers unsuitable as sources for high resolution spectroscopy.

This is the reason for the interest in generating coherent vacuum ultraviolet radiation in indirect ways - by exploiting those nonlinear processes that were made practically feasible by the high photon densities provided by lasers. In the visible and infrared regions sum and difference frequency mixing in nonlinear crystals are widely used to extend the range over which continuous frequency tuning is possible. These crystals become opaque at wavelengths of about 200 nm and cannot be used to generate radiation at wavelengths shorter than this in the ultraviolet and vacuum ultraviolet. In the ultraviolet and vacuum ultraviolet a laser source that is tunable over a wide range of frequencies and that exhibits a typical linewidth of 0.1 cm^{-1} can be generated by employing four-wave frequency mixing in a gaseous nonlinear medium.[1] Four-

[1] For an explanation why four-wave sum frequency mixing (third harmonic generation) is employed in gaseous

wave frequency mixing is a third order nonlinear optical process. In general four-wave frequency mixing is the coupling of four electromagnetic waves due to their interaction with a nonlinear optical medium resulting in the transfer of energy between the different electromagnetic fields. The two four-wave mixing processes relevant in the work described in this thesis are sum-frequency generation and third-harmonic generation. The sum-frequency generation process employed is the interaction of two incident laser beams with frequencies ω_1 and ω_2 with the nonlinear medium producing a polarisation, and therefore generating coherent radiation at the sum-frequency $\omega_s = \omega_1 + \omega_1 + \omega_2$. Third-harmonic generation is the degenerate case of sum-frequency generation where $\omega_1 = \omega_2 = \omega$ and $\omega_s = 3\omega$.

The first third-harmonic generation in a gaseous medium was reported in 1967 by W.G. Rado [34] and G.H.C. New and J.F.Ward [29] in pure noble gases. S.E. Harris and coworkers [17] (in 1971) showed that the efficiency of the process can be enhanced by orders of magnitude by using a metal vapour chosen for its high nonlinear susceptibility mixed with a noble gas to obtain a suitable index of refraction for the two-component gaseous medium in order to meet the phase matching condition. In 1974 a further advance was the discovery by D.M. Bloom [5], R.T. Hodgson [19] and K.M. Leung [23] and their coworkers that the conversion efficiency can be increased by tuning the incident frequencies to an appropriate two-photon resonance of the metal atoms.

Since then the technique of four-wave frequency mixing in a gaseous medium has become a general technique to generate coherent tunable vacuum ultraviolet for molecular spectroscopy. According to a study by Vidal [48] conversion efficiencies up to a few percent and peak powers up to 1 MW have been reported with pulsed lasers in gaseous media. A variety of gaseous media - most generally one- or two-component systems of metal vapours and/or noble gases - have been studied as media for four-wave mixing. The use of a heat pipe oven to prepare these two-component metal vapour media, as first proposed by Young et al [54], has distinct advantages.

In each experimental application the problem is to choose the most appropriate nonlinear medium and to determine those experimental conditions that give an optimal output of coherent

media whereas three-wave frequency mixing (second harmonic generation) is used in nonlinear crystals see appendix A.

vacuum ultraviolet radiation in the desired wavelength range. An experimental setup must be developed in which the gaseous medium can be prepared and in which these optimal conditions can be obtained and maintained and easily adjusted to allow for the tuning of the generated wavelength.

1.2 Aim

This thesis gives an account of a theoretical as well as experimental study of the generation of coherent vacuum ultraviolet radiation by four-wave frequency mixing processes - third-harmonic and sum-frequency generation - in a two-component gaseous medium of magnesium vapour and krypton gas prepared inside a crossed concentric heat pipe oven. The theoretical discussion and the experimental work described in this thesis have a dual aim. The practical aim is to develop an experimental source of tunable coherent vacuum ultraviolet radiation in the 140 to 160 nm wavelength range for future application in molecular laser spectroscopy, and to determine the conditions for optimal efficiency of the conversion process. The intellectual aim, that serves the practical aim, is to obtain a detailed understanding of the factors influencing the efficiency of the four-wave frequency mixing process, the reasons for the suitability of magnesium vapour as medium for the generation of vacuum ultraviolet radiation in this wavelength range, and the operation and advantages of a crossed concentric heat pipe oven for the preparation of the magnesium krypton optical medium.

1.3 Outline of thesis

Chapter 2 is dedicated to a systematic discussion of the theoretical description of third-harmonic generation as the degenerate case of four-wave frequency mixing in gaseous media. In section 2.2 the classical approach to optics is discussed in order to illustrate the coherence between the familiar theory, results and terms of linear optics and the theoretical description of the higher order processes of nonlinear optics. Section 2.2.2 shows how the processes of nonlinear optics can be seen as higher order corrections to the linear model. Section 2.3 introduces the more comprehensive quantum mechanical description used widely to describe nonlinear processes.

In chapter 3 the results of the quantum mechanical theory is applied to third-harmonic

generation in a gaseous medium in order to determine the behaviour of the nonlinear process and factors influencing the efficiency, keeping the practical implications of these results for the experimental setup with a magnesium krypton medium in mind. The conclusions at the end of section 3.6 reveal the stringent requirements which the nonlinear gaseous medium must meet in order to provide efficient third-harmonic generation. In section 3.7 the results are extended to sum-frequency generation.

In chapter 4 the principles behind the operation of a heat pipe oven are discussed and the characteristics of the heat pipe oven are illustrated by simple experimental results. It is discussed how a crossed concentric heat pipe oven facilitates the generation of a two-component gaseous nonlinear medium meeting the crucial requirements of four-wave frequency mixing in a simple setup.

The apparatus, experimental method and results obtained when applying four-wave frequency mixing in a magnesium vapour krypton gas medium as a coherent vacuum ultraviolet source, are discussed in chapter 5. Distinction is made between two parts of the experimental work: the construction, testing and characterisation of an experimental setup for third-harmonic generation in the Stellenbosch laboratory (sections 5.1 and 5.2) and the results obtained with a similar setup for sum-frequency generation in the laboratory of the Max Planck Institut für extraterrestrische Physik in Garching, Germany (sections 5.3 and 5.4).

In chapter 6 the conclusions regarding magnesium vapour as nonlinear medium, the performance of the crossed concentric heat pipe oven and the experimental results obtained are summarised and proposals for future work are made.

Chapter 2

Theory of nonlinear optics in gaseous media

This chapter gives a systematic introduction to the theoretical description of four-wave frequency mixing in a gaseous medium, as applied to the degenerate case of third-harmonic generation. The classical approach to optics discussed in section 2.2 illustrates the coherence between the familiar theory, results and terminology of linear optics and the theoretical description of the higher order processes of nonlinear optics. In the classical approach the processes of nonlinear optics can be seen as a systematic refinement of the model describing the linear phenomena. The more comprehensive quantum mechanical description used widely to model nonlinear processes is introduced in section 2.3. The theory is applied to prove that conditions can be chosen to selectively enhance either third-harmonic or sum-frequency generation as the observable nonlinear process in the interaction between monochromatic radiation and a centrosymmetric medium.

2.1 Theoretical framework for light-matter interaction

In the framework of the accepted theory on the nature of light and matter, describing the processes of light propagating through a material medium involves a description of the properties and response (i) of the atoms or molecules of the medium and (ii) of the electromagnetic wave. The problem of describing the medium response can be approached in two different ways depending on the level of the study using either a classical model or quantum mechanics.

The classical treatment of the medium is based on the classical electron oscillator model which is not intended to be a complete description of the nonlinear system, but rather describes some of the most important phenomenological aspects of nonlinear optics. The classical model is easier to visualise and is useful for an initial understanding of the subsequent quantum mechanical description of the same phenomenon.

The quantum mechanical treatment of the medium employs density matrix theory to derive the susceptibilities characterising the response of the medium to radiation. This model has been developed and interpreted to provide a much more complete description of the nonlinear processes like multi-photon absorption and frequency mixing taking all known field dependent optical effects into account simultaneously. In the mathematical models developed to describe nonlinear optical processes the electromagnetic radiation is usually treated (classically) as a wave even when the medium is treated quantum mechanically - making the so-called quantum mechanical model actually semi-classical [22].

In both the classical and the (semi-classical) quantum mechanical approaches the analysis involves the simultaneous solution of two types of equations: a Newtonian or Schrödinger equation describing the response of the particles of the medium to the local electromagnetic field (with the electrical component of the electromagnetic wave as a driving term) and the Maxwell equations describing the response of the electromagnetic field to the local properties of the medium (with the polarisation of the medium as a source term). A description of the polarisation of the medium in terms of the electromagnetic field parameters and susceptibilities of the medium serves as a link between the two sets of equations.

In general the polarisation can be expressed in terms of powers of the local electric field in an expression of the form (for monochromatic radiation, its polarisation given by the unit vector $\widehat{\varepsilon}_x$).

$$\mathbf{P}_x = \epsilon_0(\chi'_1 E_x + \chi'_2 E_x^2 + \chi'_3 E_x^3 + ...)\widehat{\varepsilon}_x \text{ in SI units} \tag{2.1}$$

$$\text{or} \qquad \mathbf{P}_x = (\chi'_1 E_x + \chi'_2 E_x^2 + \chi'_3 E_x^3 + ...)\widehat{\varepsilon}_x \text{ in cgs units} \tag{2.2}$$

where the coefficient $\chi'_i = \chi'_i(\omega, N)$ is called the electrical susceptibility of the i'th order. The susceptibility of a medium is directly proportional to its number density N for each order so

that the equation can be rewritten as

$$\mathbf{P}_x = N(\varkappa_1' E_x + \varkappa_2' E_x^2 + \varkappa_3' E_x^3 + \ldots)\widehat{\varepsilon}_x \text{ in cgs/SI units.} \tag{2.3}$$

In the work of Vidal et al as in [46] and [50] susceptibility is defined as the N independent quantity $\varkappa_i' = \varkappa_i'(\omega)$ as in expression 2.3 and is denoted by $\chi^{(i)}(\omega)$. Therefore in cgs units $\chi^{(i)}(\omega) = \varkappa_i' = \frac{\chi_i'}{N}$. In the work of Milonni et al [27] as in some other literature presenting the classical approach, $\varkappa_1'$ is called the electronic polarisability of the medium and is denoted by $\alpha(\omega)$ and the term susceptibility is reserved for the N dependent $\chi_i'(\omega, N)$. In SI units $\alpha(\omega) = \varkappa_i' = \frac{\epsilon_0 \chi_1'}{N}$. In this thesis the expressions will be in their cgs unit form for easy comparison with the extensive theoretical work done on four-wave frequency mixing in the past. (For conversion between cgs and SI units the table of Hanna et al [16, p. 315] is useful.) For the sake of uniform notation the convention of susceptibility as a quantity independent of N will be used.

2.2 Classical introduction to nonlinear optics

The first attempts to describe the interaction between light and matter were empirical and based on macroscopic observations. Michaelson in 1885 first proved that the velocity of light in a medium depends on the wavelength of the light, and defined the index of refraction for light with wavelength λ as $n_\lambda = \frac{c}{v_\lambda}$ where c is the speed of light in vacuum and v_λ is the speed of light of wavelength λ in the given medium. The change of the index of refraction n with the wavelength λ is called the dispersion of the medium. It was observed that for the visible region most of the transparent materials showed the same general trend: n increasing as λ decreases (the frequency ν increases) and the rate of increase becoming greater at shorter λ as seen in the region of normal dispersion in figure 2-1 taken from Guenther [15, p. 273]. This was called normal dispersion. In the regions near the absorption lines of the same materials in the infrared however, the refractive index was measured to decrease sharply if the wavelength approaches an absorption line from the short wavelength side. In the region of high absorption - inside the absorption line - the index of refraction could not be measured. On the long wavelength side of the absorption line the index of refraction was found to be much higher than at the short

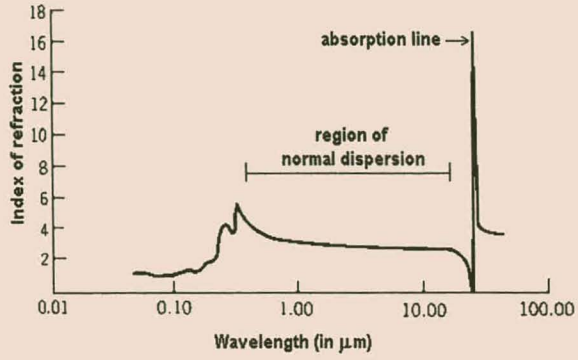

Figure 2-1: A plot of the real part of the index of refraction of gallium phosphide as function of wavelength (given in micrometer) showing normal dispersion in the region 1.0 to 10.0 micrometer and the typical anomalous dispersion at the first absorption line on the long wavelength side of its useful spectral region.

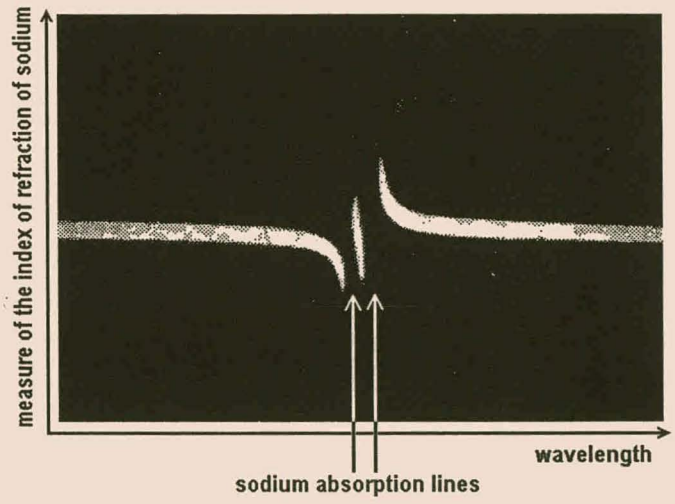

Figure 2-2: Anomalous dispersion around two absorption lines of sodium at 589.0 nm and 589.6 nm observed in sodium vapour by R.W. Wood in 1904.

wavelength side of the absorption line or in the transparent region. This phenomenon was called anomalous dispersion. Figure 2-2 taken from Jenkins and White [20, p. 469] illustrates the variation of the index of refraction with wavelength in the vicinity of absorption lines as observed in an early experiment.

Sellmeier in 1871 succeeded in describing the anomalous dispersion by postulating that the particles of the medium are bound by an elastic force allowing them to vibrate at their natural frequencies, and that the light wave exerts a periodic force on the particles forcing them to vibrate at the frequency ν of the light. As the frequency of the light approaches a natural frequency, the amplitude of the vibrations increases. Helmholtz first showed that for the description to hold very close to the absorption lines, the absorption of the light as it propagates must be taken into account. It could be done by assuming that a damping force acts on the oscillation of the particles.

Lorentz around 1900 formalised the classical description of the phenomena of linear optics by postulating that the atomic electrons in the optical medium behave like an assembly of harmonic oscillators. This is not intended as a model of the atom but as a model of the way an optical medium reacts to perturbation. The classical theory based on this Lorentz electron oscillator model describes the phenomena of linear optics quite satisfactorily and can be extrapolated to nonlinear phenomena by considering an anharmonic oscillator. This classical approach is generally used to obtain a qualitative understanding of linear and nonlinear optics [27].

2.2.1 Harmonic oscillator model and linear phenomena

The Lorentz model for an optical medium approximates the medium as an assembly of identical harmonic oscillators. With this simple model only the optical phenomena depending linearly on the electric field $\mathbf{E}$ can be described: i.e. one photon absorption and the index of refraction of the medium with its frequency dependence.

2.2.1.1 Absorbing medium and complex indices of refraction

Assume the gaseous optical medium to behave like an assembly of electrically charged harmonic oscillators - the negatively charged electron density oscillates about its equilibrium position around the positively charged nucleus - that can be forced to vibrate by an electromagnetic wave propagating through the medium. Consider a linearly polarised monochromatic plane

wave given by

$$\mathbf{E} = \widehat{\varepsilon}\frac{1}{2}\left[\widehat{E}_\omega e^{-i(\omega t - kz)} + \widehat{E}^*_\omega e^{i(\omega t - kz)}\right] \tag{2.4}$$

with $\widehat{\varepsilon}$ a unit vector in the polarisation direction and $\widehat{E}_\omega$ the constant amplitude[1] of the electric field at frequency ω. Adding the complex conjugate ensures that the electric field amplitude $|\mathbf{E}| = \frac{1}{2}\left[\widehat{E}_\omega e^{-i(\omega t - kz)} + \widehat{E}^*_\omega e^{i(\omega t - kz)}\right]$ remains a real number.

The electron oscillator is subject to the driving force $e\mathbf{E}$ exerted by the electric field of the wave, the harmonic restoring force $-m\omega_0^2\mathbf{x}$ (where $\mathbf{x}$ is the displacement from the equilibrium position, m the mass and ω_0 the natural frequency of the oscillator) and, in order to take the absorption of the propagating radiation by the medium into account, a damping force $-m\Gamma\frac{d\mathbf{x}}{dt}$. This yields the equation of motion for the electron oscillator [27, Equation 3.3.1]

$$\frac{d^2\mathbf{x}}{dt^2} + \Gamma\frac{d\mathbf{x}}{dt} + \omega_0^2\mathbf{x} = \frac{e}{m}\mathbf{E} = \widehat{\varepsilon}\frac{e}{m}\frac{1}{2}\left[\widehat{E}_\omega e^{-i(\omega t - kz)} + \widehat{E}^*_\omega e^{i(\omega t - kz)}\right]. \tag{2.5}$$

This equation has to be written and solved in the complex exponent form. The solution of this equation describes the electron's displacement as a function of time

$$\mathbf{x}(t) = \widehat{\varepsilon}\frac{1}{2}\left[\left(\frac{e/m}{\omega_0^2 - \omega^2 - i\Gamma\omega}\right)\widehat{E}_\omega e^{-i(\omega t - kz)} + \left(\frac{e/m}{\omega_0^2 - \omega^2 + i\Gamma\omega}\right)\widehat{E}^*_\omega e^{i(\omega t - kz)}\right]. \tag{2.6}$$

It is a pure sinusoidal function at the frequency of the driving force ω of which the amplitude increases as the driving frequency approaches the natural frequency ω_0 - the well known behaviour of a harmonic oscillator driven by a harmonically varying force.

When an electron is displaced from its (electrostatic) equilibrium position an induced dipole moment $\mathbf{p} = e\mathbf{x}$, where e is the electron charge, is associated with the displacement. The response of the assembly of identical oscillators (the medium) is therefore a harmonically varying polarisation density $\mathbf{P} = Ne\mathbf{x}(t)$, where N is the number of the polarisable atoms per unit volume. The induced polarisation oscillates with the same frequency ω as the electric field, but due to the damping, this polarisation density induced in the medium is out of phase with the radiation field so that a complex linear susceptibility $\chi^{(1)}(\omega)$ has to be introduced to describe

[1] General remark: The "hat" on $\widehat{E}_\omega$ does not indicate a vector, but is used here to distinguish $\widehat{E}_\omega$ from E_ω where $E_\omega = \widehat{E}_\omega e^{ik_\omega z}$. The same holds for $\widehat{P}_\omega$.

the relation between the dipole moment and the field:

$$\mathbf{P} = Ne\mathbf{x}(t) = \hat{\boldsymbol{\varepsilon}}\frac{N}{2}\left[\chi^{(1)}(\omega)\,\widehat{E}_\omega e^{-i(\omega t-kz)} + \chi^{(1)*}(\omega)\,\widehat{E}^*_\omega e^{i(\omega t-kz)}\right]. \tag{2.7}$$

By comparison of equations 2.6 and 2.7 $\chi^{(1)}(\omega)$ is given by the expression

$$\begin{aligned}\chi^{(1)}(\omega) &= \frac{e^2/m}{\omega_0^2-\omega^2-i\Gamma\omega}\\ &= \frac{e^2}{m}\frac{\omega_0^2-\omega^2}{(\omega_0^2-\omega^2)^2+\Gamma^2\omega^2} + i\frac{e^2}{m}\frac{\Gamma\omega}{(\omega_0^2-\omega^2)^2+\Gamma^2\omega^2}\\ &= \overline{\chi}^{(1)}(\omega) + i\widetilde{\chi}^{(1)}(\omega)\end{aligned} \tag{2.8}$$

where $\overline{\chi}^{(1)}$ and $\widetilde{\chi}^{(1)}$ denote the real and imaginary parts of the linear susceptibility respectively.

To obtain the response of the electromagnetic field to the polarisable medium, the polarisation density as given by equation 2.7 must be substituted as source term into the Maxwell wave equation 2.9. (Note that it is only necessary to do the substitution for one of the complex conjugate pair as the other one simply gives the complex conjugate of the answer.)

$$\boldsymbol{\nabla}^2\mathbf{E} - \frac{1}{c^2}\frac{\partial^2\mathbf{E}}{\partial t^2} = \frac{4\pi}{c^2}\frac{\partial^2\mathbf{P}}{\partial t^2} \tag{2.9}$$

$$-k^2\widehat{E}_\omega e^{-i(\omega t-kz)} + \frac{\omega^2}{c^2}\widehat{E}_\omega e^{-i(\omega t-kz)} = -\frac{4\pi\omega^2}{c^2}N\chi^{(1)}(\omega)\,\widehat{E}_\omega e^{-i(\omega t-kz)} \tag{2.10}$$

The result of equation 2.10 is a relation between the wave vector of the electromagnetic wave k_ω and the linear susceptibility $\chi^{(1)}(\omega)$ of the medium

$$k_\omega^2 = \frac{\omega^2}{c^2}\left(1+4\pi N\chi^{(1)}(\omega)\right). \tag{2.11}$$

This expression 2.11 for the wave vector together with the definition of the phase velocity $v_p = \frac{c}{n(\omega)} = \frac{\omega}{k}$ yield an expression for the index of refraction of the medium for waves of frequency ω:

$$n(\omega) = \frac{k_\omega c}{\omega} = \left(1+4\pi N\chi^{(1)}(\omega)\right)^{\frac{1}{2}} \tag{2.12}$$

Both the wave vector k_ω and the index of refraction $n(\omega)$ are complex. The complex index

of refraction $n(\omega)$ can be separated into a real and an imaginary part[2]. Under the condition that $n(\omega)$ is not much larger than 1 (i.e. $\left|N\chi^{(1)}(\omega)\right| \ll 1$) - an approximation that is valid for gases in the visible region - the square root can be approximated by a few of the lowest order terms of the series expansion $(1+x)^{\frac{1}{2}} = 1 + \frac{1}{2}x + \frac{1}{2}\left(\frac{1}{2}-1\right)x^2/2 + \ldots$ (with $x = 4\pi N\chi^{(1)}(\omega)$.) To the first order the relation between $n(\omega)$ and its real and imaginary parts reduces to the simple form

$$\begin{aligned} n(\omega) &= \left(1 + 4\pi N\left(\overline{\chi}^{(1)}(\omega) + i\widetilde{\chi}^{(1)}(\omega)\right)\right)^{1/2} \\ &\approx 1 + 2\pi N\left(\overline{\chi}^{(1)}(\omega) + i\widetilde{\chi}^{(1)}(\omega)\right) \text{ for } n \approx 1 \\ &= \overline{n}(\omega) + i\widetilde{n}(\omega). \end{aligned} \tag{2.13}$$

The real part of the complex refractive index $\overline{n}(\omega) = 1 + 2\pi N\overline{\chi}^{(1)}(\omega)$ is usually referred to as refractive index and determines the phase velocity $v = \frac{c}{\overline{n}(\omega)}$. The imaginary part $\widetilde{n}(\omega) = 2\pi N\widetilde{\chi}^{(1)}(\omega)$ is responsible for the decay of the propagating field and determines the absorption coefficient for one-photon absorption of photons of frequency ω in the medium

$$\kappa(\omega) \equiv 2\left[\widetilde{n}(\omega)\right]\omega/c = N\frac{4\pi\omega}{c}\widetilde{\chi}^{(1)}(\omega). \tag{2.14}$$

The equations for the real refractive index $\overline{n}(\omega)$ and the absorption coefficient $\kappa(\omega)$

$$\overline{n}(\omega) = 1 + 2\pi\frac{Ne^2}{m}\frac{\omega_0^2 - \omega^2}{(\omega_0^2 - \omega^2)^2 + \Gamma^2\omega^2} \tag{2.15}$$

$$\kappa(\omega) = 2\left[2\pi\frac{Ne^2}{m}\frac{\Gamma\omega}{(\omega_0^2 - \omega^2)^2 + \Gamma^2\omega^2}\right]\omega/c \tag{2.16}$$

are known as the Kramers-Kronig dispersion relations [8, p. 65]. When rewritten in terms of wavelength instead of ω these equations have essentially the same form as the empirical expressions obtained by Helmholtz in the late nineteenth century.

Near the absorption line of frequency ω_0 in the limit where $|\omega_0 - \omega| \ll \omega_0$ and therefore

[2] There are different ways to do this. In appendix D the generally used approximation method that is employed here is discussed in detail and compared to an alternative method.

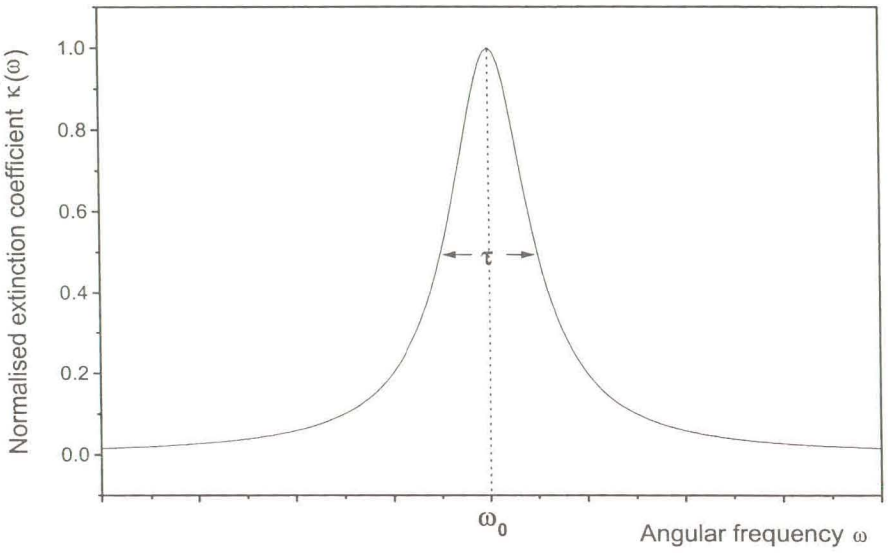

Figure 2-3: Theoretical absorption profile illustrating the variation of the absorption coefficient around an absorption linewith a natural linewidth given by Γ.

$\omega_0^2 - \omega^2 = (\omega_0 + \omega)(\omega_0 - \omega) \approx 2\omega_0(\omega_0 - \omega) \approx 2\omega(\omega_0 - \omega)$ the relations 2.15 and 2.16 reduce to

$$\overline{n}'(\omega) = 1 + \frac{\pi N e^2}{m\omega_0} \frac{\omega_0 - \omega}{(\omega_0 - \omega)^2 + \left(\frac{\Gamma}{2}\right)^2} \tag{2.17}$$

$$\kappa'(\omega) = \frac{2\pi N e^2}{mc} \frac{\left(\frac{\Gamma}{2}\right)}{(\omega_0 - \omega)^2 + \left(\frac{\Gamma}{2}\right)^2} \tag{2.18}$$

The absorption profile given by $\kappa'(\omega)$ is a Lorentzian profile with a full width at half maximum equal to Γ as illustrated in figure 2-3. This Γ is the natural width of the absorption line. The expression $\overline{n}'(\omega) - 1$ as a function of ω defines the dispersion profile of the medium near to resonance as illustrated by figure 2-4.

From figure 2-4 illustrating the dispersion profile $\overline{n}'(\omega) - 1$ it is clear that regions exist where the index of refraction $\overline{n} = \frac{c}{v} < 1$, with v the phase velocity of the radiation in the medium and c the velocity of light in a vacuum. This means that for these regions of the dispersion spectrum the phase velocity is larger than c. This is no contradiction to the theory of relativity,

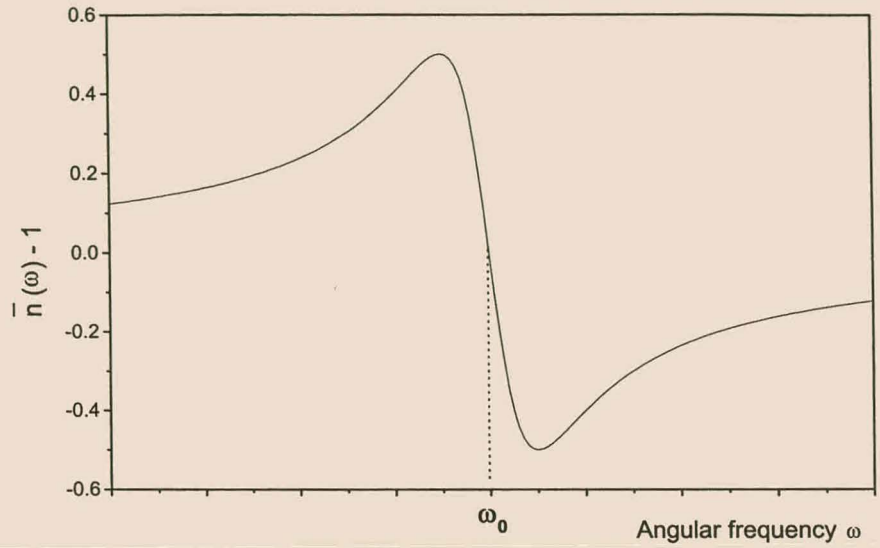

Figure 2-4: Theoretical dispersion profile illustrating the variation of the index of refraction, $\overline{n}(\omega)$, around an absorption line centred on the indicated frequency.

because the fundamental result of relativity - that c is the highest attainable velocity - applies only to velocities at which energy is transmitted. In the case of a propagating wave the energy is not transmitted at the phase velocity v but at the group velocity v_g which is always less than c as is shown in appendix B.

This "anomalous" behaviour of the index of refraction of a medium around its absorption lines makes it possible to meet the crucial phase matching condition for four-wave frequency mixing in a gaseous two component medium as discussed in section 3.5. In order to illustrate in section 3.5 how this is done an expression for the index of refraction of a mixture of gases is needed.

2.2.1.2 Index of refraction of a mixture of gases

The expression for the index of refraction, expression 2.13, derived above can be used to derive an expression for the index of refraction in a system where more than one species of atoms are present. Let the species present be labled by $a = 1, 2, 3...$ Let N_a be the number density and $\chi_a^{(1)}(\omega)$ the linear susceptibility of species a for $a = 1, 2, 3...$ and N the total number

density including all the species. The total linear polarisation (dipole moment density) is given by the sum of the polarisations of the different components

$$\begin{aligned}\mathbf{P}_{total} &= \sum_{a=1,2,3...} \mathbf{P}_a = \widehat{\varepsilon}\frac{1}{2}\sum_{a=1,2,3...} N_a\left[\chi_a^{(1)}(\omega)\,\widehat{E}_\omega e^{-i(\omega t-kz)} + cc\right] \\ &= \widehat{\varepsilon}\frac{N}{2}\sum_{a=1,2,3...}\frac{N_a}{N}\left[\chi_a^{(1)}(\omega)\,\widehat{E}_\omega e^{-i(\omega t-kz)} + cc\right]\end{aligned}$$

the sum $\sum_a \equiv \sum_{a=1,2,3...}$ being a sum over all the different species present[3]. This shows that the resultant linear susceptibility is the sum of the individual susceptibilities weighted by their relative number densities: $\chi_{res}^{(1)}(\omega) = \sum_a \frac{N_a}{N}\chi_a^{(1)}(\omega)$. Subsequently the complex index of refraction of a multi species system is given by

$$n(\omega) = \left(1 + 4\pi\sum_a N_a\chi_a^{(1)}(\omega)\right)^{\frac{1}{2}} \tag{2.19}$$

For $n(\omega) \approx 1$ which holds for gaseous media and frequencies in the optical region, the square root can be expressed as before on page 15 in terms of a series $(1+x)^{\frac{1}{2}} = 1 + \frac{1}{2}x + \frac{1}{2}\left(\frac{1}{2}-1\right)x^2/2 + ...$ of which only the lowest order terms need to be considered when $x = (n(\omega)-1)$ is much smaller than one. To the first order

$$\begin{aligned}n(\omega) &= 1 + 2\pi\sum_a N_a\chi_a^{(1)}(\omega) \\ &= \left[1 + 2\pi\sum_a N_a\overline{\chi}_a^{(1)}(\omega)\right] + i\left[2\pi\sum_a N_a\widetilde{\chi}_a^{(1)}(\omega)\right] \\ &= \overline{n}(\omega) + i\widetilde{n}(\omega)\end{aligned} \tag{2.20}$$

The expression for the real index of refraction for a mixture of gases therefore is:

$$\overline{n}(\omega) = 1 + 2\pi\sum_a N_a\overline{\chi}_a^{(1)}(\omega) \tag{2.21}$$

[3]General remark: In all disscussions following on this *cc* as used here always stands for the complex conjugate of the term preceding it.

2.2.2 Anharmonic oscillator model and nonlinear phenomena

The harmonic oscillator model does not give an indication of any of the nonlinear optical processes that are observed and applied in optical experiments facilitated by the high intensities of lasers. The model is limited by the assumption that the potential well that the atomic electron is trapped in, is a perfectly harmonic well, mathematically described by $V = \frac{1}{2}\omega_0^2 x^2$, exerting an elastic restoring force $F = -\frac{dV}{dx} = -m\omega_0^2 x$ on the atomic electrons. This is a reasonable approximation for small electrical fields causing small displacements $x(t)$ of the electrons.

To give an account of the nonlinear phenomena observed it must be assumed that the potential experienced by atomic electrons is not perfectly harmonic. Whatever the true potential function is it can always be expanded as a Taylor series in x about the equilibrium position which is defined as $x = 0$

$$V(x) = V(0) + x\left(\frac{dV}{dx}\right)_{x=0} + \frac{1}{2!}x^2\left(\frac{d^2V}{dx^2}\right)_{x=0} + \frac{1}{3!}x^3\left(\frac{d^3V}{dx^3}\right)_{x=0} + \ldots \tag{2.22}$$

In this series, $V(0)$ is a constant vanishing in the calculation of the restoring force and can be ignored; at the point of equilibrium the restoring force $F(0) = \left(\frac{dV}{dx}\right)_{x=0} = 0$, and for a stable equilibrium $\left(\frac{d^2V}{dx^2}\right)_{x=0} > 0$ must hold. Since $\left(\frac{d^2V}{dx^2}\right)_{x=0}$ is positive we can define $m\omega_0^2 = \left(\frac{d^2V}{dx^2}\right)_{x=0}$ and also $A = \frac{1}{6}\left(\frac{d^3V}{dx^3}\right)_{x=0}$, $B = \frac{1}{24}\left(\frac{d^4V}{dx^4}\right)_{x=0}$ etc. giving

$$V(x) = \frac{1}{2}m\omega_0^2 x^2 + Ax^3 + Bx^4 + \ldots \tag{2.23}$$

The anharmonicity of the oscillator is described by the higher order terms functioning as perturbations to the first harmonic term. The restoring force has the form

$$\mathbf{F}(x) = -\frac{dV}{dx}\widehat{\mathbf{x}} = \left(-m\omega_0^2 x - 3Ax^2 - 4Bx^3 - \ldots\right)\widehat{\mathbf{x}} \tag{2.24}$$

The electric field $\mathbf{E}(t)$ of the electromagnetic wave propagating through the medium exerts a force $\mathbf{F}_E(t) = e\mathbf{E}(t)$ driving the electron oscillator. Substituting the restoring force $\mathbf{F}(x)$ as well as the driving force $e\mathbf{E}(t)$ into the Newtonian equation of motion $\mathbf{F}_{total}(\mathbf{x}) = m\frac{d^2\mathbf{x}}{dt^2}$ yields

the nonlinear equation of motion for an electron according to the anharmonic oscillator model

$$\left(\frac{d^2x}{dt^2} + \omega_0^2 x + \frac{3A}{m}x^2 + \frac{4B}{m}x^3 + ...\right)\widehat{\mathbf{x}} = \frac{e}{m}\mathbf{E}(t). \tag{2.25}$$

In this equation the coefficients A, B,... the powers of x needed in the expansion and the length of the series depends on the form of the true potential. An atomic gas is a centrosymmetric medium requiring that the potential shows inversion symmetry with respect to the origin. In a one-dimensional case this means that $V(x') = V(-x')$ which requires that the coefficients of the odd order terms in the expression for $V(x)$ vanish leaving only the even order terms. The resulting restoring force therefore contains only odd order terms in x

$$\mathbf{F}(x) = \left(-m\omega_0^2 x - 4Bx^3 - ...\right)\widehat{\mathbf{x}}$$

which yields an equation of motion

$$\left(\frac{d^2\mathbf{x}}{dt^2} + \omega_0^2 x + \frac{4B}{m}x^3 + ...\right)\widehat{\mathbf{x}} = \frac{e}{m}\mathbf{E}(t). \tag{2.26}$$

This symmetry consideration, that explains the absence of even order nonlinear processes in centrosymmetric media, is discussed in more detail in appendix A.

It must be remembered that equation 2.25 (or 2.26) represents a classical model is and not intended as a complete description of an electron in an atom. The coefficients A, B... are parameters depending on the atomic potential and hence equation 2.25 or 2.26 can be used as a starting point to study the effects of perturbations of different orders in the interaction between electromagnetic radiation and a medium.

The nonlinear differential equation 2.25 (or 2.26) cannot be solved exactly but perturbation theory can be used to solve it approximately. For small displacements (as is the case for moderate intensities of the polarising radiation) the linear term $m\omega_0^2 x$ is much larger than the terms containing higher orders in x and hence the higher order terms can be neglected, as in the discussion of the harmonic oscillator. As the displacements become larger due to higher intensities of the polarising field $E(t)$ the higher order terms successively become comparable in magnitude to the linear term. Within a certain intensity range, the significant nonlinear

terms can be handled as perturbations to the linear term.

The solutions and their interpretations show that the nonlinear terms are responsible for the nonlinear optical effects observed. It can be shown that to the accuracy of first order perturbation theory the different nonlinear terms can be treated separately [15, Appendix 15-A]. Keeping only the quadratic term in the equation of motion 2.25 one arrives at a classical mathematical description of the second order nonlinear phenomena such as three-wave mixing, second harmonic generation and optical rectification. Keeping only the term cubic in x as the smallest order nonlinear term in equation 2.26, as is appropriate in centrosymmetric media (see appendix A), the resulting model describes four-wave mixing, third-harmonic generation, two-photon absorption and Raman scattering - all of them third order nonlinear phenomena. In this way the classical theory can be quite helpful in a systematic qualitative introduction to nonlinear optics.

The classical treatment of third-harmonic generation will be discussed in the following sections in order to illustrate the method, reasoning and assumptions made in the classical modeling of nonlinear optical phenomena. Other nonlinear phenomena like second harmonic generation, four-wave mixing, two-photon absorption and Raman scattering are approached classically in exactly the same way. Even in the quantum mechanical treatment of the problem as outlined in section 2.3 the reasoning and most of the assumptions made here are also used although it is often not stated explicitly in the literature.

2.2.2.1 Solving the nonlinear oscillator equation using perturbation theory

Assume that we are studying the interaction between an atomic gas medium and a single incident beam of monochromatic radiation of frequency ω (that will be called the fundamental frequency). In an atomic gas medium the even order susceptibilities vanish due to symmetry (see Appendix A) making the third order the lowest order nonlinear process that can be employed for frequency mixing. Assume that we are working in an intensity range of the incident radiation where the third order term is significant compared to the linear term and all higher order terms are negligible. The third order term is however small enough to be treated as a perturbation to the linear differential equation. The incident wave is assumed to be plane polarised and monochromatic with an electric field amplitude that is constant in time. Under these assumptions the model applies to a large range of experimental situations. It is even

used for experiments with pulsed lasers with pulse lengths of the order of ns. For systems with shorter pulses lengths the time dependence has to be taken into account.

In order to incorporate the effect of absorption into the description it is convenient to write the electric field of the incident plane wave in the complex exponential form:

$$E(t) = \frac{1}{2}\left[\widehat{E}_\omega(z)e^{-i(\omega t - k_\omega z)} + \widehat{E}^*_\omega(z)e^{i(\omega t - k_\omega z)}\right] \tag{2.27}$$

$$\text{with} \quad k_\omega = \frac{\omega n(\omega)}{c} \tag{2.28}$$

According to the anharmonic oscillator model the response of the medium to the electromagnetic radiation is described by equation 2.29. Equation 2.29 is the equation of motion of a damped anharmonic oscillator driven by the harmonic force exerted by the electric field of the incident wave. The damping constant of the oscillator is Γ, the natural frequency is ω_0 and the third order nonlinear term bx^3 is responsible for the anharmonicity of the oscillator.

$$\frac{d^2x}{dt^2} + \Gamma\frac{dx}{dt} + \omega_0^2 x + bx^3 = \frac{e}{m}\frac{1}{2}\left[\widehat{E}_\omega e^{-i(\omega t - kz)} + \widehat{E}^*_\omega e^{i(\omega t - kz)}\right] \tag{2.29}$$

In this section the perturbational method used to solve equation 2.29 is outlined and the results are given without showing the intermediate manipulations.

The zeroth order solution is obtained by solving the linear differential equation - equation 2.29 with $b = 0$ so that the nonlinear term is removed. The solution obtained is identical to expression 2.6 and is given by

$$\begin{aligned} x^{(1)}(t) &= \frac{1}{2}\left[\left(\frac{e/m}{\omega_0^2 - \omega^2 - i\Gamma\omega}\right)\widehat{E}_\omega e^{-i(\omega t - kz)} + \left(\frac{e/m}{\omega_0^2 - \omega^2 + i\Gamma\omega}\right)\widehat{E}^*_\omega e^{i(\omega t - kz)}\right] \\ &= \frac{1}{2}\left[\left(\frac{e/m}{D_\omega}\right)\widehat{E}_\omega e^{-i(\omega t - kz)} + \left(\frac{e/m}{D^*_\omega}\right)\widehat{E}^*_\omega e^{i(\omega t - kz)}\right] \end{aligned} \tag{2.30}$$

with

$$D_\omega = \omega_0^2 - \omega^2 - i\Gamma\omega. \tag{2.31}$$

The first order solution is obtained by substituting the zeroth order solution 2.30 into the cubic term in the differential equation 2.29 and solving the resulting modified linear equation.

This yields a first order solution for the displacement which can be written as

$$\begin{aligned} x^{(3)}(t) &= \frac{1}{2}\left[\left(x_\omega^{(L)} + x_\omega^{(NL)}\right)e^{-i(\omega t-kz)} + \left(x_\omega^{(L)*} + x_\omega^{(NL)*}\right)e^{i(\omega t-kz)}\right] \\ &\quad + \frac{1}{2}\left[x_{3\omega}^{(NL)}e^{-3i(\omega t-kz)} + x_{3\omega}^{(NL)*}e^{3i(\omega t-kz)}\right] \\ \text{where } x_\omega^{(L)} &= \frac{e}{m}\frac{\widehat{E}_\omega}{D_\omega} \\ x_\omega^{(NL)} &= -\frac{3b}{4}\left(\frac{e}{m}\right)^3 \frac{\left(\widehat{E}_\omega\right)^2 \widehat{E}_\omega^*}{(D_\omega)^3 D_\omega^*} \\ x_{3\omega}^{(NL)} &= -\frac{3b}{4}\left(\frac{e}{m}\right)^3 \frac{\left(\widehat{E}_\omega\right)^3}{D_{3\omega}(D_\omega)^3} \end{aligned} \tag{2.32}$$

where (L) and (NL) label linear and nonlinear contributions.

2.2.2.2 Nonlinear polarisation and third-harmonic generation

Expresssion 2.32 shows that the nonlinear response of the medium is characterised by a polarisation density (total dipole moment per unit volume) $P^{(3)} = Nex^{(3)}$ where e denotes the charge of an electron and N the number of polarisable atomic electrons per unit volume. With the aid of expression 2.32 the polarisation density can be written as:

$$\begin{aligned} P^{(3)}(z,t) &= \frac{1}{2}\left[\widehat{P}_\omega^{(L)}e^{-i(\omega t-k_\omega z)} + cc\right] \\ &\quad + \frac{1}{2}\left[\widehat{P}_\omega^{(NL)}e^{-i(\omega t-k_\omega z)} + cc\right] + \frac{1}{2}\left[\widehat{P}_{3\omega}^{(NL)}e^{-3i(\omega t-k_\omega z)} + cc\right] \\ \text{where } \widehat{P}_\omega^{(L)} &= N\frac{e^2}{m}\frac{\widehat{E}_\omega}{D_\omega} \\ P_\omega^{(NL)} &= -\frac{3Neb}{4}\left(\frac{e}{m}\right)^3 \frac{\left(\widehat{E}_\omega\right)^2 \widehat{E}_\omega^*}{(D_\omega)^3 D_\omega^*} \\ \widehat{P}_{3\omega}^{(NL)} &= -\frac{3Neb}{4}\left(\frac{e}{m}\right)^3 \frac{\left(\widehat{E}_\omega\right)^3}{D_{3\omega}(D_\omega)^3} \end{aligned} \tag{2.33}$$

where (L) and (NL) indicate linear and nonlinear polarisation terms. The linear $\widehat{P}_\omega^{(L)}$ term is the term oscillating at the fundamental frequency ω and is related to the index of refraction and the (one-photon) absorption coefficient of the medium for photons with frequency ω. The $P_\omega^{(NL)}$ term is a nonlinear polarisation at the fundamental frequency associated with a nonlinear

perturbation to the index of refraction $n(\omega)$ at high electric fields. The $\widehat{P}_{3\omega}^{(NL)}$ term oscillating at frequency 3ω gives rise to third-harmonic generation. The last two contributions both describe observable third order nonlinear optical phenomena.

To calculate the effect of the nonlinear polarisation on the electromagnetic radiation field each of the contributions to the total polarisation as given in expression 2.33 must be substituted as source terms into the Maxwell wave equation.

$$\nabla^2\mathbf{E} - \frac{1}{c^2}\frac{\partial^2\mathbf{E}}{\partial t^2} = \frac{4\pi}{c^2}\frac{\partial^2\mathbf{P}}{\partial t^2} \tag{2.34}$$

$\widehat{P}_{\omega}^{(L)}$ and $\widehat{P}_{\omega}^{(NL)}$ serve as source terms for the electric field at the fundamental frequency ω. $\widehat{P}_{3\omega}^{(NL)}$ serves as a source term that generates a third-harmonic electromagnetic field at frequency 3ω propagating through the medium. The electric field of this generated third-harmonic wave is given by

$$\begin{aligned} E_{3\omega} &= \frac{1}{2}\left(\widehat{E}_{3\omega}(z)\, e^{-i(3\omega t - k_{3\omega} z)} + \widehat{E}_{3\omega}^{*}(z)\, e^{i(3\omega t - k_{3\omega} z)}\right) \\ \text{with } k_{3\omega} &= \frac{n(3\omega)\, 3\omega}{c}. \end{aligned} \tag{2.35}$$

The medium is therefore subjected to the propagation of two electromagnetic waves at frequencies ω and 3ω, with $|E_{3\omega}| \ll |E_{\omega}|$. The third-harmonic field $E_{3\omega}$ in turn causes linear and nonlinear polarisation of the medium, but because the intensity of $E_{3\omega}$ is so much smaller than that of the fundamental wave, only the linear polarisation $\widehat{P}_{3\omega}^{(L)}$ caused by $E_{3\omega}$ has to be taken into account. The total polarisation at the third-harmonic frequency 3ω therefore consists of both linear and nonlinear polarisation contributions, and can be expressed as

$$P_{3\omega} = \frac{1}{2}\left[\widehat{P}_{3\omega}^{(L)} e^{-i(3\omega t - k_{3\omega} z)} + \widehat{P}_{3\omega}^{(NL)*} e^{-3i(\omega t - k_{\omega} z)}\right] + cc \tag{2.36}$$

Within the approximations that was already made[4] the Maxwell wave equation for the total electric field can be separated into two coupled equations describing the propagation of

[4] The formal assumption is that the total electric field in the medium and the total polarisation of the medium can both be described as discrete Fourier series, of which only the ω and 3ω terms are significant in the case of third harmonic generation, and that the Maxwell equation can be written as a set of separated (coupled) equations - one for each frequency present in the medium.

the electric fields at the fundamental and third-harmonic frequencies respectively

$$\nabla^2 \mathbf{E}_\omega - \frac{1}{c^2}\frac{\partial^2}{\partial t^2}\mathbf{E}_\omega = \frac{4\pi}{c^2}\frac{\partial^2}{\partial t^2}\left(\mathbf{P}_\omega^{(L)} + \mathbf{P}_\omega^{(NL)}\right) \tag{2.37}$$

$$\nabla^2 \mathbf{E}_{3\omega} - \frac{1}{c^2}\frac{\partial^2}{\partial t^2}\mathbf{E}_{3\omega} = \frac{4\pi}{c^2}\frac{\partial^2}{\partial t^2}\left(\mathbf{P}_{3\omega}^{(L)} + \mathbf{P}_{3\omega}^{(NL)}\right) \tag{2.38}$$

The following assumptions, called the slow amplitude approximation, are made: it is assumed that the amplitudes of both the electric field and the polarisation vary slowly in z (and in time) compared to the wavelength (or period) of the electromagnetic oscillations. (It has already been assumed on page 22 that the amplitudes are time independent, making the assumption regarding the temporal variation superfluous in this case.) Due to the slow amplitude approximation the second derivative in space of the electric field amplitude $\widehat{E}_{3\omega}(z)$ can be neglected to give

$$\nabla^2 E = \frac{\partial^2 E}{\partial z^2} \approx \frac{1}{2}\left(2ik_{3\omega}\frac{d\widehat{E}_{3\omega}}{dz} - k_{3\omega}^2 \widehat{E}_{3\omega}\right) e^{-i(3\omega t - k_{3\omega} z)} + cc \tag{2.39}$$

For the sake of simplicity consider the case where absorption in the medium is negligible ($\Gamma \to 0$ so that D_ω as well as $D_\omega^* \to \omega_0^2 - \omega^2$.) The effects of absorption are considered again in section 2.3. Using the relations 2.7 and 2.11 between the linear polarisation $P_{3\omega}^{(L)}$, the linear susceptibility $\chi^{(1)}(3\omega)$ and wave vector $k_{3\omega}$ equation 2.38 can be rewritten as an equation relating the growth of the third-harmonic field as a function of the position in the medium with the nonlinear polarisation.

$$\frac{d\widehat{E}_{3\omega}}{dz} = \frac{i2\pi(3\omega)}{cn_{3\omega}}\widehat{P}_{3\omega}^{(NL)} e^{i(3k_\omega - k_{3\omega})z} \tag{2.40}$$

$$\text{with } k_{3\omega} = \frac{(3\omega)\, n_{3\omega}}{c} \tag{2.41}$$

This equation is a special case of the fundamental equation of nonlinear optics for third-harmonic generation in an optically thin nonlinear medium where the absorption of both the fundamental and the third-harmonic waves can be neglected. Equation 2.40 indicates that third-harmonic generation would occur ($\widehat{E}_{3\omega}$ would increase as a function of position along the direction of propagation, the z-axis) as soon as a non-zero nonlinear polarisation $P_{3\omega}^{(NL)}$ exists in the medium. The amplitude of the third-harmonic wave at any position z depends

on the magnitude of the nonlinear polarisation $P_{3\omega}^{(NL)}$ and the so called phase-matching term $e^{i(3k_\omega - k_{3\omega})z}$.

2.2.2.3 Efficiency of third-harmonic generation

To analyse the process of third-harmonic generation further in order to determine the optimal conditions, requires knowledge of the form of $P_{3\omega}^{(NL)}$. From the classical deduced expression for $P_{3\omega}^{(NL)}$, equation 2.33

$$\widehat{P}_{3\omega}^{(NL)} = -\frac{3Neb}{4}\left(\frac{e}{m}\right)^3 \frac{\left(\widehat{E}_\omega\right)^3}{D_{3\omega}\left(D_\omega\right)^3}$$

it is clear that a third order nonlinear susceptibility $\chi^{(3)}(\omega)$ responsible for third-harmonic generation can be defined so that [5]

$$P_{3\omega}^{(NL)} = \frac{1}{4}N\chi^{(3)}(-3\omega;\omega,\omega,\omega)\left(\widehat{E}_\omega(z)\right)^3 \tag{2.42}$$

(Comparing expression 2.42 with the classical expression 2.33 for $P_{3\omega}^{(NL)}$ a classical expression for the susceptibility can be written down:

$$\begin{aligned}\chi^{(3)}(-3\omega;\omega,\omega,\omega) &= -3eb\left(\frac{e}{m}\right)^3 \frac{1}{D_{3\omega}\left(D_\omega\right)^3} \\ &= -3eb\left(\frac{e}{m}\right)^3 \frac{1}{\left(\omega_0^2 - (3\omega)^2 - i\Gamma 3\omega\right)\left(\omega_0^2 - \omega^2 - i\Gamma\omega\right)^3}\end{aligned} \tag{2.43}$$

with D_ω defined as in expression 2.31. Because of the simple oscillator model used, expression 2.43 is no accurate expression for the susceptibility, although it does indicate the susceptibility to show resonant enhancement when the fundamental or third-harmonic frequency approaches the natural frequency of the atom. Quantum mechanics shows the nonlinear susceptibility to be a tensor with a much more complicated structure than this expression 2.43 allowing for different atomic energy states and different transitional frequencies and probabilities corresponding to transitions between these states as well as different polarisations of the incident radiation.

With $P_{3\omega}^{(NL)}$ expressed in terms of a susceptibility (its mathematical form does not matter)

[5] The factor 1/4 comes from the notational convention for susceptibilities (see section 2.3.2.2)

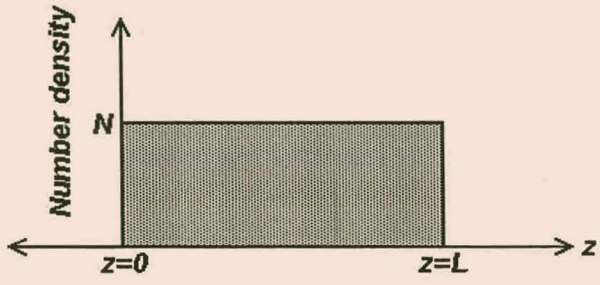

Figure 2-5: Diagram illustrating a rectangular density profile as assumed in the theoretical calculations.

the differential equation 2.40 becomes

$$\frac{d\widehat{E}_{3\omega}}{dz} = i\,(3\omega)\,\frac{2\pi}{cn_{3\omega}}\frac{1}{4}N\chi^{(3)}(-3\omega;\omega,\omega,\omega)\left(\widehat{E}_{\omega}(z)\right)^{3}e^{i\triangle kz} \tag{2.44}$$

$$\text{with } \triangle k = 3k_{\omega} - k_{3\omega} \tag{2.45}$$

now showing the coupling between the wave equations for the third-harmonic wave (equation 2.44) and the fundamental wave (equation 2.37) explicitly. The two coupled differential equations, 2.44 and 2.37, must be solved simultaneously to obtain the third-harmonic wave amplitude as a function of the position z in the medium. In the small signal limit approximations can be made that simplifies the problem. The small signal limit is in this context defined as the limit of small conversion efficiency where (i) $\widehat{E}_{3\omega} \ll \widehat{E}_{\omega}$ and (ii) it is appropriate to assume that the process of third-harmonic generation is not responsible for any significant attenuation of the fundamental wave. Therefore, $\widehat{E}_{\omega}(z)$ can be considered to be constant over the length L of the medium and the solution of equation 2.37 is simply $\widehat{E}_{\omega}(z) = \widehat{E}_{\omega}(0)$ (absorption is not taken into account here).

To simplify the integration of equation 2.44 it is assumed that the medium has a rectangular density profile. A rectangular density profile, as illustrated in figure 2-5, can be expressed as

the following function of the position z along the optical path:

$$\begin{aligned} Number\ density(z) &= 0 \quad \text{for } z < 0 \\ &= N \quad \text{for } 0 < z < L \\ &= 0 \quad \text{for } L < z \end{aligned}$$

where L is the medium length. Making these assumptions, equation 2.44 can easily be integrated and the following solution for the third-harmonic electric field as a function of z is obtained

$$\begin{aligned} \widehat{E}_{3\omega}(z) &= i\,(3\omega)\,\frac{2\pi}{cn_{3\omega}}\frac{1}{4}N\chi^{(3)}(-3\omega;\omega,\omega,\omega)\left(\widehat{E}_{\omega}(0)\right)^{3}\int_{0}^{z}e^{i\triangle kz} \quad \text{for } 0 < z < L \\ &= i\,(3\omega)\,\frac{2\pi}{cn_{3\omega}}\frac{1}{4}N\chi^{(3)}(-3\omega;\omega,\omega,\omega)\left(\widehat{E}_{\omega}(0)\right)^{3}ze^{i\triangle kz/2}\left(\frac{\sin\triangle kz/2}{\triangle kz/2}\right) \end{aligned} \tag{2.46}$$

The result that is of practical interest is the intensity of the generated third-harmonic wave at the exit window:

$$\begin{aligned} I_{3\omega}(L) &= \frac{1}{2}\frac{n_{3\omega}c}{4\pi}\left|\widehat{E}_{3\omega}(L)\right|^{2} \\ &= \frac{1}{16}\left(\frac{4\pi}{c}\right)^{4}\frac{1}{(n_{\omega})^{3}n_{3\omega}}(3\omega)^{2}\left(N\chi^{(3)}(-3\omega;\omega,\omega,\omega)\right)^{2}(I_{\omega}(0))^{3}L^{2}\left(\frac{\sin\triangle kL/2}{\triangle kL/2}\right)^{2} \end{aligned} \tag{2.47}$$

An intensity conversion efficiency for third-harmonic generation e_{THG} can be defined as

$$e_{THG} = \frac{I_{3\omega}(L)}{I_{\omega}(0)} = \frac{1}{16}\left(\frac{4\pi}{c}\right)^{4}\frac{1}{(n_{\omega})^{3}n_{3\omega}}(3\omega)^{2}\left(N\chi^{(3)}(-3\omega;\omega,\omega,\omega)\right)^{2}(I_{2\omega}(0))^{2}L^{2}\left(\frac{\sin\triangle kL/2}{\triangle kL/2}\right)^{2} \tag{2.48}$$

From equation 2.47 the requirements for efficient third-harmonic generation in the small signal limit in a medium where absorption losses are negligible are obtained. The fundamental intensity is important as the intensity of the generated third-harmonic radiation is directly proportional to the cube of the fundamental intensity. Secondly the efficiency depends critically on the properties of the medium. The microscopic requirement is that the medium must have a sufficiently large nonlinear susceptibility $\chi^{(3)}$ for third-harmonic generation at the specific fundamental frequency used. (The nonlinear susceptibility is frequency dependent and greatly

enhanced by exploiting atomic resonances as indicated by expression 2.43.) The critical macroscopic requirement is called phase matching and is contained in the last factor $\left(\frac{\sin \triangle kL/2}{\triangle kL/2}\right)^2$. This factor shows a sharp peak where the $\triangle kL = 0$ (See figure 3-3), but reduces the efficiency of third-harmonic generation drastically towards positive or negative values of $\triangle kL$. The third-harmonic intensity in the small signal limit also depends on the length and density of the medium. In chapter 3 these considerations, applied to a specific experimental setup, are discussed in more detail.

2.3 Quantum mechanical approach to nonlinear optics

The quantum mechanical approach discussed in this section is, as mentioned in section 2.1, not a full quantum mechanical treatment, but rather a semi-classical approach. The nonlinear medium is treated by quantum mechanics, but the ratiation field is described classically by a wave model. The classical treatment of the radiation field is valid when the radiation field is strong, which is the case in the experimental situations discussed here.

An analysis of the interaction of electrical fields with a nonlinear medium using quantum mechanical theory again involves the simultaneous solution of two equations: the Schrödinger and Maxwell equations. The Schrödinger equation describes the response of the atoms or molecules of the medium to the local properties of the electromagnetic wave in terms of electric susceptibilities of different orders. The Maxwell equations describe the response of the electromagnetic fields to the local properties of the medium as characterised by the susceptibilities. The Maxwell equations, with the assumption that the amplitudes of E and P are varying very slowly in space and time and that the radiation is a plane monochromatic wave, yield the fundamental equation of nonlinear optics [31, Equation 1], [46, Equation 1]

$$\frac{d\widehat{E_q}}{dz} = i\frac{2\pi\omega_q^2}{c^2 k_q} P_q^{NL} \exp\left(-ik_q z\right) - \frac{\sigma^{(1)}(\omega_q)}{2} N\widehat{E}_q \tag{2.49}$$

Here E_q and P_q^{NL} are the Fourier components of the electrical field and polarisation at the frequency ω_q.

In the case of third harmonic generation in an optically thin medium when $\sigma^{(1)}(\omega) \to 0$, equation 2.49 reduces exactly to the classical result, equation 2.40.

2.3.1 Derivation of the fundamental equation of nonlinear optics

The Maxwell equations governing the interaction of an electromagnetic wave with a scattering medium are [50, Equation 13.45]:

$$\begin{aligned} \nabla \cdot \mathbf{D} &= 4\pi\rho \\ \nabla \times \mathbf{E} &= -\frac{1}{c}\frac{\partial \mathbf{B}}{\partial t} \\ \nabla \cdot \mathbf{B} &= 0 \\ \nabla \times \mathbf{H} &= \frac{4\pi}{c}\mathbf{j} + \frac{1}{c}\frac{\partial \mathbf{D}}{\partial t} \end{aligned} \tag{2.50}$$

with $\mathbf{D} = \mathbf{E} + 4\pi\mathbf{P} = \epsilon\mathbf{E}$ the electric displacement, $\mathbf{B} = \mathbf{H} + 4\pi\mathbf{M} = \mu\mathbf{H}$ the magnetic induction, $\mathbf{j}$ the current density and ρ the charge density.

For nonlinear optics in gaseous media the following simplifying assumptions can be made: $\mathbf{M} = 0$ (therefore $\mathbf{B} = \mathbf{H}$) because the medium is nonmagnetic, $\rho = 0$ because the medium is charge free and $\mathbf{j} = 0$ the medium being currentless. The simplified Maxwell equations describing such a medium are:

$$\nabla \cdot \mathbf{D} = 0 \tag{2.51}$$

$$\nabla \times \mathbf{E} = -\frac{1}{c}\frac{\partial \mathbf{B}}{\partial t} \tag{2.52}$$

$$\nabla \cdot \mathbf{B} = \nabla \cdot \mathbf{H} = 0 \tag{2.53}$$

$$\nabla \times \mathbf{H} = \nabla \times \mathbf{B} = \frac{1}{c}\frac{\partial \mathbf{D}}{\partial t} = \frac{1}{c}\frac{\partial \mathbf{E}}{\partial t} + \frac{4\pi}{c}\frac{\partial \mathbf{P}}{\partial t} \tag{2.54}$$

Substitution and simplification of these four equations yield the well known Maxwell wave equation

$$\nabla^2\mathbf{E} - \frac{1}{c^2}\frac{\partial^2 \mathbf{E}}{\partial t^2} = \frac{4\pi}{c^2}\frac{\partial^2 \mathbf{P}}{\partial t^2} \tag{2.55}$$

Without any loss of generality, $\mathbf{P}$ can be split into a linear $\mathbf{P}^{(L)}$ and a nonlinear component $\mathbf{P}^{(NL)}$. With small electrical fields the polarisation induced in any medium is proportional to the electric field amplitude. This is called the linear polarisation $\mathbf{P}^{(L)}$. In a medium subjected to large electrical fields the nonlinear polarisation terms proportional to the electrical field amplitude to some higher power become significant. These contributions are represented by

$\mathbf{P}^{(NL)}$ and can be written in general as a series expansion of contributions of different orders

$$\mathbf{P}^{(NL)} = \sum_{n=2}^{\infty} \mathbf{P}^{(n)} \tag{2.56}$$

summing over the orders n ($n \geq 2$) of the nonlinear contributions [50, Equation 13.31]. $\mathbf{P}^{(n)}$ is completely defined by the Fourier expansion in equation 2.59 and the general expression 2.78 for the Fourier coefficients in the discussion of section 2.3.2.

The Maxwell wave equation can now be rewritten

$$\begin{aligned} \nabla^2\mathbf{E} - \frac{1}{c^2}\frac{\partial^2\mathbf{E}}{\partial t^2} - \frac{4\pi}{c^2}\frac{\partial^2\mathbf{P}^{(L)}}{\partial t^2} &= \frac{4\pi}{c^2}\frac{\partial^2\mathbf{P}^{(NL)}}{\partial t^2} \\ &= \frac{4\pi}{c^2}\frac{\partial^2}{\partial t^2}\sum_{n=2}^{\infty}\mathbf{P}^{(n)} \end{aligned} \tag{2.57}$$

and depending on the orders of the terms allowed in the sum solutions of different orders can be obtained for the Maxwell wave equation. Using first order perturbation theory equation 2.57 can be solved separately for the different orders of n, each solution describing the nonlinear optical phenomena in the electromagnetic wave material medium interaction belonging to that order.

It is convenient for the rest of the discussion to describe the electric field in terms of its Fourier components [50, p. 294]:

$$\begin{aligned} \mathbf{E}(r,t) &= \frac{1}{2}\sum_j \left[\widehat{\varepsilon}_j \widehat{E}(r,\omega_j)\, e^{-i(\omega_j t - k_j z)} + cc\right] \\ &= \frac{1}{2}\sum_j \left[\widehat{\varepsilon}_j E(r,\omega_j)\, e^{-i\omega_j t} + cc\right] \\ \text{with } E(r,\omega_j) &= \widehat{E}(r,\omega_j)\, e^{ik_j z} \end{aligned} \tag{2.58}$$

$\widehat{\varepsilon}_j$ is the unit vector in the direction of polarisation of component j. (For the applications discussed in this thesis it is appropriate to consider the electric field as consisting of a superposition of (quasi-) monochromatic waves and therefore the discrete sum instead of an integral is used.) In the same way each contribution to the polarisation density can also be expanded

as Fourier series:

$$\mathbf{P}^{(n)}(r,t) = \frac{1}{2}\sum_j \left[\widehat{\varepsilon}_j P^{(n)}(r,\omega_j)\, e^{-i\omega_j t} + cc\right]. \tag{2.59}$$

This Fourier expansion of the polarisation density can be made for each of the linear and nonlinear contributions: n can be 1 (linear) or $2,3,4...$(nonlinear, higher order contributions). The Fourier expansion is independent of the expansion of $\mathbf{P}^{(NL)}$ as the sum of contributions over different orders as in expression 2.56.

To summarise: the polarisation density can be expressed as

$$\mathbf{P} = \mathbf{P}^{(L)} + \mathbf{P}^{(NL)} = \mathbf{P}^{(L)} + \sum_{n=2}^{\infty} \mathbf{P}^{(n)} \tag{2.60}$$

where a Fourier series expansion can be made for the linear part

$$\mathbf{P}^{(L)}(r,t) = \frac{1}{2}\sum_j \left[\widehat{\varepsilon}_j P^{(L)}(r,\omega_j)\, e^{-i\omega_j t} + cc\right]$$

as well as for each of the nonlinear contributions of different orders.

$$\begin{aligned} \mathbf{P}^{(2)}(r,t) &= \frac{1}{2}\sum_j \left[\widehat{\varepsilon}_j P^{(2)}(r,\omega_j)\, e^{-i\omega_j t} + cc\right] \\ \mathbf{P}^{(3)}(r,t) &= \frac{1}{2}\sum_j \left[\widehat{\varepsilon}_j P^{(3)}(r,\omega_j)\, e^{-i\omega_j t} + cc\right] \text{ etc.} \end{aligned} \tag{2.61}$$

Written in terms of the Fourier coefficients equation 2.57 becomes[6]

$$\begin{aligned} &\nabla^2\left(\widehat{E}(r,\omega_j)\, e^{-i(\omega_j t - k_j z)}\right) - \frac{1}{c^2}\frac{\partial^2}{\partial t^2}\left(\widehat{E}(r,\omega_j)\, e^{-i(\omega_j t - k_j z)}\right) \\ = &\frac{4\pi}{c^2}\frac{\partial^2}{\partial t^2}\left(P^{(L)}(r,\omega_j)\, e^{-i\omega_j t}\right) + \frac{4\pi}{c^2}\frac{\partial^2}{\partial t^2}\left(P^{(NL)}(r,\omega_j)\, e^{-i\omega_j t}\right) \end{aligned} \tag{2.62}$$

Each of the Fourier coefficients $P^{(n)}(r,\omega_j)$ of the polarisation density can be expressed in terms of susceptibilities and Fourier coefficients of the electric fields as will be discussed in section 2.3.2 giving the general expression 2.78. The relation for the linear polarisation is well

[6] In the equality, comparing terms with equal time dependent exponents, one can get rid of the sums and complex conjugates.

known. The complete quantum mechanical expression for the linear polarisation is

$$P_{\alpha_s}^{(L)}(r,\omega_j) = N\sum_{\alpha_1}\chi_{\alpha_s\alpha_1}^{(1)}(-\omega_j;\omega_j)\,E_{\alpha_1}(r,\omega_j) \tag{2.63}$$

(for an explanation of the tensor notation see the paragraph following expression 2.78) but for the purpose of this discussion the simplified expression

$$\begin{aligned} P^{(L)}(r,\omega_j) &= N\chi^{(1)}(\omega_j)E(r,\omega_j) && (2.64)\\ &= N\chi^{(1)}(\omega_j)\widehat{E}(r,\omega_j)\,e^{ik_jz} && (2.65)\end{aligned}$$

can be used, showing the linear susceptibility $\chi^{(1)}(\omega_j)$ to be the proportionality constant in the direct proportionality between the linear polarisation and the electric field at frequency ω_j. In general the linear susceptibility $\chi^{(1)}$ is frequency dependent and complex with $\overline{\chi}^{(1)}$ and $\widetilde{\chi}^{(1)}$denoting the real and imaginary parts of the linear susceptibility respectively. The derivation of the relation between the real and imaginary parts of $\chi^{(1)}$ and the wave vector, index of refraction and absorption coefficient is discussed in detail in appendix C. The results are used here. The real part $\overline{\chi}^{(1)}(\omega)$ is related to the real index of refraction n of the medium and therefore to the phase velocity v of the propagating electromagnetic wave of frequency ω. From equation 7.10 in appendix C:

$$1+4\pi N\overline{\chi}^{(1)}(\omega_j) \equiv \epsilon_r = \overline{n}_j^2 = \left(\frac{c}{v}\right)^2. \tag{2.66}$$

The imaginary part of the linear susceptibility $\widetilde{\chi}^{(1)}$ can be shown (see equation 7.15 in appendix C) to determine the absorption coefficient κ [50, equation 13.30]

$$4\pi N\widetilde{\chi}^{(1)}(\omega_j) \equiv \epsilon_i = \frac{cn_j\kappa_j}{\omega_j} \tag{2.67}$$

$$\text{or} \quad \kappa_j = N\frac{4\pi\omega_j}{cn_j}\widetilde{\chi}^{(1)}(\omega_j) \tag{2.68}$$

or the one-photon absorption cross-section $\sigma^{(1)}$ [46, equation 4] (see equation 7.16)

$$\sigma_j^{(1)} = \frac{4\pi\omega_j}{cn_j}\widetilde{\chi}^{(1)}(\omega_j). \tag{2.69}$$

In some definitions of $\sigma_j^{(1)}$ as in Puell et al ([31]) and Vidal et al ([46] and [50])as well as in the results derived in section 2.2.1 the factor $\frac{1}{n_j}$ is left out, an acceptable approximation if $n_j \approx 1$. Two different ways to obtain the expressions for κ_j and $\sigma_j^{(1)}$ and the approximations made in both are compared in appendix C.

The expression for the linear polarisation, equation 2.65, leads to a simplification of the nonlinear Maxwell equation. Equation 2.62 becomes

$$\begin{aligned} &\nabla^2\left(\widehat{E}\left(r,\omega_j\right)e^{ik_jz}\right) - \frac{1}{c^2}\frac{\partial^2}{\partial t^2}\left(\widehat{E}\left(r,\omega_j\right)e^{ik_jz}\right) - \frac{4\pi}{c^2}N\chi^{(1)}\frac{\partial^2}{\partial t^2}\left(\widehat{E}\left(r,\omega_j\right)e^{ik_jz}\right) \\ = \;& \frac{4\pi}{c^2}\frac{\partial^2}{\partial t^2}P^{(NL)}\left(r,\omega_j\right) \end{aligned} \tag{2.70}$$

and after rearrangement

$$\begin{aligned} \nabla^2\left(\widehat{E}\left(r,\omega_j\right)e^{ik_jz}\right) - \frac{1}{c^2}\left(1+4\pi N\chi^{(1)}\right)\frac{\partial^2}{\partial t^2}\left(\widehat{E}\left(r,\omega_j\right)e^{ik_jz}\right) &= \frac{4\pi}{c^2}\frac{\partial^2}{\partial t^2}P^{(NL)}\left(r,\omega_j\right) \\ \nabla^2\left(\widehat{E}\left(r,\omega_j\right)e^{ik_jz}\right) - \frac{1}{c^2}\left(n_j^2+i\epsilon_i\right)\frac{\partial^2}{\partial t^2}\left(\widehat{E}\left(r,\omega_j\right)e^{ik_jz}\right) &= \frac{4\pi}{c^2}\frac{\partial^2}{\partial t^2}P^{(NL)}\left(r,\omega_j\right) \end{aligned} \tag{2.71}$$

with ϵ_i and n_j^2 as defined in expressions 2.67 and 2.66

For a detailed study of the nonlinear optical process, the spatial dependence of the electric fields Fourier coefficients $\widehat{E}\left(r,\omega_j\right)$ need to be specified. For a general discussion the plane wave approximation can be used. These results hold approximately for not too tightly focussed beams. A Gaussian or more complicated spacial distribution has to be considered when studying the optics of focussed beams [53].

In the plane wave approximation the electric field and polarisation density have the simplified forms

$$\mathbf{E}\left(z,t\right) = \frac{1}{2}\sum_j\left[\widehat{\varepsilon}_j\widehat{E}_j\left(z\right)e^{-i(\omega_jt-k_jz)} + cc\right] = \frac{1}{2}\sum_j\left[\widehat{\varepsilon}_jE_j(z)e^{-i(\omega_jt)} + cc\right] \tag{2.72}$$

$$\text{with} \qquad E_j(z) = \widehat{E}_j(z)\exp(ik_j z)$$

$$\text{and} \qquad \mathbf{P}(z,t) = \frac{1}{2}\sum_j \left[\widehat{\varepsilon}_j P_j(z)\, e^{-i\omega_j t} + cc\right] \tag{2.73}$$

with z the chosen direction of propagation. The wave equation 2.71 then depends on only one Cartesian coordinate, z, and ∇^2 can be replaced by $\frac{\partial^2}{\partial z^2}$.

It is assumed that the amplitudes of the electric field and polarisation density vary very slowly in time and space compared to the period and wavelength of the oscillations. In this slow amplitude approximation $\frac{\partial \widehat{E_j}}{\partial t} \ll \omega_j \widehat{E_j}$ and $\frac{\partial \widehat{E_j}}{\partial z} \ll k_j \widehat{E_j}$ (and for $P_j^{(NL)}$ correspondingly.) Calculating the derivatives in equation 2.71 the second derivatives of the amplitudes are considered to be negligible, but the first derivatives are retained giving

$$\begin{aligned}
\nabla^2\mathbf{E} &= \frac{1}{2}\sum_j \widehat{\varepsilon}_j \left(2ik_j\frac{\partial \widehat{E_j}}{\partial z} - (k_j)^2\widehat{E_j}\right) e^{-i(\omega_j t - k_j z)} + cc \\
\frac{\partial^2\mathbf{E}}{\partial t^2} &= \frac{1}{2}\sum_j \widehat{\varepsilon}_j \left(-2i\omega_j\frac{\partial \widehat{E_j}}{\partial t} - (\omega_j)^2\widehat{E_j}\right) e^{-i(\omega_j t - k_j z)} + cc \\
\frac{\partial^2\mathbf{P}^{(NL)}}{\partial t^2} &= \frac{1}{2}\sum_j \widehat{\varepsilon}_j \left(-2i\omega_j\frac{\partial P_j^{(NL)}}{\partial t} - (\omega_j)^2 P_j^{(NL)}\right) e^{-i\omega_j t} + cc
\end{aligned}$$

Substituting this into the Maxwell wave equation 2.71 yields

$$\begin{aligned}
&\left(2ik_j\frac{\partial \widehat{E_j}}{\partial z} - (k_j)^2\widehat{E_j}\right) e^{ik_j z} - \frac{1}{c^2}\left(n_j^2 + i\epsilon_i\right)\left(-2i\omega_j\frac{\partial \widehat{E_j}}{\partial t} - (\omega_j)^2\widehat{E_j}\right) e^{ik_j z} \\
= \;& \frac{4\pi}{c^2}\left(-2i\omega_j\frac{\partial P_j^{(NL)}}{\partial t} - (\omega_j)^2 P_j^{(NL)}\right)
\end{aligned}$$

Using the relation 7.10 in appendix C

$$\overline{k}_j^2 = \frac{\omega_j^2\overline{n}_j^2}{c^2} = \frac{\omega_j^2}{c^2}(1 + 4\pi N\overline{\chi}_j^{(1)}) \tag{2.74}$$

this gives

$$2ik_j\left(\frac{\partial \widehat{E_j}}{\partial z} + \frac{n_j}{c}\frac{\partial \widehat{E_j}}{\partial t}\right) - \frac{2\epsilon_i\omega_j}{c^2}\frac{\partial \widehat{E_j}}{\partial t} + \frac{i\epsilon_i\omega_j^2}{c^2}\widehat{E_j} = \frac{4\pi}{c^2}\left(-2i\omega_j\frac{\partial P_j^{(NL)}}{\partial t} - (\omega_j)^2 P_j^{(NL)}\right) e^{-ik_j z} \tag{2.75}$$

The slow amplitude approximation means that the terms containing the time derivatives of $\widehat{E_j}$ and P_j can now be neglected. Using the expression for the total derivative $\frac{\partial \widehat{E_j}}{\partial z} + \frac{n}{c}\frac{\partial \widehat{E_j}}{\partial t} = \frac{d\widehat{E}_j}{dz}$ the fundamental equation of nonlinear optics is obtained

$$\frac{d\widehat{E}_j}{dz} = i\frac{2\pi\omega_j}{n_j c} P_j^{(NL)} e^{-ik_j z} - \frac{\epsilon_i \omega_j}{2cn_j}\widehat{E_j}$$

In terms of the absorption coefficient κ_j it has the form

$$\frac{d\widehat{E}_j}{dz} = i\frac{2\pi\omega_j}{n_j c} P_j^{(NL)} e^{-ik_j z} - \frac{\kappa_j}{2}\widehat{E_j} \tag{2.76}$$

or as equation 2.49 in terms of the one-photon absorption cross section $\sigma_j^{(1)} = \sigma^{(1)}(\omega_j)$.

$$\frac{d\widehat{E}_j}{dz} = i\frac{2\pi\omega_j}{n_j c} P_j^{(NL)} e^{-ik_j z} - \frac{\sigma_j^{(1)}}{2} N\widehat{E_j} \tag{2.77}$$

The fundamental equation of nonlinear optics (see equations 2.49, 2.76 or 2.77), together with knowledge of the nonlinear susceptibilities for different nonlinear phenomena contained in $P_q^{(NL)}$ and their structure as provided by quantum mechanics, give a complete mathematical description of any nonlinear system. To describe a nonlinear system where a number of M different frequencies (incident and generated frequencies) are considered to be present in a significant intensity in the medium, a set of M coupled equations of the form of equation 2.77 is needed. Each of the M frequencies can in principle have nonlinear polarisations of several orders contributing to it - as expression 2.56 implies. In general, mathematically, M goes to infinity making the problem impossible to solve. Therefore, considering a physical situation, physical insight is needed and care must be taken to include the relevant polarisation contributions and to exclude those that are negligible.

To use the fundamental equation of nonlinear optics for evaluation of any physical system the mathematical structure of the significant contributions $P_q^{(NL)}$ needs to be known. Quantum mechanical methods yield expressions for the nonlinear polarisation contributions in terms of Fourier components of the electric fields present in the medium and the nonlinear susceptibilities characterising the response of the medium.

2.3.2 Nonlinear susceptibilities

Schrödinger's equation for the atoms or molecules of the medium yields those properties of the medium influenced by the electric field as contained in the linear and especially the nonlinear polarisation density $P_q^{(NL)}$. $P_q^{(NL)}$ can be evaluated in one of two ways [31]. The first method uses the density matrix formalism consistently to arrive at intensity dependent susceptibilities including all intensity dependent effects directly. The set of equations and their interpretation become very complicated. The second method treats atoms originally excited to different energy levels as separate species, applies time-dependent perturbation theory to each excited atomic state separately, and finally calculates the sum over all the excited states weighed by their populations and finds the total nonlinear polarisation. Rate equations are needed to calculate the populations of the different excited states. The second method as employed by Armstrong et al [1] and Puell et al [31] does not include all effects like Stark shift, coherent excitation and saturation directly, but makes it easier to distinguish between the different processes and realise the limitations [31]. The results of the second method are discussed further in this section.

2.3.2.1 Tensor properties of the nonlinear susceptibility

In the discussion of third-harmonic generation in the classical context a third order nonlinear susceptibility was introduced in equation 2.42. $\chi^{(3)}(-3\omega;\omega,\omega,\omega)$ has been defined, apart from the number density and a numerical factor, as the proportionality constant between the induced third order nonlinear polarisation density at frequency 3ω and the inducing electrical field amplitude to the third power.

In 2.42 we have tacitly assumed that the incident waves and the polarisation are linearly polarised in the same direction. In general, however, three electric fields (three photons) polarised in different directions can couple to generate a field and produce a photon polarised in yet another direction. The quantum mechanical definition of the nth order nonlinear susceptibility [16, equation 2.7] takes this into account:

$$P_{\alpha_s}^{(n)}(r,\omega_s) = \frac{n!N}{2^{n-1}} \sum_{\alpha_1 \ldots \alpha_n} \chi_{\alpha_s \alpha_1 \ldots \alpha_n}^{(n)}(-\omega_s;\omega_1 \ldots \omega_n)\, E_{\alpha_1}(r,\omega_1) \ldots E_{\alpha_n}(r,\omega_n) \qquad (2.78)$$

$$\text{where } \omega_s = \omega_{1+}\omega_{2+} \ldots + \omega_n.$$

Equation 2.78 defines the tensor form of the nonlinear optical susceptibility tensor $\chi^{(n)}_{\alpha_s\alpha_1...\alpha_n}$ that characterises the nonlinear response of the medium to the simultaneous interaction with $n+1$ different waves. $\chi^{(n)}_{\alpha_1...\alpha_n}$ couples n electric fields of frequencies $\omega_1, \omega_2...\omega_n$ to the induced polarisation density $P^{(n)}_{\alpha_s}$ at frequency $\omega_s = \omega_1 + \omega_2 + ... + \omega_n$ and must therefore be a tensor of rank $(n+1)$ by definition. $P^{(n)}_{\alpha_i}$ and E_{α_i} are the Fourier coefficients of the α_i components of the polarisation density and electrical field. The α_i describes the "polarisation orientation" of the component - in terms of the Cartesian coordinates x, y and z or alternatively cylindrical or spherical coordinates. The indices $\alpha_1...\alpha_n$ may, for plane polarised waves, be Cartesian subscripts (x, y or z) over which must be summed to include all the contributions to the full polarisation density in the Cartesian direction α_s. (The summation signs are sometimes left out accepting the Einstein summation convention that there must always be summed over repeated indices.) N is the number density of the medium, the $n!$ factor takes the permutation symmetry of the susceptibility tensor into account - for the case when all the frequencies are non-zero and different. The factor $\frac{1}{2^{n-1}}$ is the result of the convention in defining susceptibilities as discussed in the next subsection.

The nonlinear susceptibility tensors possesses an intrinsic permutation symmetry - that they are invariant under permutation of the pairs $\alpha_1\omega_1,..., \alpha_n\omega_n$ identifying the incident waves. This permutation symmetry is responsible for the $n!$ factor in expression 2.78. If none of the frequencies $\omega_s, \omega_1, \omega_2...\omega_n$ or combinations of them are resonant with transition frequencies in the medium, then to a good approximation the nonlinear susceptibility is also invariant under permutations of the pairs $\alpha_s - \omega_s; \alpha_1\omega_1,..., \alpha_n\omega_n$ called "overall" permutation symmetry.

This general expression, equation 2.78, includes the generation of all possible different linear combinations of $\omega_1, \omega_2...\omega_n$. The conventional notation is that a frequency ω_i that must be subtracted in calculating the resultant ω_s, is replaced by $-\omega_i$ in equation 2.78 and $E(r, \omega_i)$ by $E(r, -\omega_i) \equiv E^*(r, \omega_i)$.

As an example the linear susceptibility is in general a tensor of rank 2 (equivalent to a matrix). Its general expression is

$$P^{(1)}_{\alpha_s}(r, \omega) = N \sum_{\alpha_1=x,y,z} \chi^{(1)}_{\alpha_s\alpha_1}(-\omega; \omega) E_{\alpha_1}(r, \omega) \tag{2.79}$$

having chosen Cartesian components to specify the polarisation directions. It is clear that $\chi^{(1)}_{\alpha_s\alpha_1}(-\omega;\omega)$ has $3\times3=9$ tensor elements for example $\chi^{(1)}_{xx}(-\omega;\omega)$, $\chi^{(1)}_{xy}(-\omega;\omega)$... For example the x-component of the polarisation density is given by

$$\begin{aligned} P^{(1)}_x(r,\omega) &= N\left[\chi^{(1)}_{xx}(-\omega;\omega)E_x(r,\omega)+\chi^{(1)}_{xy}(-\omega;\omega)E_y(r,\omega)+\chi^{(1)}_{xz}(-\omega;\omega)E_z(r,\omega)\right] \\ (\text{with } E_z(r,\omega) &= 0 \text{ if } z \text{ is the direction of propagation}) \end{aligned} \tag{2.80}$$

For $P^{(1)}_y$ and $P^{(1)}_z$ similar expressions can be written down. For the linear susceptibility this can be written in matrix notation

$$\begin{bmatrix} P^{(1)}_x \\ P^{(1)}_y \\ P^{(1)}_z \end{bmatrix} = N \begin{bmatrix} \chi^{(1)}_{xx} & \chi^{(1)}_{xy} & \chi^{(1)}_{xz} \\ \chi^{(1)}_{yx} & \chi^{(1)}_{yy} & \chi^{(1)}_{yz} \\ \chi^{(1)}_{zx} & \chi^{(1)}_{zy} & \chi^{(1)}_{zz} \end{bmatrix} \begin{bmatrix} E_x \\ E_y \\ E_z \end{bmatrix}$$

In anisotropic media the matrix elements of the susceptibility with different x, y, z indices may have different values giving rise to refractive indices that are different for different field polarisations or directions of propagation. In an isotropic medium such as an atomic gas simplifications can be made to the expression 2.78. This can be illustrated by examples.

In an isotropic medium the linear susceptibility $\chi^{(1)}_{\alpha_s\alpha_1}$ is diagonal meaning that

$$\chi^{(1)}_{\alpha_s\alpha_1} = \chi^{(1)}_{\alpha_1\alpha_1}\delta_{\alpha_s\alpha_1},$$

in matrix notation

$$\chi^{(1)}_{\alpha_s\alpha_1} = \begin{bmatrix} \chi^{(1)}_{xx} & 0 & 0 \\ 0 & \chi^{(1)}_{yy} & 0 \\ 0 & 0 & \chi^{(1)}_{zz} \end{bmatrix}$$

and the expression for the (say) α component of the polarisation $P^{(1)}_\alpha(r,\omega)$ as given by expression 2.79 reduces to only one term depending only on the α component of the electrical field

$$P^{(1)}_\alpha(r,\omega) = N\chi^{(1)}_{\alpha\alpha}(-\omega;\omega)E_\alpha(r,\omega)$$

$$\text{or simply } P^{(1)}(r,\omega) = N\chi^{(1)}(-\omega;\omega)\,E(r,\omega)$$

For third order the nonlinear susceptibility is in general

$$P^{(3)}_{\alpha_s}(r,\omega_s) = \frac{3N}{2}\sum_{\alpha_1=x,y,z}\sum_{\alpha_2=x,y,z}\sum_{\alpha_3=x,y,z}\chi^{(3)}_{\alpha_s\alpha_1\alpha_2\alpha_3}(-\omega_s;\omega_1,\omega_2,\omega_3)\,E_{\alpha_1}(r,\omega_1)\,E_{\alpha_2}(r,\omega_2)\times E_{\alpha_3}(r,\omega_3) \tag{2.81}$$

$$\text{with } \omega_s = \omega_1+\omega_2+\omega_3 \tag{2.82}$$

$\chi^{(2)}_{\alpha_s\alpha_1\alpha_2}(-\omega_s;\omega_1,\omega_2)$ is the fourth rank nonlinear susceptibility tensor coupling fields of frequencies ω_1, ω_2 and ω_3 to induce a field with frequency ω_s. The tensor $\chi^{(3)}_{\alpha_s\alpha_1\alpha_2\alpha_3}(-\omega_s;\omega_1,\omega_2,\omega_3)$ consists of $3\times3\times3\times3=81$ tensor elements, for example $\chi^{(2)}_{zyxx}(-\omega_s;\omega_1,\omega_2,\omega_3)$ coupling the electric field vectors of frequencies ω_1 polarised in the y-direction, ω_2 polarised in the x-direction and ω_3 polarised in the x-direction to form one term contributing to the total polarisation at frequency ω_s in the z-direction.

When the general expression is applied to third-harmonic generation in an isotropic atomic vapour the same simplifications can be made. Assume that the incident wave is polarised linearly in the y-direction; therefore $E_y(r,\omega)$ is the only non-zero component of the electric field. The expression for the third order nonlinear polarisation density is then reduced to only one component

$$P^{(3)}_y(r,\omega_s) = \frac{3}{2}N\chi^{(3)}_{yyy}(-\omega_s;\omega_1,\omega_2,\omega_3)\,E_y(r,\omega_1)\,E_y(r,\omega_2)\,E_y(r,\omega_3) \tag{2.83}$$

$$(\text{with } \omega_1 = \omega_2 = \omega_3 = \omega \text{ and } \omega_s = 3\omega \text{ for third harmonic})$$

or simply written as

$$P^{(3)}(r,\omega_s) = \frac{3}{2}N\chi^{(3)}(-\omega_s;\omega_1,\omega_2,\omega_3)\,E(r,\omega_1)\,E(r,\omega_2)\,E(r,\omega_3) \tag{2.84}$$

This is, especially for third-harmonic generation of a dye laser beam in an atomic gas medium, a realistic assumption because the single incident dye laser beam, coming from a Lambda Physik dye laser, is strongly (ratio 20:1) linearly polarised in the vertical direction, therefore $E_y \gg E_x$ (and $E_z = 0$ when z is taken as the direction of propagation.) Because the atomic gas medium

is isotropic this practically vertical polarised electric field produces only a vertical polarised polarisation field, leaving the polarisation contribution given by expression 2.83 as the only significant polarisation term.

2.3.2.2 Convention for nonlinear susceptibilities

The factor $\frac{1}{4}$ in expression 2.42, $\frac{3}{2}$ in expression 2.82 and the factor $\frac{n!}{2^{n-1}}$ in the formal definition of nonlinear susceptibility, expression 2.78, is connected to the convention used in relating polarisation density to the inducing electric fields. This can be best illustrated by examples.

Consider third-harmonic generation. The incident monochromatic fundamental wave has the form

$$E(\omega) = \frac{1}{2}\left[E(\omega)e^{-i\omega t} + E^*(\omega)e^{i\omega t}\right] \tag{2.85}$$

For the third order nonlinear process it is the third power of the fundamental wave that determines the nonlinear polarisation.

$$\begin{aligned} E^3(\omega) &= \left[\frac{1}{2}E(\omega)e^{-i\omega t} + \frac{1}{2}E^*(\omega)e^{i\omega t}\right]^3 \\ &= \frac{1}{8}E^3(\omega)e^{-i3\omega t} + \frac{3}{8}E^2(\omega)E^*(\omega)e^{-i\omega t} + \frac{3}{8}E(\omega)E^{*2}(\omega)e^{i\omega t} + \frac{1}{8}E^{*3}(\omega)e^{i3\omega t} \end{aligned} \tag{2.86}$$

The resultant polarisation is

$$P(3\omega) = \frac{1}{2}\left[P^{(L)}(3\omega)e^{-i3\omega t} + cc\right] + \frac{1}{2}\left[P^{(NL)}(3\omega)e^{-i3\omega t} + cc\right] \tag{2.87}$$

The nonlinear susceptibility $\chi(-3\omega;\omega,\omega;\omega)$ is defined by the proportionality of the $P^{(NL)}$ term in equation 2.87 and the $E^3(\omega)$ term in equation 2.86 (terms with equal exponents) with $N\chi(-3\omega;\omega,\omega;\omega)$ as proportionality constant:

$$\begin{aligned} \frac{1}{2}P^{(NL)}(3\omega)e^{-i3\omega t} &= N\chi(-3\omega;\omega,\omega;\omega)\frac{1}{8}E^3(\omega)e^{-i3\omega t} \\ P^{(NL)}(3\omega) &= \frac{1}{4}N\chi(-3\omega;\omega,\omega;\omega)E^3(\omega). \end{aligned} \tag{2.88}$$

This yields the factor $\frac{1}{4}$ in expression 2.42.

The factor $\frac{n!}{2^{n-1}}$ in the definition 2.78 is valid in the general case where all the frequencies of the coupling waves are different and non-zero. Consider this definition for $n = 3$ describing the general process called four wave frequency mixing where three waves of frequencies ω_1, ω_2 and ω_3 are coupled to produce a wave at frequency ω_s that can be any linear combination of the two incident frequencies, for example sum-frequency generation with $\omega_3 = \omega_s = \omega_1 + \omega_2 + \omega_3$. (Third-harmonic generation is the degenerate case of this process.) In four wave frequency mixing the electric field, the third power of which generates the nonlinear polarisation, is the sum of three fields with frequencies ω_1, ω_2 and ω_3 respectively.

$$\begin{aligned} E^3 &= \left[\frac{1}{2}E(\omega_1)e^{-i\omega_1 t} + cc + \frac{1}{2}E(\omega_2)e^{i\omega_2 t} + cc + \frac{1}{2}E(\omega_3)e^{i\omega_3 t} + cc\right]^3 \\ &= \frac{6}{8}E(\omega_1)E(\omega_2)E(\omega_3)e^{-i(\omega_1+\omega_2+\omega_3)t} + \frac{1}{8}E^3(\omega_1)e^{-i3\omega_1 t} + \frac{1}{8}E^3(\omega_2)e^{-i3\omega_2 t} + \ldots \end{aligned} \tag{2.89}$$

The polarisation at the sum frequency is

$$P(\omega_s) = \frac{1}{2}\left[P^{(NL)}(\omega_s)e^{-i(\omega_1+\omega_2+\omega_3)t} + cc\right].$$

The nonlinear susceptibility $\chi(-\omega_s;\omega_1,\omega_2,\omega_3)$ is again defined as the proportionality constant between $\frac{1}{2}P^{(NL)}(\omega_s)e^{-i(\omega_1+\omega_2+\omega_3)t}$ and the $e^{-i(\omega_1+\omega_2+\omega_3)t}$ term in expression 2.89.

$$\begin{aligned} \frac{1}{2}P^{(NL)}(\omega_s)e^{-i(\omega_1+\omega_2+\omega_3)t} &= N\chi(-\omega_s;\omega_1,\omega_2,\omega_3)\frac{6}{8}E(\omega_1)E(\omega_2)E(\omega_3)e^{-i(\omega_1+\omega_2+\omega_3)t} \\ P^{(NL)}(\omega_s) &= \frac{3}{2}N\chi(-\omega_s;\omega_1,\omega_2,\omega_3)E(\omega_1)E(\omega_2) \end{aligned} \tag{2.90}$$

The numerical factor is $\frac{3}{2}$ as predicted by $\frac{n!}{2^{n-1}}$ in expression 2.78 with $n = 3$.

2.3.2.3 Quantum mechanical expressions for nonlinear susceptibilities

Quantum mechanical time dependent perturbation theory does not only give a complete definition of the nonlinear susceptibilities of any order, but also explicit expressions for the susceptibility tensors. These expressions are derived by means of density matrix theory and time-dependent perturbation theory where all the excited states of the atoms and their relative populations have to be taken into account [31], as first done by Armstrong et al [1].

The result of time-dependent perturbation theory is expressions for the susceptibilities in

terms of the expectation values of the transition electric dipole moments

$$\mu_{nm}^{\alpha} = \langle n| \mu_{\alpha}(\omega) |m\rangle \tag{2.91}$$

and the transition frequencies

$$\omega_{nm} = \Omega_{nm} - i\Gamma_{nm} \tag{2.92}$$

for a transition between states n and m of the atoms. In expression 2.91 $\langle n| \mu_{\alpha}(\omega) |m\rangle$ is the dipole matrix element of the α-th directional component of the dipole operator component $\mu(\omega)$ between states n and m where the vector $\mu(\omega)$ is parallel to the electrical field at ω [19]. (Therefore α is determined by the polarisation of the radiation causing the transition.) In expression 2.92 Ω_{nm} is the real transition frequency corresponding to the energy difference $E_n - E_m$ of the two states and Γ_{nm} is the damping constant (absorption linewidth) of the transition.

The complete theoretical expressions for the nonlinear susceptibilities are complicated expressions with several contributing terms (for example [7, equation 2.15] and [27, Equation 18.2.5]) corresponding to different possible ways in which the interaction can take place, and associated with distinguishable Feynman diagrams [7], but for general purposes only the most significant term (with the smallest denominator) is cited in literature (see [23], [19], [50, equation 13.38], [7, equation 2.14]). The purpose of this discussion is to understand the general structure of the expression for the nonlinear susceptibility in order to understand the way resonance enhancement and angular momentum selection rules govern its behaviour.

According to Hanna et al [16] and Vidal [50] the general expression[7] for the n-th order nonlinear susceptibility is given by

$$\chi^{(3)}_{\alpha_s\alpha_1\alpha_2\ldots\alpha_n}(-\omega_s;\omega_1\ldots\omega_n) = \tag{2.93}$$

$$\frac{S_T}{n!\hbar^n}\sum_{g,b_1\ldots b_n}\rho(g)\frac{\langle g| \mu_{\alpha_s}(\omega_s) |b_1\rangle \langle b_1| \mu_{\alpha_1}(\omega_1) |b_2\rangle \ldots \langle b_n| \mu_{\alpha_n}(\omega_n) |b_g\rangle}{(\omega_{b_1 g} - \omega_1 - \omega_2 \ldots - \omega_n)(\omega_{b_2 g} - \omega_2 \ldots - \omega_n)\ldots(\omega_{b_n g} - \omega_n)}$$

[7] Vidal (1998) uses only the real part of the transitional frequencies Ω_{nm} in the denominator which can be done far from resonance, but in general the complex transitional frequency ω_{nm} has to be used as done by Hodgson et al (1974) and Puel et al (1976) and discussed by Hanna et al (1979) in section 2.5.

The sum over all atomic (or molecular) states $b_1 ... b_n$ as well as over all the possible initial states g weighed by their unperturbed population densities $\rho(g)$ must be calculated. S_T is a permutation operator indicating that there must be summed over all permutations of the $n+1$ interacting waves, therefore all permutations of the parameter pairs $\alpha_s - \omega_s$, $\alpha_1\omega_1$, ..., $\alpha_n\omega_n$.

For the linear susceptibility $\chi^{(1)}$ defined by $P_{\alpha_\omega}{}^{(L)}(r,\omega) = \sum_{\alpha_\omega\alpha_\omega} N\chi^{(1)}_{\alpha_\omega\alpha_\omega} E_{\alpha_\omega}(r,\omega)$ time dependent perturbation theory provides the expression [46, Equation 5]

$$\chi^{(1)}_{\alpha_\omega\alpha_\omega}(-\omega;\omega) = \frac{1}{\hbar}\sum_g \rho(g) \sum_n \left[\frac{\mu^{\alpha_\omega}_{gn}\mu^{\alpha_\omega}_{ng}}{\omega_{ng}-\omega} + \frac{\mu^{\alpha_\omega}_{ng}\mu^{\alpha_\omega}_{gn}}{\omega_{ng}+\omega}\right]. \tag{2.94}$$

The summation over n is done to include the contributions of transitions to all excited states n accessible from the initial state g. It is obvious that the first of the two terms in the brackets will always have a larger contribution due to the smaller value of its denominator. For this reason the second term is often neglected in the expression of the linear susceptibility which is then given by

$$\chi^{(1)}_{\alpha_\omega\alpha_\omega}(-\omega;\omega) = \frac{1}{\hbar}\sum_g \rho(g) \sum_n \frac{\mu^{\alpha_\omega}_{gn}\mu^{\alpha_\omega}_{ng}}{\omega_{ng}-\omega}.$$

In the case of the cubic susceptibility responsible for third-harmonic generation the permutation operator S_T is responsible for four distinct terms ([16, equation 2.18], [7, equation 2.15])

$$\begin{aligned}\chi^{(3)}_{\alpha_{3\omega}\alpha_\omega\alpha_\omega\alpha_\omega}(-3\omega;\omega,\omega,\omega) = \frac{1}{\hbar^3}\sum_g \rho(g) \sum_{l,m,n} \Bigg(&\frac{\mu^{\alpha_{3\omega}}_{gl}\mu^{\alpha_\omega}_{lm}\mu^{\alpha_\omega}_{mn}\mu^{\alpha_\omega}_{ng}}{(\omega_{gl}-3\omega)(\omega_{mg}-2\omega)(\omega_{ng}-\omega)} \\ &+\frac{\mu^{\alpha_\omega}_{gl}\mu^{\alpha_{3\omega}}_{lm}\mu^{\alpha_\omega}_{mn}\mu^{\alpha_\omega}_{ng}}{(\omega_{gl}+\omega)(\omega_{mg}-2\omega)(\omega_{ng}-\omega)} \\ &+\frac{\mu^{\alpha_\omega}_{gl}\mu^{\alpha_\omega}_{lm}\mu^{\alpha_{3\omega}}_{mn}\mu^{\alpha_\omega}_{ng}}{(\omega_{gl}+\omega)(\omega_{mg}+2\omega)(\omega_{ng}-\omega)} \\ &+\frac{\mu^{\alpha_\omega}_{gl}\mu^{\alpha_\omega}_{lm}\mu^{\alpha_\omega}_{mn}\mu^{\alpha_{3\omega}}_{ng}}{(\omega_{gl}+\omega)(\omega_{mg}+2\omega)(\omega_{ng}+3\omega)}\Bigg)\end{aligned} \tag{2.95}$$

As in the case of the linear susceptibility the first term will generally contribute most to the susceptibility due to the difference factors in the denominator and the susceptibility for third-

harmonic generation is often given in terms of the first term only [47].

$$\chi^{(3)}_{\alpha_{3\omega}\alpha_\omega\alpha_\omega\alpha_\omega}(-3\omega;\omega,\omega,\omega) = \frac{1}{\hbar^3}\sum_g \rho(g)\sum_{l,m,n}\frac{\mu_{gl}^{\alpha_{3\omega}}\mu_{lm}^{\alpha_\omega}\mu_{mn}^{\alpha_\omega}\mu_{ng}^{\alpha_\omega}}{(\omega_{gl}-3\omega)(\omega_{mg}-2\omega)(\omega_{ng}-\omega)} \tag{2.96}$$

Note that in these expressions the summation over g is required to include the contributions of atoms in different unperturbed initial states. Every term in this summation is weighed by the population density $\rho(g)$ of the unperturbed initial state. In atomic media however the contribution of the atoms in the atomic ground state is dominant and those of the excited states can be neglected. In this case $\rho = 1$ for the atomic ground state and $\rho \approx 0$ for all states with higher energy and the sum over g reduces to one term.

2.3.2.4 Selection rules and the conservation of angular momentum

Every nonlinear susceptibility of order n contains $n+1$ factors of the form $\langle a|\,\mu_{\alpha_i}(\omega_i)\,|b\rangle$ where $\langle a|\,\mu_{\alpha_i}(\omega_i)\,|b\rangle$ is the dipole matrix element of the α_i-th component of $\mu(\omega_i)$ between the atomic eigenstates a and b where $\mu(\omega_i)$ is the dipole operator component which is parallel to the electrical field at ω_i. The dipole operator $\mu_{\alpha_i}(\omega_i)$ transforms as a tensor of rank 1 (or a vector operator) and its orientation is given by α_i that is also the orientation of the electric field at frequency ω_i. When the matrix elements of such a tensor operator is evaluated with respect to angular momentum eigenstates, which atomic eigenstates are, the conservation of angular momentum is responsible for selection rules that have important implications for the dependence of the nonlinear process on the polarisation of the incident electric fields. Let the atomic eigenstate be expressed by $|b\rangle \equiv |\gamma_b J_b m_b\rangle$ where J_b is the angular momentum quantum number, m_b the magnetic quantum number and γ_b represents all other quantum numbers needed to describe state b.

The Wigner-Eckart theorem states that the matrix element of a spherical tensor $T_q^{(k)}$ of rank k with magnetic quantum number q between angular momentum eigenstates $|a\rangle$ and $|b\rangle$

$$\langle a|\,T_q^{(k)}\,|b\rangle = \langle \gamma_a J_a m_a|\,T_q^{(k)}\,|\gamma_b J_b m_b\rangle$$

can be factorised into a Clebsch-Gordan coefficient factor, that immediately gives the selection rules in terms of the selection rules for angular momentum, and a second factor - the reduced

Polarisation $\boldsymbol{\alpha_i}$	Magnetic quantum number $\triangle \mathbf{m}_i$
plane polarised, x direction	$+1$ or -1 with equal probability
plane polarised, y direction	$+1$ or -1 with equal probability
right circularly polarised	$+1$
left circularly polarised	-1

Table 2.1: The angular momentum of photons with different polarisations.

matrix element - that is independent of m_a, m_b and q but dependent on the nature of the tensor.

The dipole moment operator $\mu_{\alpha_i}(\omega_i) \equiv \mu^{(1)}_{\alpha_i}$ is a spherical tensor. Its rank is $k = 1$ and depending on its orientation (or polarisation) given by α_i it has a magnetic quantum number, that I will call $\triangle m_i$, its dependence on the polarisation given in table 2.1 (z is the propagation direction).

The Wigner-Eckart theorem ([35, equation 3.10.31], [9, equation 5.4.1]) applied to the dipole operator has the form

$$\begin{aligned}
\langle \gamma_a J_a m_a | \, \mu^{(1)}_{\alpha_i} \, | \gamma_b J_b m_b \rangle &= (-1)^{J_b - m_b} \frac{\langle (k=1) \triangle m_i J_b m_b | \, (k=1) J_b J_a m_a \rangle}{(2J_a+1)^{1/2}} \langle \gamma_a J_a | \left| \mu^{(1)} \right| | \gamma_b J_b \rangle \\
&= (-1)^{J_a - m_a} \begin{pmatrix} J_a & (k=1) & J_b \\ -m_a & \triangle m_i & m_b \end{pmatrix} \langle \gamma_a J_a | \left| \mu^{(1)} \right| | \gamma_b J_b \rangle
\end{aligned}$$

where $\langle \gamma_a J_a | \left| \mu^{(1)} \right| | \gamma_b J_b \rangle$ is the reduced matrix element giving the transition moment between the m-degenerate states $|\gamma_a J_a\rangle$ and $|\gamma_b J_b\rangle$. It is independent of the magnetic quantum numbers m_a, m_b and $\triangle m_i$. The middle factor in each line contains a Clebsch-Gordan coefficient for adding J_b and k to get J_a. It depends only on the geometry and orientation of the system to the z-axis and not on the nature of $\mu^{(1)}_{\alpha_i}$. This factor is governed by the selection rules for the addition of angular momentum.

The first selection rule is the triangular rule: for the matrix element to be non-zero the vectors $\overrightarrow{J}_a$, $\overrightarrow{J}_b$ and $\overrightarrow{k} = \overrightarrow{1}$ must form a closed triangle. The second m-selection rule requires that $-m_a + \triangle m_i + m_b = 0$. This selection rule can be applied to the susceptibility of a general four-wave mixing process by considering the general expression 2.93 with $n = 3$. It yields the

following conditions for the susceptibility to be non-zero:

$$\begin{aligned} -m_g + \triangle m_s + m_{b_1} &= 0 \\ -m_{b_1} + \triangle m_1 + m_{b_2} &= 0 \\ -m_{b_2} + \triangle m_2 + m_{b_3} &= 0 \\ -m_{b_3} + \triangle m_3 + m_g &= 0 \end{aligned}$$

When these equations are summed they yield the important result

$$\triangle m_s + \triangle m_1 + \triangle m_2 + \triangle m_3 = 0. \tag{2.97}$$

It has the implication that when circularly polarised incident waves are used and two of the three incident waves are circularly polarised in the same direction, say right-hand circularly polarised with $\triangle m_1 = \triangle m_2 = +1$, then the third incident wave must be left-hand circularly polarised with $\triangle m_3 = -1$ in order to satisfy the selection rule given by equation 2.97 and a left-hand circularly polarised sum-frequency with $\triangle m_s = -1$ will be generated. When all three incident waves have the same circular polarisation the selection rule cannot be satisfied and sum frequency generation (or third-harmonic generation) is suppressed. Sum-frequency generation of three incident waves that are linearly polarised in the same direction is allowed, because a linearly polarised photon carries angular momentum of $+1$ or -1 with equal probability.

The generation of the third harmonic of a single plane polarised incident beam is therefore allowed, but the generation of the third harmonic is suppressed when the incident laser beam is completely circularly polarised.

The second result of the selection rules is that the states $|g\rangle$ and $|b_2\rangle$ have the same parity which is opposite to that of $|b_1\rangle$ and $|b_3\rangle$. This has implications for the choice of the resonance employed to enhance the nonlinear susceptibility as will be discussed in detail in section 3.1.

2.3.3 Quantum mechanical approach to third-harmonic generation

In a homogenous isotropic medium the coefficients of the even powers of E vanish due to symmetry. The fourth rank tensors $\chi^{(3)}$ describing four-wave frequency mixing processes, with

third-harmonic generation as the degenerate case, are then the lowest order nonlinear susceptibilities.

Consider a linearly polarised plane wave of fundamental frequency ω propagating through such a nonlinear medium. Working in an intensity range where the susceptibilities of orders higher than third order can be neglected the observable nonlinear process that takes place will be third-harmonic generation and the medium will as result be subjected to the propagation of two waves: the wave at the fundamental frequency ω and the wave at the third-harmonic frequency 3ω; with the amplitude of the third-harmonic wave much smaller than the amplitude of the fundamental wave - $E_3 \ll E_1$. In the total nonlinear polarisation the terms P_1^{NL} and P_3^{NL} (nonlinear polarisations at frequencies ω and 3ω respectively) both dependent on the electrical fields[8] E_1 and E_3 can be distinguished.

Applying all the results of the discussion in sections 2.3.2.1, 2.3.2.2 and 2.3.2.3 the expressions for the total nonlinear polarisation at frequencies ω and 3ω are [31, Equation 4]

$$\begin{aligned} P_1^{NL} &= \sum_i \{ \frac{N_i}{4} \left[3\chi_{iT}^{(3)}(\omega) E_3 E_1^* E_1^* + \chi_{iS}^{(3)}(\omega) E_1 |E_1|^2 + \chi_{iS}^{(3)}(\omega, 3\omega) E_1 |E_3|^2 \right] \\ &\quad - (N_{0i} - N_i) \chi_i^{(1)}(\omega) E_1 \} \end{aligned} \tag{2.98}$$

$$\begin{aligned} P_3^{NL} &= \sum_i \{ \frac{N_i}{4} \left[\chi_{iT}^{(3)}(3\omega) E_1 E_1 E_1 + \chi_{iS}^{(3)}(3\omega) E_3 |E_3|^2 + \chi_{iS}^{(3)}(3\omega, \omega) E_3 |E_1|^2 \right] \\ &\quad - (N_{0i} - N_i) \chi_i^{(1)}(3\omega) E_3 \} \end{aligned} \tag{2.99}$$

where the sum over index i is a sum over the different energy levels that were initially populated and have to be taken into account separately according to the assumption that the atoms initially in different energy levels can be treated as separate species and their contributions summed (see discussion at the beginning of section 2.3.2 and the end of section 2.3.2.3).

Alternative shorter labels for the susceptibilities [47] have been used above:

$$\chi_i^{(1)}(\omega) \equiv \chi_i^{(1)}(-\omega;\omega) \qquad \chi_i^{(1)}(3\omega) \equiv \chi_i^{(1)}(-3\omega;3\omega)$$
$$\chi_{iT}^{(3)}(3\omega) \equiv \chi_i^{(3)}(-3\omega;\omega,\omega,\omega) \qquad \chi_{iT}^{(3)}(\omega) \equiv \chi_i^{(3)}(-\omega;-\omega,-\omega,3\omega)$$

[8] E_q and P_q represents the electrical field and polarisation density at the frequency $q\omega$

$$\begin{aligned} \chi^{(3)}_{iSA}(\omega) &\equiv \chi^{(3)}_i(-\omega;-\omega,\omega,\omega) \quad \chi^{(3)}_{iSA}(3\omega) \equiv \chi^{(3)}_i(-3\omega;-3\omega,3\omega,3\omega) \\ \chi^{(3)}_{iSB}(\omega,3\omega) &\equiv \chi^{(3)}_i(-\omega;\omega,-3\omega,3\omega) \quad \chi^{(3)}_{iSB}(3\omega,\omega) \equiv \chi^{(3)}_i(-3\omega;\omega,-\omega,3\omega) \end{aligned} \quad (2.100)$$

It can be verified by inspection that these listed susceptibilities include all possible four-wave mixing processes that can take place in the case of a single incident beam, generating radiation fields at frequencies ω and 3ω.

The physical interpretation of the different terms in equations 2.98 and 2.99 according to the literature ([31] and [46]) is:

- The last (linear) term in each equation describes the changes in index of refraction due to population changes caused by absorption. $\chi^{(1)}_i(q\omega) \equiv \chi^{(1)}_i(-q\omega;q\omega)$ is the linear susceptibility of excited state i that has initial number density N_{0i} and final number density N_i due to absorption. (Usually most of the atoms are in their electronic ground state so that the initial number density of the ground state $N_{0i=1} = N =$ *the total number density of the system* and the initial number densities of the excited states $N_{0i} = 0$ for $i > 1$.) The real and imaginary parts of $\chi^{(1)}_i$ gives the index of refraction and the one photon absorption coefficient respectively as in equations 2.66 and 2.67.

- The first term in each equation: $\chi^{(3)}_{iT}(3\omega) \equiv \chi^{(3)}_i(-3\omega;\omega,\omega,\omega)$ is responsible for the third-harmonic generation process and $\chi^{(3)}_{iT}(\omega) \equiv \chi^{(3)}_i(-\omega;-\omega,-\omega,3\omega)$ for the inverse process that regenerates the fundamental frequency from the third harmonic.

- The second and third terms: The real parts of $\chi^{(3)}_{iSA}(\omega) \equiv \chi^{(3)}_i(-\omega;-\omega,\omega,\omega)$, $\chi^{(3)}_{iSA}(3\omega) \equiv \chi^{(3)}_i(-3\omega;-3\omega,3\omega,3\omega)$, $\chi^{(3)}_{iSB}(\omega,3\omega) \equiv \chi^{(3)}_i(-\omega;\omega,-3\omega,3\omega)$ and $\chi^{(3)}_{iSB}(3\omega,\omega) \equiv \chi^{(3)}_i(-3\omega;\omega,-\omega,3\omega)$ are responsible for the intensity dependent changes of the refractive index (second order Kerr effect [32]). The imaginary parts of $\chi^{(3)}_{iSA}(\omega)$ and $\chi^{(3)}_{iSA}(3\omega)$ describe two-photon absorption of the frequencies ω and 3ω respectively. The imaginary parts of $\chi^{(3)}_{iSB}(\omega,3\omega)$ and $\chi^{(3)}_{iSB}(3\omega,\omega)$ are responsible for Raman-scattering type losses.

The semi-classical model of third-harmonic generation in a nonlinear gaseous medium according to the quantum mechanical approach is obtained by combining the following results:

- The fundamental equation of nonlinear optics (equation 2.49) describing the behaviour of the electromagnetic field in the medium where a polarisation exists.

- Knowledge of the different nonlinear polarisations that contribute (as given by equations 2.98 and 2.99) and the structure of these polarisation densities in terms of nonlinear susceptibilities and electric fields.

- The explicit quantum mechanical expressions (such as 2.95 and other derived from expression 2.93) for the nonlinear susceptibilities.

In combining these results and constructing the model, the assumptions made and limitations set in the derivation of each of the results that are used must be taken into account. A complete discussion of this semi-classical model is found in Puell et al [31]. Puell et al discusses the expressions for the nonlinear susceptibilities in the case of two-photon resonant third-harmonic generation, considers the steady state populations in an atomic medium and arrives at analytical and numerical solutions for the problem of describing third-harmonic generation in general.

The aim of this discussion is not to find detailed or general mathematical solutions, but to study the implications of the theory for a specific experimental setup: third-harmonic generation in a two-component metal vapour noble gas medium prepared inside a crossed concentric heat pipe oven. The question that is addressed is a practical one: What must the conditions in the nonlinear medium be for efficient third-harmonic generation in such an experimental setup? Therefore the discussion in the chapter that follows will concentrate on the limited conclusions based on approximations relevant to this experimental setup, while making use of results of the mathematical framework outlined in previous sections.

Chapter 3

Efficient third-harmonic generation in a gaseous medium

The theory described in the previous chapter is applied in this chapter to a specific experimental setup: the generation of tunable coherent vacuum ultraviolet radiation by four-wave frequency mixing in a magnesium vapour krypton gas medium that is prepared inside a crossed concentric heat pipe. The aim of the discussion in this chapter is to determine the parameters that influence the conversion efficiency most in order to answer the following questions: What are the medium requirements for efficient (optimal) four-wave frequency mixing in a gaseous nonlinear medium, and following from these results, what are the reasons for choosing magnesium vapour and krypton gas as the two components of the nonlinear medium? The application of the theory to third-harmonic generation, as the most simple degenerate case of four-wave frequency mixing, is discussed in detail in sections 3.1 to 3.6. Third-harmonic generation instead of general four-wave frequency mixing is discussed in such detail since the description of third-harmonic generation is mathematically simple and it illustrates all the physical principles involved in four-wave mixing. In the second place third-harmonic generation is important in the study of nonlinear media because it is generally used as a test case to characterise the nonlinear medium, because the experimental setup for third-harmonic generation is simple and easily reproducable and the theory is well studied (see references such as [21], [31], [37], [38].) By comparing the theoretical and experimental results, optical characteristics of the medium such as optical depth, density

profile, and the values of the susceptibilities can be obtained.

To achieve efficient third-harmonic generation in a nonlinear medium, the following three properties are required of the medium

- The microscopic requirement: Every volume element of the medium exposed to the fundamental frequency must have a sufficiently large nonlinear susceptibility for third-harmonic generation. In the first place this implies that the nonlinear medium has to be chosen to provide a large nonlinear susceptibility. The quantum mechanical expressions for the nonlinear susceptibilities show that the nonlinear susceptibility in the chosen medium must, secondly, adhere to the selection rules of angular momentum and can, thirdly, be enhanced by a suitable resonance. The selection rules were discussed in section 2.3.2 and the conclusion was drawn that third-harmonic generation is allowed for a linearly polarised incident beam but suppressed if the incident beam is circularly polarised. Resonant enhancement of the nonlinear susceptibilities is discussed in section 3.1.

- The macroscopic requirement: The third-harmonic contributions generated in different volume elements of the active medium must interfere constructively. This is called the phase matching condition. Phase matching was introduced at the end of section 2.2.2 and is discussed in more detail in this chapter. In sections 3.2 and 3.3 the effect of different experimental variables such as optical depth of the medium and focusing of the incident beam on phase matching is discussed theoretically. In section 3.5 techniques to satisfy the phase matching condition for third-harmonic generation in a mixture of two gases are discussed.

- Competing processes: The conditions in the experimental setup must be chosen so that the influence of the linear and other nonlinear processes competing with third-harmonic generation is minimised. The optimization of the susceptibility for third-harmonic generation with respect to competing processes involves careful consideration of several factors. The medium and resonances used should be well chosen to give enhancement of the susceptibility without destroying the small optical depth of the medium for either the fundamental and third-harmonic waves. These factors are discussed in sections 3.1 and 3.2. In raising the fundamental beam intensity it must be taken into account that at

very high intensities other competing higher order processes are becoming significant (see sections 3.3 and 3.4 on saturation effects.)

In section 3.6 the theoretical results are applied to the specific case of third-harmonic generation in a magnesium vapour krypton gas medium.

In section 3.7 the theoretical results on third-harmonic generation in a magnesium vapour krypton gas medium are extrapolated to the generation of tunable coherent vacuum-ultraviolet radiation by non-degenerate sum-frequency generation in the same medium.

3.1 Resonant enhancement of the nonlinear susceptibilities

In studying the optimal medium conditions for third-harmonic generation it is important to maximise the value of the susceptibility $\chi_T^{(3)}$ responsible for third-harmonic generation and also to optimise $\chi_T^{(3)}$ relative to the $\chi_S^{(3)}$ susceptibilities in the expressions for the nonlinear polarisation density given by equations 2.98 and 2.99. The $\chi_S^{(3)}$ susceptibilities are responsible for intensity dependent changes of the refractive indices that destroy the phase matching in the medium. Theoretical expressions for the different susceptibilities give insight in their behaviour. The dominant contributions in the case of third-harmonic generation [46, equations 14 to 16] are given by

$$\chi_T^{(3)}(3\omega) \equiv \chi_i^{(3)}(-3\omega;\omega,\omega,\omega) = \frac{1}{\hbar^3}\sum_{l,m,n}\frac{\mu_{gl}\mu_{lm}\mu_{mn}\mu_{ng}}{(\omega_{gl}-\omega)(\omega_{gm}-2\omega)(\omega_{gn}-3\omega)} \tag{3.1}$$

$$\chi_{SA}^{(3)}(\omega) \equiv \chi_i^{(3)}(-\omega;-\omega,\omega,\omega) = \frac{1}{\hbar^3}\sum_{l,m,n}\frac{\mu_{gl}\mu_{lm}\mu_{mn}\mu_{ng}}{(\omega_{gl}-\omega)(\omega_{gm}-2\omega)(\omega_{gn}-\omega)} \tag{3.2}$$

$$\chi_{SB}^{(3)}(3\omega,\omega) \equiv \chi_i^{(3)}(-3\omega;\omega,-\omega,3\omega) = \frac{1}{\hbar^3}\sum_{l,m,n}\frac{\mu_{gl}\mu_{lm}\mu_{mn}\mu_{ng}}{(\omega_{gl}-3\omega)(\omega_{gm}-2\omega)(\omega_{gn}-3\omega)} \tag{3.3}$$

and illustrated diagrammatically (for the two-photon resonant case) in figure 3-1. For these expressions to hold near resonance, ω_{ab} must be the complex transition frequency of the transition $|a\rangle \rightarrow |b\rangle$. When the Stark effect on the energy levels is neglected, then $\omega_{ab} = \Omega_{ab} - i\Gamma_{ab}$ with

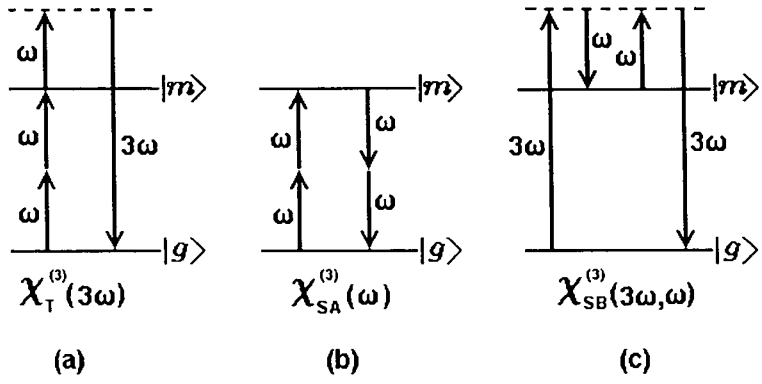

Figure 3-1: Diagrammatic representation of the three dominant nonlinear susceptibilities associated with third harmonic generation, illustrated for the two-photon resonant case: (a) the susceptibility responsible for third harmonic generation, (b) the susceptibility responsible for two-photon absorption and contributing significantly to intensity dependent changes of the index of refraction and (c) the susceptibility responsible for Raman-type losses.

Ω_{ab} giving the energy separation between the unperturbed energy levels and Γ_{ab} the linewidth of the transition. The sum in each expression is a sum over all possible intermediate energy states l, m and n. In these equations the sum over the ground state g as well as the explicit tensor nature of the susceptibility is neglected. The sum over g can be neglected in an atomic gas medium because in the unperturbed state the population densities and therefore contributions of excited atomic states are very small. The tensor notation can be neglected because in the experimental setup the incident beam, coming from a Lambda Physik dye laser, is highly polarised in the vertical direction and only one of the tensor components, $\chi_{yyyy}^{(3)}$, is contributing significantly.

$\chi_T^{(3)}(3\omega)$ can clearly be optimised by choosing an appropriate fundamental frequency that minimises one of the difference factors in the denominator of expression 3.1. The three possibilities for resonance are illustrated in figure 3-2. According to the dipole transition selection rule g and m must have the same parity and l and n must have the opposite parity for $\chi_T^{(3)}(3\omega)$ to be non-zero as discussed in section 2.3.2. This means that $|g\rangle \rightarrow |l\rangle$ and $|g\rangle \rightarrow |n\rangle$ are dipole

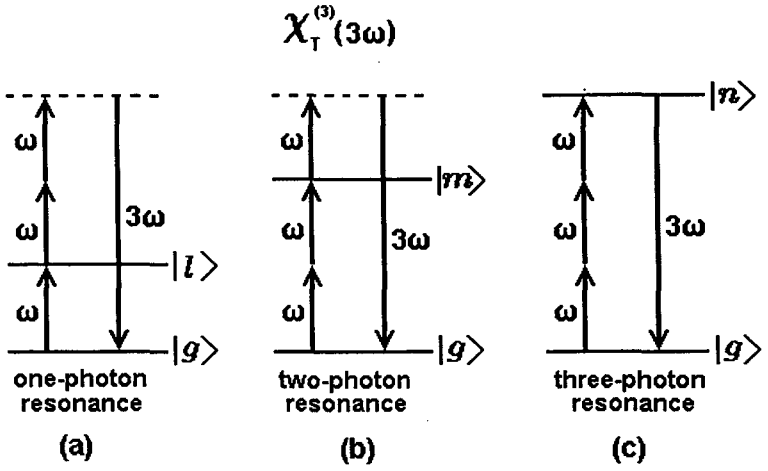

Figure 3-2: Diagrammatic representation of the three possibilities for resonant enhancement of the third order susceptibility responsible for third harmonic generation: (a) one-photon resonance - associated with one-photon absorption of the fundamental wave by the allowed dipole transition from the ground state to state l, (b) two-photon resonance and (c) three-photon resonance - associated with three-photon absorption of the third harmonic wave by the allowed dipole transition from the ground state to state n.

allowed transitions but the transition $|g\rangle \rightarrow |m\rangle$ is forbidden. An attempt to use one-photon ($\omega = \omega_{gl}$) or three-photon resonance ($3\omega = \omega_{gn}$) in order to minimise the denominator would therefore give rise to strong one-photon absorption of the fundamental or the third-harmonic wave by the dipole allowed transitions $|g\rangle \rightarrow |l\rangle$ or $|g\rangle \rightarrow |n\rangle$. Two-photon resonance however, with $2\omega = \omega_{gm}$ does not open up the possibility for one-photon absorption by an allowed transition and can be used to enhance the susceptibility for third-harmonic generation if the two-photon absorption due to $\widetilde{\chi}_{SA}^{(3)}(\omega)$ is sufficiently small. The susceptibility for two-photon absorption - being a third order nonlinear process - is usually much smaller than that for one-photon absorption by an allowed transition. The value of the two-photon absorption cross-section of a medium depends on the position of the intermediate energy levels. For example: The two-photon absorption cross-section in strontium vapour is much larger than in magnesium vapour due to intermediate energy levels that are nearly one-photon resonant with the two-photon resonant frequency - illustrated by adding the energy state $|l\rangle$ of figure 3-2 (a) to the two-photon case of 3-2 (b) - enhancing of the two-photon absorption cross-section.

The energy of the suitable atomic energy states that can be used for two-photon resonance is the determining factor in the choice of nonlinear medium for resonant sum-frequency generation in a certain spectral region. Atomic strontium has a two-photon resonance at 575.9 nm and is therefore a suitable medium for the generation of sum-frequencies around 190 nm [37]. A magnesium vapour medium can be used to generate shorter wavelengths (137 - 160 nm) due to its two-photon resonance at 431 nm [21].

Under the condition of two photon resonance $2\omega = \omega_{gm}$ the sum over m is eliminated in expressions 3.1, 3.2 and 3.3 yielding

$$\chi^{(3)}_{TR}(3\omega) \equiv \chi^{(3)}_{iR}(-3\omega;\omega,\omega,\omega) = \frac{1}{\hbar^3}\frac{1}{(\omega_{gm}-2\omega)}\left[\sum_l \frac{\mu_{gl}\mu_{lm}}{(\omega_{gl}-\omega)}\right]\left[\sum_n \frac{\mu_{mn}\mu_{ng}}{(\omega_{gn}-3\omega)}\right] \tag{3.4}$$

$$\chi^{(3)}_{SR}(\omega) \equiv \chi^{(3)}_{iR}(-\omega;-\omega,\omega,\omega) = \frac{1}{\hbar^3}\frac{1}{(\omega_{gm}-2\omega)}\left[\sum_l \frac{\mu_{gl}\mu_{lm}}{(\omega_{gl}-\omega)}\right]^2 \tag{3.5}$$

$$\chi^{(3)}_{SR}(3\omega,\omega) \equiv \chi^{(3)}_{iR}(-3\omega;\omega,-\omega,3\omega) = \frac{1}{\hbar^3}\frac{1}{(\omega_{gm}-2\omega)}\left[\sum_l \frac{\mu_{gl}\mu_{lm}}{(\omega_{gl}-3\omega)}\right]^2 \tag{3.6}$$

These expressions for the resonant susceptibilities ([46] and [16, equation 2.20]), as illustrated diagrammatically in figure 3-1, show that two-photon resonant conditions enhance both $\chi^{(3)}_T$ responsible for third-harmonic generation and $\chi^{(3)}_S$ responsible for the destruction of phase matching in the same way, making two-photon resonance not an unconditional way of increasing the third-harmonic generation efficiency. The two-photon resonant factor in the preceding expressions determines the real and imaginary part of each susceptibility [46] according to

$$\frac{1}{(\omega_{gm}-2\omega)} = \frac{(\Omega_{gm}-2\omega)+i\Gamma_{gm}}{(\Omega_{gm}-2\omega)^2+\Gamma^2_{gm}}$$

From this expression it is clear that in two-photon resonant conditions when $(\omega_{gm}-2\omega)\rightarrow 0$ the susceptibilities are dominated by the imaginary parts of expressions 3.4, 3.5 and 3.6 and in off-resonant conditions by the real parts. The consequence can be shown to be that different processes are responsible for saturation in two-photon resonant and nonresonant third-harmonic

generation. All saturation processes involve the field dependent destruction of phase matching by one or another competing process. Section 3.4 discusses the implications of saturation in practice.

3.2 The small signal limit and the effect of optical depths

As the electric field amplitudes grow, the number of different competing processes that significantly contribute to the nonlinear polarisation and therefore have to be included in the description of the nonlinear system, increases. It is therefore informative to discuss the two opposite cases:

- the small signal limit and
- the high intensity regime where the onset of saturation occurs.

Theoretically the intensity of the generated third-harmonic field is proportional to the third power of the intensity of the incident beam at the fundamental frequency, as seen in equation 2.47. The small signal limit is the regime where a low intensity of the incident beam has the result that the conversion efficiency is very small, and therefore $|\mathbf{E}_3| \ll |\mathbf{E}_1|$. The onset of saturation at high incident intensity is characterised thereby that the proportionality between the third-harmonic intensity and the third power of the incident intensity breaks down. This indicates that the conversion efficiency is becoming increasingly limited by competing processes. In this section the small signal limit is discussed and in section 3.4 the conditions for onset of saturation and the processes responsible for it.

In the small signal limit the electric field amplitude of the third-harmonic wave is much smaller than the electric field amplitude of the fundamental wave, $|\mathbf{E}_3| \ll |\mathbf{E}_1|$. For an atomic medium it can also be assumed all atoms are and remain in the ground state and that the contributions of atoms in excited states are neglegible. With these assumptions the experssion for the nonlinear polarisation density at the third-harmonic frequency, equation 2.99, reduces to only one term:

$$P_3^{NL} = \frac{N}{4}\chi_T^{(3)}\left(-3\omega;\omega,\omega,\omega\right)E_1E_1E_1$$

Substituting this result into the fundamental equation of nonlinear optics, equation 2.49, yields a differential equation[1] describing the growth of the electric field $\widehat{E_3}(z)$ at frequency 3ω in terms of $\widehat{E_1}(z)$.

$$\frac{d\widehat{E_3}}{dz} = i\frac{2\pi 3\omega}{cn_3}\frac{N}{4}\chi_T^{(3)}(-3\omega;\omega,\omega,\omega)\left(\widehat{E_1}\right)^3\exp(-i\triangle kz) - \frac{\sigma^{(1)}(3\omega)}{2}N\widehat{E_3} \tag{3.7}$$

with

$$\triangle k = k_{3\omega} - 3k_\omega$$

The differential equation for the change of $E_1(\omega)$ with z is simplified by assuming that the fundamental pump wave intensity is not reduced significantly by the third-harmonic generation or by two-photon absorption. This assumption reduces equation 2.98 to $P_1^{NL} = 0$. Substituting this result into the fundamental equation of nonlinear optics, equation 2.49, gives a differential equation for $\widehat{E_1}(z)$ that takes only one-photon absorption of the fundamental wave into account:

$$\frac{d\widehat{E_1}}{dz} = -\frac{N\sigma^{(1)}(\omega)}{2}\widehat{E_1}. \tag{3.8}$$

Equation 3.8 has the well known solution

$$\widehat{E_1}(z) = \widehat{E_1}(0)\exp\left(-\frac{N\sigma^{(1)}(\omega)z}{2}\right). \tag{3.9}$$

With these simplifications, that can be made in the small signal limit, the set of coupled differential equations describing the propagation of the electromagnetic field in the nonlinear medium mathematically, is reduced to two equations, 3.7 and 3.8, that can be solved simultaneously. Substituting expression 3.9 into equation 3.7 gives an uncoupled differential equation for the third-harmonic wave, namely

$$\begin{aligned}\frac{d\widehat{E_3}(z)}{dz} &= i\frac{\pi 3\omega}{cn_3}\frac{N}{2}\chi_T^{(3)}(-3\omega;\omega,\omega,\omega)\left(\widehat{E_1}(0)\right)^3\exp\left(-\left(\frac{3N\sigma^{(1)}(\omega)}{2}+i\triangle k\right)z\right)\\ &\quad -\frac{N\sigma^{(1)}(3\omega)}{2}\widehat{E_3}(z)\end{aligned}$$

[1] In the constant term $1/k_{3\omega}$ has been replaced by $c/3\omega n_3$ where $n_3 \equiv n(3\omega)$.

This equation can be integrated over the length of the medium to give an expression for $\widehat{E_3}(L)$.

$$\widehat{E_3}(L) = i\frac{\pi 3\omega}{2cn_3} NL\chi_T^{(3)}\left(-3\omega;\omega,\omega,\omega\right)\left(\widehat{E_1}(0)\right)^3 \frac{\exp(-\Gamma_s/2)}{\frac{\Gamma_s-\Gamma_i}{2} - i\triangle kL}\left(\exp\left(\frac{\Gamma_s-\Gamma_i}{2} - i\triangle kL\right) - 1\right)$$

In the integration it is assumed that the medium has a rectangular density profile as illustrated before in figure 2-5, page 27

$$\begin{aligned} N(z) &= N \quad \text{for } 0 < z < L \\ &= 0 \quad \text{for } z < 0,\ z > L \end{aligned}$$

The absorption cross sections are rewritten as optical depths: $\Gamma_s = \Gamma_3 = \kappa_3 L = \sigma^{(1)}(3\omega)NL$ is the optical depth of the medium for the third-harmonic wave, and $\Gamma_i = 3\Gamma_1 = 3\kappa_1 L = 3\sigma^{(1)}(\omega)NL$ is the total optical depth for the fundamental wave.[2]

Taking the modulus squared of the equation to rewrite it for intensities according to

$$I_q(z) = \frac{n_q c}{8\pi}\left|\widehat{E_q}(z)\right|^2$$

gives an expression for the intensity conversion efficiency (equivalent to the result of Vidal [50, Equation 13.65])

$$\frac{I_3(L)}{I_1(0)} = \frac{16\pi^4\left(3\omega\right)^2}{c^4 n_3\left(n_1\right)^3}\left[NL\left|\chi_T^{(3)}\left(-3\omega;\omega,\omega,\omega\right)\right|\right]^2\left[I_1(0)\right]^2 F(\triangle kL,\Gamma_i,\Gamma_s) \tag{3.10}$$

Here $F(\triangle kL,\Gamma_i,\Gamma_s)$ is the phase matching factor. In the general case taking the optical depths into account, the phase matching factor [48, Equation 11.66] is given by

$$F(\triangle kL,\Gamma_i,\Gamma_s) = \frac{\exp(-\Gamma_i) + \exp(-\Gamma_s) - 2\exp(-\frac{\Gamma_s-\Gamma_i}{2})\cos(\triangle kL)}{\left(\frac{\Gamma_s-\Gamma_i}{2}\right)^2 + (\triangle kL)^2} \tag{3.11}$$

It is instructive to look at the form of the phase matching factor as a function of the phase mismatch, $\triangle kL$, and the optical depths, Γ_s and Γ_i, for some special cases as observed

[2] The optical depth $\Gamma = \sigma^{(1)}(\omega)NL$ quantifies the total one-photon absorption by a medium with a number density N and length L. It can be expressed mathematically: $I(L) = I(0)e^{-\Gamma}$ where $I(0)$ is the incident intensity and $I(L)$ the intensity leaving the medium.

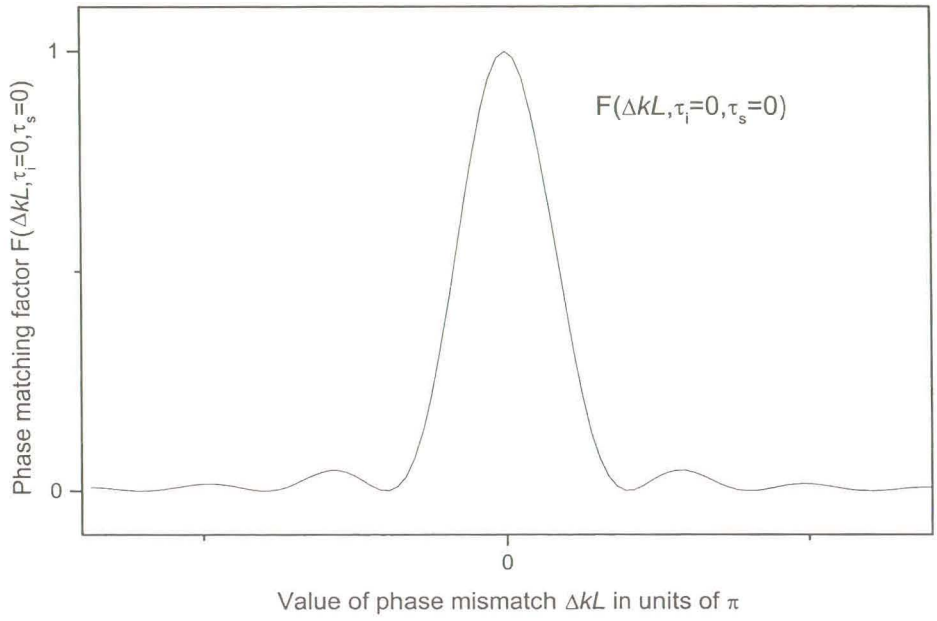

Figure 3-3: Theoretical phase matching curve for an optically thin medium (linear scale on both axes.)

experimentally.

For an optically thin medium where Γ_s and Γ_i go to zero, the phase matching factor has the form

$$F(\triangle kL, \Gamma_i \to 0, \Gamma_s \to 0) \approx \left(\frac{\sin(\triangle kL/2)}{\triangle kL/2} \right)^2 \tag{3.12}$$

as illustrated in figure 3-3. The same expression was derived previously (see equation 2.47) using classical theory.

In practice it is relatively easy to choose the medium and incident (fundamental) frequency so that the fundamental frequency does not correspond with a electric dipole allowed transition and thus minimise Γ_i. The absorption of the third-harmonic wave, however, is often associated with auto-ionisation or photo-ionisation of the medium that cannot be minimised and has to

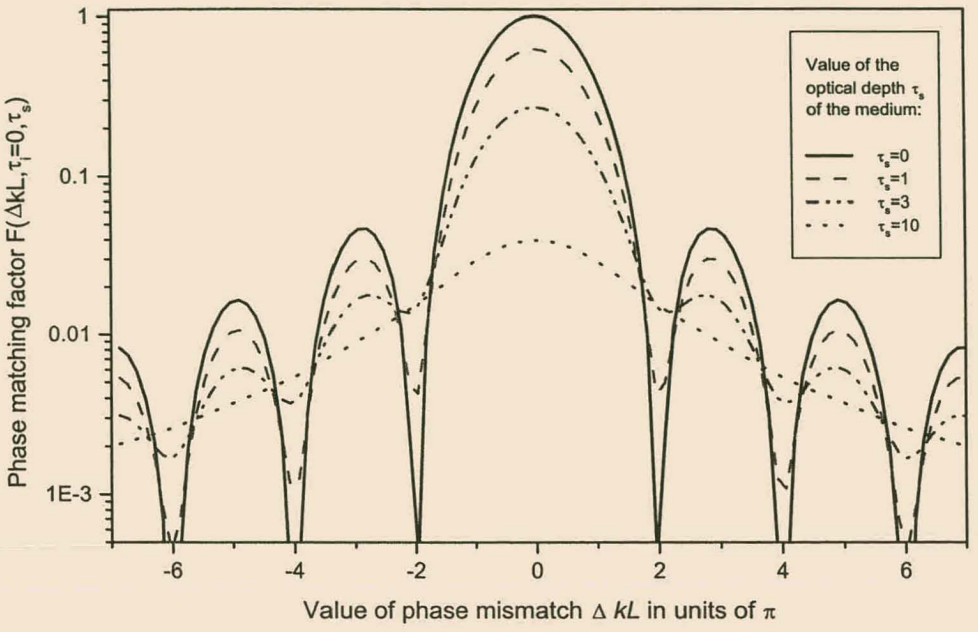

Figure 3-4: Theoretical phase matching curves for different values of the optical depth. (Logarithmic scale is used to make the oscillatory structure clearly observable.)

be taken into account. In this case, when $\Gamma_i \ll 1$, the phase matching factor is given by

$$F(\triangle kL, \Gamma_i \ll 1, \Gamma_s) \approx F(\triangle kL, \Gamma_s) = \frac{1 + \exp(-\Gamma_s) - 2\exp(-\frac{\Gamma_s}{2})\cos(\triangle kL)}{\left(\frac{\Gamma_s}{2}\right)^2 + (\triangle kL)^2} \tag{3.13}$$

The effect of the optical depth is that the minima in the phase matching curve fill up as the optical depth Γ_s increases, as illustrated in figure 3-4, and in the limit of an optically thick system with $\Gamma_s \gg 1$ a Lorenzian type of profile is obtained:

$$F(\triangle kL, \Gamma_i \ll 1, \Gamma_s \gg 1) \approx \frac{1}{\left(\frac{\Gamma_s}{2}\right)^2 + (\triangle kL)^2} \tag{3.14}$$

The dependence of the oscillatory structure of the phase matching curve on the optical depth makes it possible to deduce the optical depth Γ_s of a nonlinear medium from the experimental

third-harmonic phase matching curve. This is described in more detail in chapter 5.

The magnitude of the phase matching factor in a medium where the phase matching condition is satisfied, i.e. $\triangle k = 0$, influences the optimal conversion efficiency of the medium. To determine the phase matching factor in a phase matched medium for different absorption conditions, equations 3.11, 3.13 and 3.14 are considered for $\triangle k \rightarrow 0$. For a phase matched medium the general phase matching factor as given by expression 3.11, becomes

$$F(\triangle kL = 0, \Gamma_i, \Gamma_s) = \left[\frac{\exp(-\Gamma_i/2) - \exp(-\Gamma_s/2)}{\Gamma_s/2 - \Gamma_i/2}\right]^2 \tag{3.15}$$

The phase matching factor of a phase matched optically thin system can be approximated by

$$F(\triangle kL = 0, \Gamma_i \ll 1, \Gamma_s \ll 1) \approx 1 - \frac{\Gamma_s + \Gamma_i}{2} \tag{3.16}$$

making use of the expansion for $e^x = 1 + x + \frac{x^2}{2!} + ...$

For a phase matched system with larger values of the optical depth Γ_s but with $\Gamma_i \ll \Gamma_s$ as in many practical media, the phase matching factor 3.14 reduces to

$$F(\triangle kL = 0, \Gamma_i \ll \Gamma_s) \approx \left[\frac{2}{\Gamma_s}\right]^2$$

giving a conversion efficiency

$$\frac{I_3(L)}{I_1(0)} = \frac{64\pi^4 (3\omega)^2}{c^4 n_3 (n_1)^3} \left[\frac{\left|\chi_T^{(3)}(-3\omega; \omega, \omega, \omega)\right|}{\sigma^{(1)}(3\omega)}\right]^2 [I_1(0)]^2 \tag{3.17}$$

Important conclusions from equation 3.17 are that the conversion efficiency of such a phase matched system that is optically thick for the third-harmonic wavelength is independent of the density N and length L of the medium (obviously N and L must be within reasonable limits so that the assumptions that have been made above still hold). The efficiency depends only on the ratio of the nonlinear susceptibility $\chi_T^{(3)}$ to the one-photon absorption cross section $\sigma^{(1)}(3\omega)$ for the third-harmonic wave. This stresses the advantage of a small one-photon absorption cross section for the third harmonic, as provided by a magnesium vapour medium due to its lack of auto-ionising levels near the third-harmonic energy.

Auto-ionising levels in the continuum at the energy of the sum frequency photons give rise to one-photon resonance of the generated sum frequency with these auto-ionising levels. Hanna et al [16, Section 4.3.2] show that under certain conditions in certain nonlinear media the presence of such an auto-ionising resonance greatly enhances the nonlinear susceptibility and therefore the efficiency of sum-frequency generation. According to Scheingraber et al [36] an auto-ionising resonance may also reduce the third-harmonic output if it causes strong absorption of the generated third harmonic. According to Junginger et al [21] one of the advantages of a magnesium vapour medium for third-harmonic generation is that atomic magnesium does not have auto-ionising levels causing strong absorption near the energy of the generated third harmonic. The energy levels of Mg and Mg^+ as tabulated by Moore [28] confirm this. This makes magnesium vapour a low-loss medium for third-harmonic generation at about 140 to 160 nm.

To obtain these results it was assumed that the nonlinear medium has a rectangular density profile. Using a phase matched metal vapour as generated inside a concentric heat pipe oven as the nonlinear medium, this is not the case. The active medium, a homogeneous mixture of a metal vapour and a buffer gas, is bordered on both sides by a narrow transition zone over the width of which the density of the metal vapour decreases with a certain gradient to more or less zero in the pure buffer gas confining the medium, as illustrated in figure 4-7 on page 94. In a metal vapour buffer gas medium $\triangle k$ depends on the relative pressures of the metal vapour and the buffer gas. The density gradients at the ends of the medium column cause the phase matching factor to become asymmetrical with respect to the phase matching peak at $\triangle k = 0$. To the side of the maximum where the buffer gas pressure is lower than at the phase matching peak the secondary maxima (as seen in the experimental phase matching curves in figures 5-16, page 130 and 5-22, page 139) are pronounced and the curve decreases slowly to the left, but to the side of a higher buffer gas pressure the secondary maxima virtually vanish and the curve falls rapidly towards zero. The physical reason for this effect is explained in more detail in section 4.3.2.

To calculate phase matching curves that can be compared to experimental phase matching curves measured in a heat pipe oven, the density profile in the transition zones has been

approximated by Puell et al [32] by

$$N(z) = \frac{1}{2}N\left[1 + \tanh\left(\alpha|z| - \left|\frac{L}{2}\right|\right)\right] \text{ for } |z| > \frac{L}{2}$$

where α is a measure of the gradient that has to be determined by fitting the theoretical phase matching curve to the experimental data.

3.3 The effect of focusing on the efficiency of third-harmonic generation

The plane wave approximation that has been used so far is not valid in all practical situations. It is approximately valid in experimental situations where the incident laser beam has a beam waist in the medium, but the confocal parameter is much larger than the medium length, i.e. approaching the so-called parallel beam limit where $b \rightarrow \infty$. The conversion efficiency can often be increased by focusing the incident fundamental laser beam, in this way increasing the fundamental intensity in the active part of the medium. A focussed beam cannot be described by a plane wave. In order to determine the effect of focusing on the conversion efficiency and phase matching curve, it is instructive to consider a Gaussian intensity distribution. The focussed incident beam would only have a true Gaussian intensity distribution if the laser is producing a single longitudinal TEM_{00} mode. This can be achieved experimentally. Focussed incident beams of lasers that do not meet this requirement can however be approximated as Gaussian for most practical purposes. Focusing optics often cause losses that promote the propagation of the TEM_{00} mode that has its intensity concentrated on the beam axis and discriminate against the other longitudinal modes with wider radial intensity distributions, enhancing the Gaussian character of the beam. For nonlinear processes high intensities of the incident radiation is very important since the conversion of a nonlinear process of order n depends on the intensity of the fundamental radiation to the power n. Therefore, compared to the other longitudinal modes, the TEM_{00} mode where the energy is concentrated in the one anti-node in the centre of the beam cross-section has the highest intensity for a given power and makes the most significant contribution to a nonlinear process [47].

It is therefore instructive to consider a beam with a Gaussian intensity distribution which

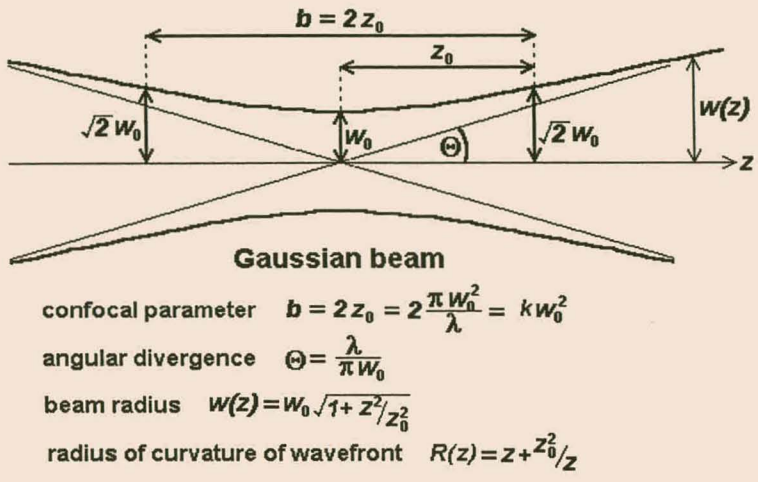

Figure 3-5: Illustration of the parameters used to describe a focussed Gaussian beam near the beam waist.

has the form ([52], [50, equation 3.114])

$$E_q(r,z,t) = E_q(r,z)\frac{b}{b+2iz}\exp\left(\frac{-k_q r^2}{b+2iz}\right)\exp\left(ik_q z\right) \tag{3.18}$$

where

$$b = 2z_0 = \frac{2\pi w_0^2}{\lambda} = kw_0^2$$

is the confocal parameter with w_0 the $1/e^2$ radius of the intensity distribution in the focal plane (see figure 3-5). If the incident beam(s) are approximately Gaussian (and colinear aligned with the same confocal parameter if there are more than one beam,) then the beam produced by sum-frequency generation in the small signal limit is also Gaussian with the same focal parameter as the incoming beam(s) and therefore an even smaller angular divergence θ, because of the shorter wavelength [52].

In order to calculate the effect of focusing on the phase matching curve the following assumptions are made. Absorption is neglected as absorption may obscure the effects of focusing, and only the small signal limit is considered as before. The medium is assumed to be close to phase

matching so that $\triangle k \ll k_q$ since this is the condition that is of practical interest. Therefore, when substituting the electric field of the Gaussian beam 3.18 into the fundamental equation of nonlinear optics, equation 2.49, the slow varying radial dependence of the exponential factor in equation 3.18 can be neglected. An expression for the conversion efficiency in form identical to expression 3.10 is obtained ([52], [32], [47]), but with the phase matching factor given by

$$F(\triangle k \cdot L, b/L) = \frac{1}{L^2}\left[\int_{-L/2}^{+L/2} \frac{\exp(-i\triangle kz)}{(1+2iz/b)^2} dz\right]^2 \tag{3.19}$$

This reduces to expression 3.12 again when $b \to \infty$ in the parallel beam limit. For multimode laser beams the phase matching curve differ significantly from that of the TEM_{00} mode [53], but in the parallel beam ($b \to \infty$) limit the mode structure has no influence.

The practically important case of tight focusing when $L \gg b$ can be solved analytically (because in this case only the medium in the beam waist of length b contributes to the nonlinear process, the length of the medium L is unimportant and the integral limits can be extended to infinity). The result is (see [52, equation III.22] or [47, equation 3.54])

$$\begin{aligned} F(\triangle kb, b/L \ll 1) &= 0 && \text{for } \triangle kb \geq 0 \\ \text{or} \quad &= \frac{\pi^2}{4}\left(\frac{b}{L}\right)^2 (\triangle kb)^2 \exp(\triangle kb) && \text{for } \triangle kb < 0 \end{aligned} \tag{3.20}$$

as illustrated in figure 3-6. The function reaches a maximum of

$$F(\triangle kb = 2, b/L \ll 1) = \left(\frac{\pi b}{eL}\right)^2 \tag{3.21}$$

at $\triangle kb = -2$. The effect of tight focusing on third-harmonic or sum-frequency generation is therefore a shift of the phase matching maximum towards a negative[3] value of $\triangle k$. The experimental observation of this shift of the optimal conversion efficiency towards negative $\triangle k$ (at a lower krypton-magnesium pressure ratio in a krypton magnesium medium) is reported by Junginger et al [21] and confirmed by comparing the experimental results obtained with a focussed and a nearly parallel laser beam in the same experimental setup as discussed in section

[3] Different convensions are used for the sign of $\triangle k$. The convention is used here is $\triangle k = k_{3\omega} - 3k_{\omega}$.

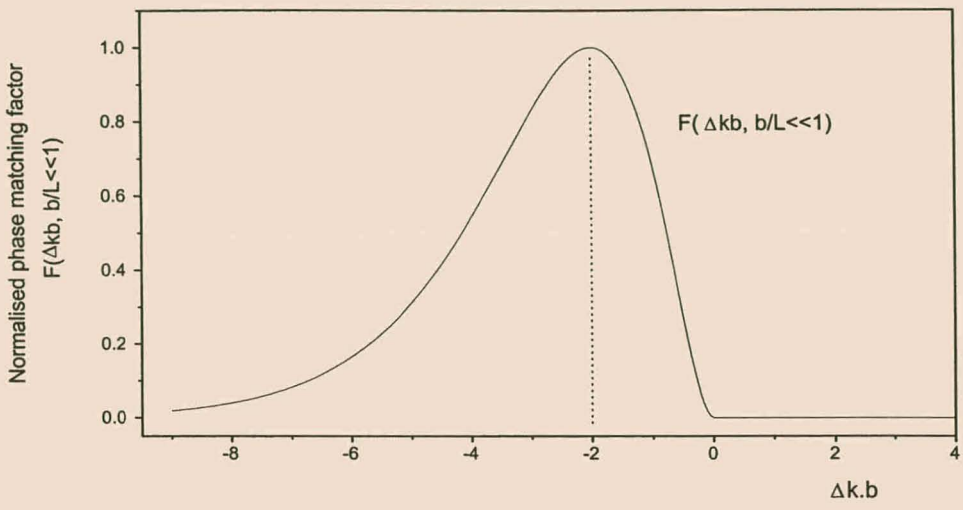

Figure 3-6: Theoretical phase matching curve for a tightly focussed Gaussian beam, for which the confocal parameter b is much smaller than the medium length L, illustrating the shift of the maximum conversion towards the negative value of $\triangle k$: $\triangle k = -2/b$.

5.2.2.

There is a physical reason for the shift of the maximum conversion efficiency towards a negative value of $\triangle k$ [52]. In a focussed laser beam not all components of the electromagnetic wave propagate parallel in exactly the same direction as for ideal colinear plane waves. In a medium where the phase mismatch $\triangle k$ for parallel waves has a small negative value, meaning that $|k_{3\omega}| < 3\,|k_{\omega}|$, some non-parallel plane wave components existing within the focussed beam can meet the phase matching condition and contribute significantly to the third-harmonic generation. Figure 3-7 illustrates how the wave vectors for three fundamental beam components directed at small angles $-\delta$, 0 and δ to the beam direction can be phase matched to a third-harmonic wave vector parallel to the beam direction. In a tightly focussed beam the contribution of non-parallel components become significant, causing the phase matching maximum to shift towards a negative $\triangle k$ value.

To determine the optimal focusing in a practical setup, the relevant criterium is the power conversion efficiency. The power of a Gaussian beam is proportional to $w_0^2 I \propto bI$, using the definition of the confocal parameter, $b = kw_0^2$. Rewriting the conversion efficiency, equation

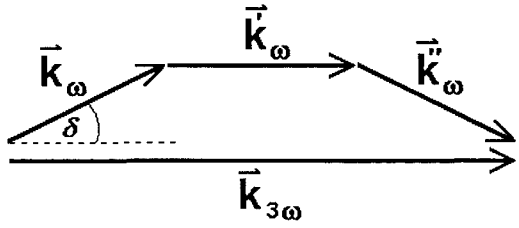

Figure 3-7: Vector diagram illustrating phase matching of noncolinear beam components in a focussed beam.

3.10, to give the power conversion, and using the form of the phase matching factor for a tightly focussed beam as given by expression 3.21, shows that the power conversion efficiency becomes independent of the confocal parameter b under the condition of tight focusing, $b/L \ll 1$. Physically this means that for a tightly focussed beam, when b is much smaller than the length L of the medium, the effect of the higher intensity due to focusing is counteracted by the shorter effective length of the nonlinear medium. Tighter focusing then does not increase the power conversion efficiency any further, but can on the contrary decrease the effectivity of the system due to perturbing higher order nonlinear polarisations that are induced by the increased intensity - see section 3.4 on saturation effects. Vidal [50, p. 312] gives $b \simeq L$ as a rule of thumb for the optimal focusing condition for a phase matched system. According to Scheingraber et al [37] the conversion efficiency is less sensitive to phase matching under this focusing condition than for a parallel beam - an observation that can be explained by the shorter effective medium length.

The effect of focussing on the phase matching curve can be observed by comparing the three experimental phase matching curves in chapter 5 with one another. Figure 5-22, page 139 shows a phase matching curve taken with a incident beam that approaches the parallel beam limit. In the case of figure 5-16, page 130 the incident beam was focussed with a 80 cm focal length lens and in the case of figure 5-15, page 128 it was rather tightly focussed with a 20 cm focal length lens. It becomes clear that tighter focusing does not only shift the peak towards larger

negative values of $\triangle k$, but also smears out the oscillatory structure, to give the long smoothly decreasing slope towards larger negative $\triangle k$ (as seen in figure 3-6) in the $b/L \ll 1$ limit. As the value of b/L increases the oscillatory structure becomes more pronounced until the opposite limit of a parallel beam gives the solid curve in figure 3-4.

3.4 Saturation effects

As can be seen in equation 3.10 for the intensity conversion efficiency for third-harmonic generation, the intensity of the third harmonic is proportional to the fundamental intensity to the third power. Raising the fundamental intensity in order to raise the third-harmonic intensity however, leads to saturation long before the theoretical limit of depletion of the fundamental wave according to energy conservation can be reached.

Different physical processes are responsible for the onset of saturation under different experimental conditions. A magnesium krypton medium at a total pressure of ca. 30 kPa falls into the category of a high density system according to Junginger et al [21]. The high density of the nonlinear medium can compensate for a lower input intensity of the fundamental radiation. Moderate input intensities have the advantage that optical Stark shifts, power broadening and ionization of the medium do not become limitations. In a high density medium however, phase matching is important and saturation is usually caused by processes that become significant as the intensity rises and destroy the phase matching condition. The effect of field dependent changes on the phase matching condition can to some extent be compensated for. The system can be arranged to have an initial phase mismatch at low input intensities so that the field dependent changes of the indices of refraction will bring the system to the phase matching condition at a certain higher intensity. The success of this method to facilitate the use of higher intensities is limited as pulsed lasers are generally used in third-harmonic generation. The laser pulse has an intensity distribution varying in time and space - the larger the input intensity, the larger this variation. The phase matching condition, holding at some specific intensity, would therefore only hold for a small fraction of the pulse.

The dominant processes causing the onset of saturation are associated with the real and imaginary parts of the $\chi_S^{(3)}$ terms in equations 2.98 and 2.99. It has already been shown in

section 3.1 that the susceptibilities of competing processes (see expressions 3.4, 3.5 and 3.6) are dominated by their imaginary and real parts under two-photon resonant and nonresonant conditions respectively, indicating that different processes are responsible for saturation under these two conditions. Puell et al in 1976 [32] showed, by using a phase matched nonresonant Rb-Xe system, that under nonresonant conditions saturation is caused by intensity dependent changes of the refractive index. In the nonresonant Rb-Xe medium the onset of saturation was found to occur at an incident beam intensity of about 10^8 Wcm^{-2} for 300 ps pulses. The quadratic Kerr effect, as described by the real parts of the $\chi_S^{(3)}$ terms, is the main cause of saturation. The real part of the third order nonlinear susceptibility $\chi_S^{(3)}(\omega) \equiv \chi^{(3)}(-\omega;\omega-\omega\omega)$ determines the first nonlinear correction term, quadratic in E_1, to the index of refraction of the atomic gas medium [7]:

$$\overline{n}^2(\omega) = 1 + 4\pi N\overline{\chi}^{(1)}(-\omega;\omega) + 4\pi N\overline{\chi}^{(3)}(-\omega;\omega-\omega\omega)\left[E_1\right]^2 .$$

In 1980 Puell et al [31] showed that for a two-photon resonant phase matched Sr-Xe system two-photon absorption (therefore the imaginary part of $\chi_S^{(3)}(\omega)$) is responsible for saturation at significantly lower intensity levels than in the nonresonant case. In the resonant Sr-Xe medium the onset of saturation was observed at an intensity of the incident beam of 5×10^6 Wcm^{-2} for 600 ns pulses. In the two-photon resonant case two-photon absorption, with cross section [31, Equation 8]

$$\sigma^{(2)}(\omega) = \left(\frac{\pi\omega}{c}\right)\widetilde{\chi}_S^{(3)}(\omega)\left|\widehat{E}_1\right|^2$$

where $\widetilde{\chi}_S^{(3)}(\omega)$ is the imaginary part of the susceptibility, causes not only depletion of the fundamental wave but also changes of the energy level populations. The changes in the population densities cause changes to the refractive index of the medium destroying the phase matching condition. For this reason an efficient two-photon resonant system should not only have a small one-photon absorption cross section $\sigma^{(1)}(3\omega)$ but also a small two-photon absorption cross section $\sigma^{(2)}(\omega)$ to delay the onset of saturation effects. A magnesium krypton system is such a low loss medium according to Junginger et al [21].

To summarise: Two-photon resonance is responsible for significant resonance enhancement of the generated third-harmonic wave at moderate input intensities, but also for the advanced

onset of saturation at higher input intensities when compared to the nonresonant system. The result is that for moderate input intensities the conversion efficiency peaks at the two-photon resonant frequency, but for very high input intensities the highest conversion efficiency is obtained slightly off resonance on both sides of the two-photon resonance frequency [47].

The higher the intensity of the incident radiation the larger the number of processes that have to be taken into account. Higher order processes become significant causing perturbations to the third order susceptibilities or acting as additional competing nonlinear processes. When intensities above the threshold for saturation are used, two other processes that are not taken into account by the perturbational treatment of the theory - the optical Stark effect and multiphoton ionisation - must also be taken into account. The optical Stark effect can cause a shift in the energy of the two-photon resonant level influencing resonant enhancement by smearing out the two-photon resonance [47]. Multiphoton ionisation brings about the attenuation of the incident beam and the production of ions and photo-electrons that can induce Stark broadening. In general it must be taken into account that above the saturation threshold the nonlinear medium itself is changing because of the redistribution of population densities due to two-photon absorption and other processes. This causes the values of the index of refraction and other susceptibilities to become intensity dependent and the simple theoretical model to fail.

For optimal conversion efficiency it is recommended that the intensity range near the onset of saturation is used where the behaviour of the system is still well understood [47]. Experimental results indicate that a further increase in the intensity does not raise the third-harmonic energy obtained very much [31].

3.5 Phase matching for third-harmonic generation in a gaseous medium

It was shown mathematically in sections 2.2.2 and 3.2 that the intensity conversion efficiency for third-harmonic generation depends critically on the phase matching factor. In sections 3.1 to 3.4 the most important parameters influencing the phase matching factor were discussed, i.e.

- the wave vector mismatch Δk,

- the absorption cross sections for the fundamental and third-harmonic frequencies,
- the focusing of the incident laser beam as quantified by b/L and
- the mode structure of the incident laser beam.

The last two depend on qualities of the incident laser beam, whereas the first two are determined by the characteristics of the nonlinear medium. To phase match a nonlinear medium for a nonlinear process, such as third-harmonic generation, means to minimise the wave vector mismatch Δk between the fundamental and the generated third-harmonic frequencies. For different optical media there are different ways to obtain phase matching. In this section the possible mechanisms of phase matching in a two-component gaseous medium are discussed.

Firstly the physical reason for phase matching has to be considered. For different experimental setups the phase matching factor acquires different forms, but for not too tightly focussed beams it reaches its peak value at the minimum value of the phase mismatch Δk. Physically this means that the fundamental and third-harmonic waves must have the same phase velocity ($v_{phase} = \frac{c}{n_i} = \frac{\omega_i}{k_i}$) for the third-harmonic waves generated in different volume elements of the medium to interfere constructively. In general a phase mismatch will develop between third-harmonic radiation generated in different positions along the optical path because the third-harmonic field propagates with the phase velocity $c/n_{3\omega}$, whereas the nonlinear polarisation density generating it has a phase velocity c/n_{ω} as deduced from equation 2.36. The phase mismatch that develops over a medium length L is given by

$$\begin{aligned} e^{i(k_{3\omega}-3k_{\omega})L} &= e^{i\triangle kL} \\ \text{with } \triangle kL &= (k_{3\omega} - 3k_{\omega})\, L = \frac{3\omega}{c}\,(n_{3\omega} - n_{\omega})\, L \end{aligned}$$

This phase mismatch gives rise to the phase matching factor as in equations 2.48 and 3.11 (pages 28 and 59).

The phase matching requirement is a direct result of the requirement for conservation of linear momentum. The wave vector $\mathbf{k}$ is related to the linear momentum of the photon associated with the wave by $\mathbf{p} = \hbar\mathbf{k}$. Conservation of momentum $\mathbf{p}_1 + \mathbf{p}_2 + \mathbf{p}_3 = \mathbf{p}_{sum}$ therefore

requires

$$\mathbf{\Delta k} = \mathbf{k}_{sum} - (\mathbf{k}_1 + \mathbf{k}_2 + \mathbf{k}_3) = 0 \tag{3.22}$$

In the case of third-harmonic generation with a single incident beam the fundamental and the harmonic beams are colinear. In this case $k_1 = k_2 = k_3 = k_\omega = \frac{\omega n(\omega)}{c}$ and $k_{sum} = k_{3\omega} = \frac{3\omega n(3\omega)}{c}$ giving

$$\begin{aligned} \Delta k &= k_{3\omega} - 3k_\omega \\ &= \frac{3\omega n(3\omega)}{c} - 3\frac{\omega n(\omega)}{c} \\ &= \frac{3\omega}{c}\left(n(3\omega) - n(\omega)\right) = 0. \end{aligned}$$

The phase matching condition is indeed met when

$$n(3\omega) = n(\omega) \tag{3.23}$$

and the fundamental and harmonic wave propagate through the medium with the same phase velocity.

Three methods to obtain phase matching in a gaseous medium are described now.

A practical way to meet this requirement is to use a two-component gaseous system. If one of the gaseous components is positive dispersive in the spectral region between ω and 3ω (meaning that $n(\omega) < n(3\omega)$) and the other component exhibits negative dispersion ($n(\omega) > n(3\omega)$), a pressure ratio can be found for which $n(\omega)_{mixture} = n(3\omega)_{mixture}$. This is illustrated by the schematic dispersion curve for magnesium and krypton in figure 3-8. The correct density (pressure) ratio for phase matching for third-harmonic generation in a two component gaseous system can be calculated if the real parts of the linear susceptibilities of both components at both the fundamental and the third-harmonic frequencies are known. According to equation 2.21 the indices of refraction of the two-component system with species a and b at ω and 3ω are given by

$$\begin{aligned} n(\omega) &= 1 + 2\pi\left[N_a\overline{\chi}_a^{(1)}(\omega) + N_b\overline{\chi}_b^{(1)}(\omega)\right] \\ n(3\omega) &= 1 + 2\pi\left[N_a\overline{\chi}_a^{(1)}(3\omega) + N_b\overline{\chi}_b^{(1)}(3\omega)\right] \end{aligned} \tag{3.24}$$

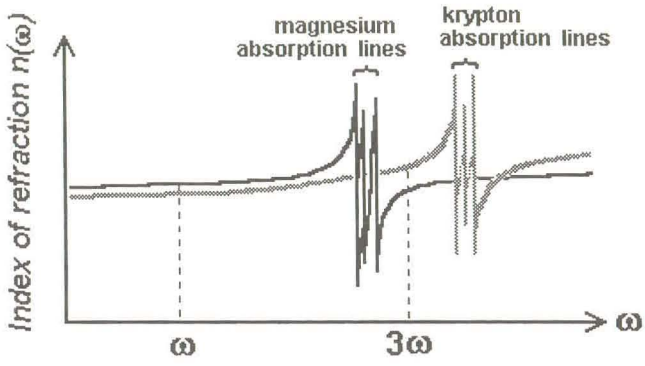

Figure 3-8: Schematic illustration of the dispersion curves of magnesium vapour and krypton gas in the spectral region between the fundamental frequency and the third harmonic frequency.

where N_a and N_b are the number densities of species a and b respectively. Phase matching is achieved when

$$\begin{aligned} n(\omega) &= n(3\omega) \\ \left[N_a\overline{\chi}_a^{(1)}(\omega) + N_b\overline{\chi}_b^{(1)}(\omega)\right] &= \left[N_a\overline{\chi}_a^{(1)}(3\omega) + N_b\overline{\chi}_b^{(1)}(3\omega)\right] \\ N_a\left[\overline{\chi}_a^{(1)}(\omega) -_a \overline{\chi}_a^{(1)}(3\omega)\right] &= N_b\left[\overline{\chi}_b^{(1)}(3\omega) - \overline{\chi}_b^{(1)}(\omega)\right] \end{aligned}$$

giving

$$\frac{N_a}{N_b} = \frac{\overline{\chi}_b^{(1)}(3\omega) - \overline{\chi}_b^{(1)}(\omega)}{\overline{\chi}_a^{(1)}(\omega) - \overline{\chi}_a^{(1)}(3\omega)} \tag{3.25}$$

This condition has to be met over the whole path length of the laser beam in the gaseous medium imposing a stringent homogeneity requirement on the medium.

When two incident laser beams, both at the fundamental frequency, are used, phase matching can be achieved in a different way. Consider third-harmonic generation by the coupling of two incident beams at the fundamental frequency ω but propagating in different directions, overlapping inside the nonlinear medium. Let the propagation vector for the one beam be

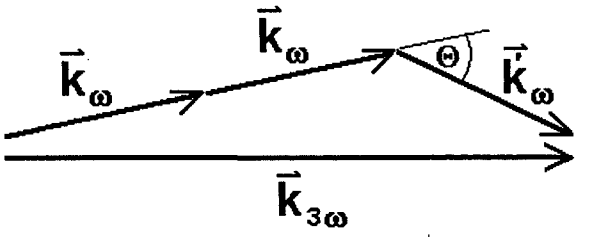

Figure 3-9: Vector diagram illustrating phase matching with two non-colinear beams in a negatively dispersive medium.

$\mathbf{k}_\omega$ and for the other one $\mathbf{k}'_\omega$ such that their absolute values are equal $|\mathbf{k}'_\omega| = |\mathbf{k}_\omega|$, but their directions differ slightly. Now the phase matching condition is the vector equation

$$2\mathbf{k}_\omega + \mathbf{k}'_\omega = \mathbf{k}_{3\omega} \tag{3.26}$$

If the medium is negatively dispersive, that means $|2\mathbf{k}_\omega| + |\mathbf{k}'_\omega| > |\mathbf{k}_{3\omega}|$, then equation 3.26 can be satisfied by the correct angle between $\mathbf{k}_\omega$ and $\mathbf{k}'_\omega$ determined by the ratio of $n(\omega)$ and $n(3\omega)$, as illustrated in figure 3-9. The advantage is that phase matching can be obtained without changing the composition of the medium, but this method has the disadvantage that high intensity pump beams are needed to compensate for the limited spatial overlap of two non-colinear beams.

This angular phase matching occurs spontaneously in focussed beams and is responsible for the shift of the conversion maximum towards negative $\triangle k$ values as discussed in section 3.3.

The third method to obtain phase matching for the generation of a certain sum-frequency ω_s in a specific atomic medium (without changing the medium composition or the colinear alignment) is to adjust the incident frequencies ω_1, ω_2 and ω_3 to satisfy the phase matching

condition

$$\omega_s \overline{\chi}^{(1)}(\omega_s) = \omega_1 \overline{\chi}^{(1)}(\omega_1) + \omega_2 \overline{\chi}^{(1)}(\omega_2) + \omega_3 \overline{\chi}^{(1)}(\omega_3)$$

Scanning the sum-frequency when this method is used, however requires computer controlled lasers with an intricate feedback and control system.

3.6 Application to a magnesium vapour krypton gas medium

In the magnesium vapour krypton gas system studied in this thesis the magnesium vapour is chosen for its suitability as a medium for the generation of vacuum ultraviolet radiation around 140 nm by third-harmonic and sum-frequency generation. Some of the reasons are explained in this section.

Wallace and Zdasiuk [51] first investigated two-photon resonant third-harmonic generation and four-wave mixing in magnesium vapour, mixed with helium gas, but not phase matched. They reported a wide continuous tuning range of the generated vacuum ultraviolet in the 140 to 160 nm region and a very high power conversion efficiency of 0.2 ± 0.1 percent at 30 kW input power although their explanation for it and calculated value for $\chi_T^{(3)}(3\omega)$ are disputed. Junginger et al in 1980 [21] investigated a magnesium vapour medium phase matched with krypton gas and presented it as a suitable low loss, high density medium. Junginger obtained a intensity conversion efficiency of up to 1.2×10^{-4} and a peak third harmonic power of about 3 W using a nitrogen laser pumped dye laser. Vidal and collaborators (for example [38], [25] and [41]) reported that a magnesium krypton medium prepared in a concentric heat pipe oven to is convenient and reliable medium for the generation of tunable vacuum ultraviolet for spectroscopy purposes by four-wave frequency mixing.

Magnesium vapour provides a sufficiently large nonlinear susceptibility for third-harmonic generation as well as a suitable two-photon resonance at 431 nm allowing the generation of a third harmonic at 143 nm. It was found that using the $3s^2 - 3s3d$ two-photon resonance of magnesium both the one- and two-photon absorption of the fundamental frequency (431 nm) are sufficiently small due to the lack of one-photon resonant intermediate energy levels. The one-photon absorption of the third-harmonic frequency, which is in the vacuum ultraviolet region, is in general a problem because the photon energy is enough to cause photo-ionisation

in the medium, but the lack of auto-ionising states near the third-harmonic photon energy (at 143 nm) gives magnesium vapour a small one-photon absorption cross-section for the generated third-harmonic frequency. The small one-photon and two-photon absorption cross-sections of magnesium at the fundamental and third-harmonic frequencies (leading to Junginger's term: low loss medium) have a dual advantage. Due to the small two-photon absorption cross-section the onset of saturation due to two-photon absorption is delayed so that higher intensities can be used. The effect of low one-photon absorption is that, a given intensity, the column density NL of the phase matched medium (where N is the number density and L the medium length) can be increased to enhance the conversion without getting saturation due to large optical depths [38].

A magnesium vapour medium can be phase matched by the addition of an inert gas. Magnesium vapour exhibits negative dispersion between 430 nm and 140 nm meaning that the index of refraction at 140 nm is smaller than at 430 nm - see the diagrammatic illustration of the dispersion of magnesium in figure 3-8. Positively dispersive krypton gas (for which the index of refraction increases continuously with decreasing wavelength in the 430 to 140 nm spectral region) is added as buffer gas to achieve phase matching by careful adjustment of the partial pressure ratio as explained in the previous section. The phase matching condition is given by

$$\frac{N_{Kr}}{N_{Mg}} = \frac{P_{Kr}}{P_{Mg}} = \frac{\overline{\chi}^{(1)}_{Mg}(3\omega) - \overline{\chi}^{(1)}_{Mg}(\omega)}{\overline{\chi}^{(1)}_{Kr}(\omega) - \overline{\chi}^{(1)}_{Kr}(3\omega)}$$

($P = (\frac{kT}{V})N$ and $\frac{kT}{V}$ is a constant for the experiment so that $\frac{N_{Kr}}{N_{Mg}} = \frac{P_{Kr}}{P_{Mg}}$.)

Junginger et al [21] used this equation, with the krypton linear susceptibilities calculated from measured values of the index of refraction and theoretically calculated values for the linear susceptibilities of magnesium, to calculate the pressure ratio needed for phase matching. The experimentally measured value of the pressure ratio for phase matching was then used to adjust the matrix elements with the highest uncertainty in the theoretical calculation to give the values for the linear susceptibilities of magnesium and krypton tabulated in table 3.1.[4]

The pressure ratio for phase matching obtained experimentally by Junginger et al is $\frac{P_{Kr}}{P_{Mg}} =$ 12.7. This relatively low pressure ratio for phase matching makes it possible to work with

[4]Note: explanation of cgs-units (ESU) in Hanna, Cotter and Yuratich (1979), p. 315-316.

Wavelength λ in nm	Frequency ω in rad.s^{-1}	$\overline{\chi}^{(1)}_{Mg}(\omega)$ in cgs	$\overline{\chi}^{(1)}_{Kr}(\omega)$ in cgs
Fundamental: 431	4.373×10^{15}	17.5×10^{-24}	2.59×10^{-24}
Third harmonic: 143	1.318×10^{16}	-5.35×10^{-24}	4.37×10^{-24}

Table 3.1: The frequencies and susceptibilities relevant to the calculation of the density ratio for phase matching in the magnesium krypton system.

a higher absolute magnesium vapour pressure (high density medium) without reducing the effective nonlinear susceptibility due to pressure broadening. Calculations using the tabulated values for the susceptibilities as well as the schematic illustration of the dispersion of magnesium and krypton in figure 3-8 (the illustration is qualitatively correct, although not quantitatively accurate) shows that a krypton magnesium pressure ratio higher than 12.7 corresponds to a positive value of $\triangle k$ ($\triangle k = k_{3\omega} - k_{\omega} > 0$) and a lower pressure ratio to a negative value of $\triangle k$.

This method of phase matching requires the two-component medium to be very homogeneous and the partial pressures of the magnesium vapour and krypton gas to be well defined and stable. Under the experimental conditions applicable to the phase matching curve in figure 5-22, a change in the krypton magnesium pressure ratio of only 0.3 percent causes a 10 percent reduction in the third harmonic energy output. This means that the temperature of the medium, that determines the pressure of the vapour, must be very stable and constant over the medium volume. How these requirements can be met in a heat pipe oven is discussed in chapter 4.

3.7 Sum-frequency generation and frequency tunability

In a general four-wave frequency mixing process three waves of frequencies ω_1, ω_2 and ω_3 are coupled to produce a wave at frequency ω_4 that can be any linear combination of the three incident frequencies, for example sum-frequency generation, with $\omega_4 = \omega_1 + \omega_2 + \omega_3$. Third-harmonic generation is the degenerate case where $\omega_1 = \omega_2 = \omega_3 = \omega$ and $\omega_4 = 3\omega$.

When employing third-harmonic generation as a source of coherent vacuum ultraviolet radiation, the generated third harmonic can in principle be frequency tuned by tuning the frequency of the single fundamental beam. Under moderate incident intensities the conversion efficiency for third-harmonic generation however, depends on the two-photon resonance of the fundamental frequency. The restriction that the fundamental frequency can only be tuned inside the

bandwidth of the two-photon resonance makes the effective tuning range small.

Sum-frequency generation by partly degenerate four–wave frequency mixing using two incident beams with different frequencies (say ω_1 and ω_2) overcomes this restriction. The frequency ω_1 can be tuned to two-photon resonance to obtain the crucial resonant enhancement of the nonlinear susceptibility. The frequency ω_2 of the other beam can be tuned independently to give a tunable sum frequency $\omega_{sum} = 2\omega_1 + \omega_2$ without affecting the resonance. The phase matching condition will require adjustment of the medium conditions when tuning over a large frequency range. The four-wave frequency mixing process generating the sum frequency $\omega_{sum} = 2\omega_1 + \omega_2$ is the process used generally for the experimental generation of frequency tunable vacuum ultraviolet in a magnesium krypton medium. This process will be referred to as sum-frequency generation in the discussion that follows.

Although the mathematical expressions describing the process of sum-frequency generation are more complicated than those for third-harmonic generation, all the results obtained for third-harmonic generation in the previous sections in principle also hold for sum-frequency generation. To summarise:

- The susceptibility for sum-frequency generation $\chi^{(3)}(-\omega_{sum}; \omega_2, \omega_1, \omega_1)$ can be enhanced by a one-photon resonance of either of the incident frequencies, a two-photon resonance of (say) ω_1 or a three-photon resonance. Using the two-photon resonance has the advantage that it does not bring about strong one-photon absorption of either the incident frequencies or the sum-frequency by dipole allowed transitions, as is the case with one- and three-photon resonances. This has the practical implication mentioned above that ω_1 must be tuned to the two-photon resonance leaving ω_2 tunable to obtain a tunable sum frequency at $\omega_{sum} = 2\omega_1 + \omega_2$.

- For efficient sum-frequency generation the medium must be phase matched, meaning that the sum-frequency wave generated in different volume elements of the medium must interfere constructively. The phase matching curve shows that the efficiency of sum-frequency generation depends critically on the phase matching condition. The conservation of linear momentum - which is the physical principle behind phase matching - can be reduced for colinear incident beams to a relation between the frequencies and indices of refraction of

the incident and sum-frequency waves

$$2\omega_1 n(\omega_1) + \omega_2 n(\omega_2) = \omega_s n(\omega_s) \tag{3.27}$$

(see the derivation of equation 3.23 from equation 3.22 on page 73.) In a two-component gaseous nonlinear medium such as magnesium and krypton the phase matching condition as given by equation 3.27 can be satisfied by the correct ratio of partial pressures of the two components. It can be expected that the pressure ratio for phase matching for sum-frequency generation changes continuously as the nonresonant incident frequency ω_2 and therefore the sum frequency is tuned.

- A crossed concentric heat pipe oven can be used to provide the crucial temperature stability and homogeneity needed in the medium as well as the possibility to adjust the partial pressures of the metal vapour and the inert gas independently to obtain and maintain phase matching; without electronic control or a stabilised heating power.

- The linear and nonlinear processes competing with sum-frequency generation and influencing the efficiency of the process must be minimised by the choice of the medium and incident frequencies. These processes are one-photon absorption of the incident and sum-frequency waves, two-photon absorption of the two-photon resonant incident frequency that causes saturation under resonant conditions at high input laser intensities and other third and higher order processes that cause saturation under non-resonant conditions, including third-harmonic generation.

In the case of sum-frequency generation the generation of the third harmonics of the fundamental frequencies ω_1 and ω_2 competes strongly with the sum-frequency generation process. In order to make sum-frequency generation the dominating process, third-harmonic generation must be suppressed. This can be done by using circular polarised incident beams. The physical principle is the conservation of angular momentum that leads to the selection rule, equation 2.97, page 47. For sum-frequency generation it can be expressed as:

$$\triangle m_s + \triangle m_1 + \triangle m_1 + \triangle m_2 = 0.$$

When the incident beam at frequency ω_1 is right-hand circularly polarised so that each photon carries an angular momentum $\triangle m_1 = +1$ and the incident beam at frequency ω_2 is left-hand circularly polarised having angular momentum $\triangle m_2 = -1$, then the sum-frequency $\omega_s = 2\omega_1 + \omega_2$ is allowed and will have an angular moment $\triangle m_s = -1$ (left-hand circularly polarised) to satisfy the selection rule. The third harmonics of either of the incident waves however are not allowed by the selection rule because

$$\triangle m_s + \triangle m_i + \triangle m_i + \triangle m_i = \triangle m_s + (\pm 1 \pm 1 \pm 1) = \triangle m_s \pm 3 = 0$$

cannot be satisfied. The single sum-frequency photon cannot carry an angular momentum of magnitude 3.

The conclusion is that once third-harmonic generation is obtained in an experimental setup, where the medium is generated inside a crossed concentric heat pipe oven, tunable sum-frequency generation can also be realised without major changes to the setup by adding a second dye laser and the necessary polarising optical components to polarise the two incident beams circularly in opposite directions.

Chapter 4

The heat pipe oven as apparatus in spectroscopy

In chapter 2 the most important medium requirement for efficient four-wave frequency mixing in a metal vapour medium is shown to be the constructive interference of the contributions to the sum frequency wave generated in different parts of the medium - the phase matching condition. In section 3.5 it is discussed in theory how phase matching can be achieved in a two component gaseous system by tuning the pressure ratio. In this chapter the characteristics of heat pipes, especially the crossed concentric heat pipe oven, are discussed in order to show how a crossed concentric heat pipe oven facilitates the preparation of a vapour medium that meets the phase matching condition.

In practice the phase matching condition for efficient four-wave frequency mixing in a magnesium vapour and krypton gas medium sets extremely stringent requirements to the two component mixture.

- In order to have a sufficiently large magnesium particle density the temperature of the medium must be about 760 degrees Celsius. (At 1020 K (747 °C) the magnesium vapour pressure is about 2.3 kPa giving a particle density of approximately 1.6×10^{17} atoms per cm^3.)

- To obtain phase matching the temperature must be constant within a degree Celsius over a path length of a few centimeters as well as absolutely stable in time.

- The mixture of the magnesium vapour and krypton gas must be homogeneous and extremely stable [37].
- The partial pressures of the magnesium vapour and krypton gas must be well defined and independently adjustable to facilitate the fine-tuning of the pressure ratio to meet the critical phase matching condition.

It will be shown that these stringent requirements can be met inside a crossed concentric heat pipe oven.

4.1 Development of the heat pipe as spectroscopic instrument

Gaugler of the General Motors Corporation patented the first true heat pipe with a wick structure in 1944 in the USA as a proposed solution to a refrigeration problem. However, it was only in the 1960's in connection with the space program of the USA that the idea was reinvented by Grover (who coined the term heat pipe) and developed further. Grover, Cotter and Erickson [13] did experimental work on heat pipes with different working materials and obtained some preliminary theoretical results. The interest in heat pipes was due to the properties of a heat pipe as a "synergistic engineering structure which is equivalent to a material having a thermal conductivity greatly exceeding that of any known metal" [14], operating also under gravity-free conditions. The heat pipe for heat transfer purposes consists of a closed container containing the working material. At the heat source the working material is evaporated and the vapour flows due to a small vapour pressure gradient towards the heat sink region where it is condensed. The latent heat of evaporation is transfered from source to sink. The condensate is returned to the heat source by the capillary pressure in a wick structure. The evaporation and condensation takes place at the same temperature so that a large heat flow is maintained in the heat pipe over a very small temperature difference (one degree Kelvin or less) giving a very large thermal conductivity. Research on, and application of heat pipes as thermal devices have developed rapidly since the middle 1960's. Heat pipes are today widely used for heat transfer purposes in engineering and industry.

The fact that the heat pipe can be used to solve common difficulties in providing a homogeneous vapour sample of well defined optical path length was first recognised and investigated in

1969 by Vidal and Cooper [42]. Vidal and Cooper developed the double open-ended gas loaded heat pipe as a spectroscopic device. In spectroscopic applications the term heat pipe oven is often used to distinguish the modified spectroscopic heat pipe models from the closed heat pipes used in engineering and to emphasise their function as an oven in which metal vapours confined by inert gases are generated. A heat pipe oven can provide a column of homogeneous pure metal vapour with a well defined pressure, temperature and optical path length. The inert gas confining the vapour column protects the windows, solving the window problem of the metal being deposited on the window surface. The measurement of vapour pressure curves (as described in section 4.2.1), oscillator strengths and the generation of metal vapour plasmas are some laboratory applications.

The need to generate homogeneous metal vapour inert gas mixtures of which the partial pressures could be adjusted independently led to the development of the concentric heat pipe oven [43], followed by the crossed concentric heat pipe oven [37] as well as its advanced model as described in reference [38]. Both designs consist of two independent heat pipes, the outer one functioning as an isothermal oven for the section of the inner one in contact with its vapour column. The designs differ in the relative orientation of the two heat pipes giving the crossed concentric heat pipe oven the advantage of a fixed geometrically defined column length and shorter warm up time. The crossed concentric heat pipe oven is the model that is of relevance in this thesis and its operation is discussed in detail in section 4.3. Its prime application is the generation of suitable phase matched medium for four-wave frequency mixing.

4.2 Principles of operation of a heat pipe oven

The principle difference between the heat pipe ovens employed in spectroscopy and the heat pipes used in engineering for heat transfer is that a heat pipe for heat transfer consists of a closed container (the working material constitutes a constant volume system) whereas a spectroscopic heat pipe oven has a mechanism to keep the pressure inside the oven constant.

In order to develop a qualitative understanding of the thermodynamic conditions in a constant pressure system, consider the following ideal model: a thermally isolated container sealed off by a movable piston to which a constant external pressure is applied. The working material,

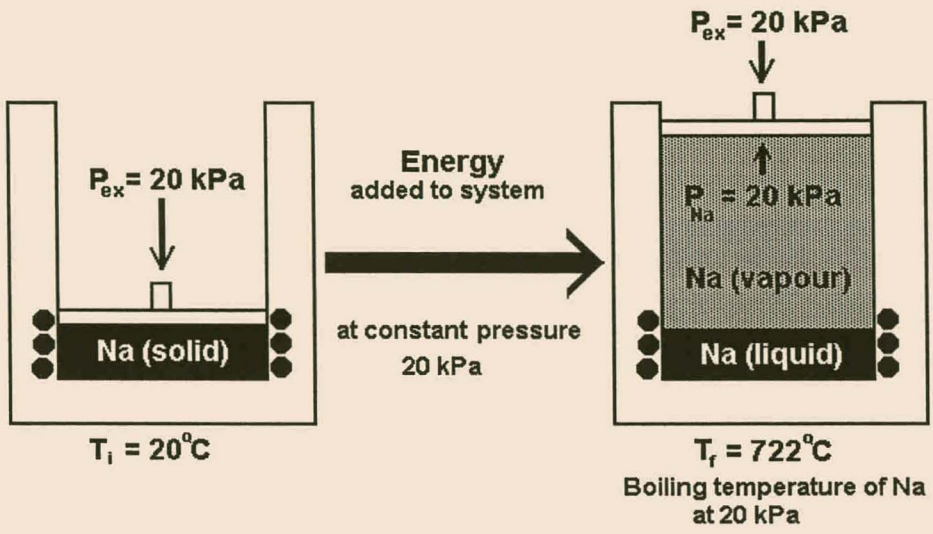

Figure 4-1: Schematic illustration of a liquid-phase equilibrium in an isolated constant pressure system.

for example sodium, fills the whole volume of the container (figure 4-1). There must also be a mechanism to add energy to the system, for example a heating element.

At room temperature and (external) pressure of (for example) 20 kPa sodium is in its solid phase. For 20 grams of sodium the first 3,2 kJ of energy raises the temperature of the solid sodium to 78 degrees Celsius, its melting temperature at a pressure of 20 kPa. At this temperature and pressure the solid and liquid sodium are in equilibrium. The next 2,3 kJ of energy causes the solid sodium to liquefy gradually without any raise in temperature because of the solid-liquid phase equilibrium exsisting in the system. After all the sodium has been melted the next 19,1 kJ of energy added raises the temperature of the liquid sodium from 78 to 722 degrees Celsius, the boiling temperature of sodium at 20 kPa. Adding any more energy (up to 77,5 kJ) to the system will not change the temperature but will evaporate a corresponding quantity of the sodium and bring the system to a dynamic sodium liquid-vapour phase equilibrium. (Adding more than 77,5 kJ energy would cause evaporation of all the liquid sodium and the equilibrium would no longer exist.)

It is the characteristics of the liquid-vapour phase equilibrium that are important. Con-

sidering the forces on the movable piston it is obvious that the vapour pressure of the sodium vapour formed by evaporation must be equal to the pressure applied externally. The vapour pressure determines the boiling temperature of the sodium according tot the sodium vapour pressure curve and therefore the temperature inside the container. The temperature is not influenced by fluctuations in the total energy in the system as long as the equilibrium conditions are maintained. The equilibrium is called dynamic because evaporation and condensation are continuously taking place (at equal total rates) at all liquid-vapour interfaces. In this equilibrium model with the heater switched off and heat losses ignored, there is no net flow of heat from a heat source to a heat sink.

To summarise: by adding sufficient energy to the isolated system at the constant pressure of 20 kPa, a sodium liquid-vapour phase equilibrium is obtained with the sodium vapour pressure P_{Na} equal to the external pressure P_{ex} = 20 kPa and the temperature of the whole system equal to the boiling temperature (phase equilibrium temperature) of sodium at that pressure. The vapour pressure curve is a plot of the change of the equilibrium temperature with pressure. The external pressure dictates the temperature in the system and as long as the equilibrium is maintained the exact amount of energy in the system has no influence on the temperature. These are the characteristics of a dynamic liquid-vapour phase equilibrium.

In practice a sodium heat pipe oven differs from the simple isolated equilibrium system in being thermally poorly isolated and the constant pressure being applied by a noble gas buffer (say argon gas) at some external pressure P_{ex} instead of a piston - see figure 4-2.

To keep the heat pipe in operation a continual energy supply (the heating element at the bottom) is needed so that the heating power, in its stable operating state, balances the energy losses from the surface of the upper part of the heat pipe oven. In this case a well defined heat source (the heating element at the bottom of the heat pipe) and heat sink (the cooler environment to which the upper part of the heat pipe loses its heat) can be distinguished. A dynamic liquid-vapour phase equilibrium[1] exists in the heat pipe with the sodium evaporating at the heat source (taking up its latent heat of evaporation), the vapour flowing upwards due to a slight pressure gradient and condensing at the heat sink in the upper part of the vapour

[1] Due to the continuous nett flow of energy it is no true equilibrium state, but when in stable operation the system exhibits the characteristics of a dynamic phase equlibrium.

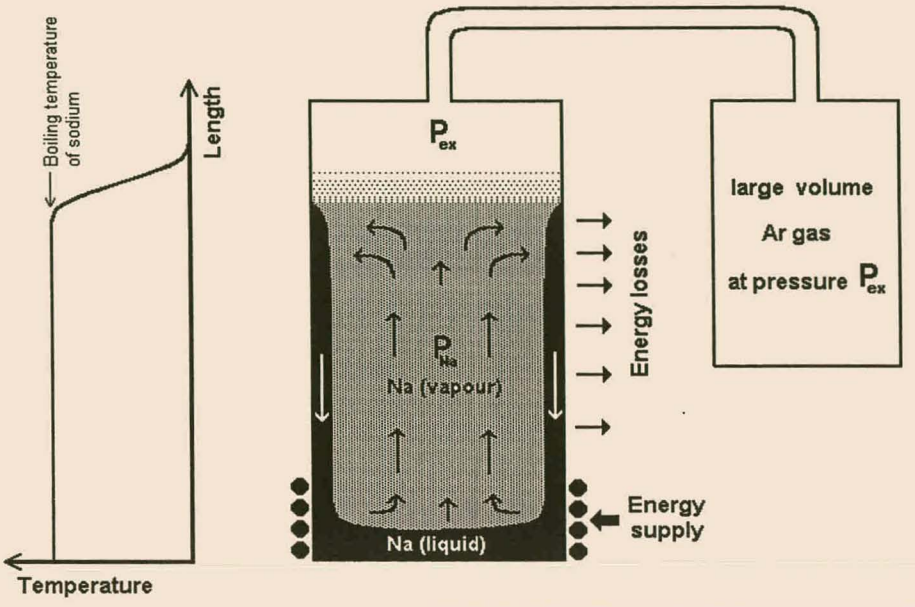

Figure 4-2: Schematic illustration of the functioning of a true heat pipe.

column, releasing the latent heat again. The effect of the heat sink and source is that the processes of evaporation and condensation that maintain the dynamic equilibrium are separated spatially but the two processes are still part of one dynamic equilibrium and take place at the same equilibrium temperature. In order to maintain the equilibrium the condensate has to be returned to the evaporation zone. This is accomplished by gravitation as well as capillary forces in a wick that is attached to the inner surface of the heat pipe. The menisci in the evaporation zone are highly curved due to the removal of liquid in the wick pores. In the condensation zone the menisci are nearly flat. Due to the surface tension of the liquid the difference in curvature causes a capillary pressure gradient along the length of the wick returning the liquid to the evaporation zone.

The most important operational properties of the heat pipe oven are:

- Due to the equilibrium conditions existing through the whole length of the vapour column, the temperature difference between the heat source and sink is less than one degree Celsius [42]. (The amount of heat transferred in the form of latent heat from source to sink with

such a low temperature gradient gives the heat pipe oven a very large thermal conductivity - orders larger than any solid metal rod of the same dimensions.)

- The molecular pumping action of the flowing vapour expels the buffer gas (and any other vaporised impurities) to the volume above the active vapour column making the system self-purifying. When the heat pipe oven has reached a stable operation state the only mixing of sodium vapour and argon gas occurs in the narrow transition zone between the pure sodium vapour and the argon gas - its width of the order of the mean free path of the atoms of the working material in the buffer gas [6]. The buffer gas functions as movable boundary confining the metal vapour.

- The sodium vapour pressure P_{Na} in the column is equal[2] to the external pressure of the argon gas P_{ex} and can therefore be measured easily and accurately.

- Due to the equilibrium conditions the temperature of the liquid-vapour system is determined by the sodium vapour pressure according to the sodium vapour pressure curve.

- The heating power determines the length of the vapour column. An increase in heating power causes the rate of evaporation to exceed the rate of condensation temporally and therefore cause the vapour column to expand until the heat losses through the expanded heated surface balance the higher heating power. The heating power has no effect on the equilibrium temperature.

4.2.1 Experimental method and results

The heat pipe used in this preliminary experiment to verify the thermal properties of a heat pipe oven is the vertical heat pipe of a prototype crossed concentric heat pipe oven (similar, but slightly smaller than the one described in chapter 5 and illustrated in figure 5-4, page 107) of which the horizontal pipe is not in use and is open to the atmosphere. It is made of stainless steel (type 316) with a wall thickness of ca. 3 mm. It is 360 mm long with a diameter of 50.8 mm. The lower 65 mm of the pipe is in contact with the electrical heating element coiled around the

[2] In principle the velocity of the flowing vapour causes its pressure to differ from the pressure of the argon gas in the reservoir volume by the velocity dependent term in the Bernoulli equation but this can for most practical purposes be neglected for moderate flow velocities.

heat pipe. Up to a height of 270 mm the heat pipe is covered by 50 mm thick thermal isolating material. The top cover with the inlet for the argon gas is water cooled. Along the length of the heat pipe above the heating element nickel-chromium/nickel-aluminium thermocouples are spotwelded directly to the outer surface of the stainless steel wall at regular intervals. The reference Ni-Cr/Ni-Al junction was placed in a water and ice mixture. The temperature at the different positions along the heat pipe was obtained by reading the potential difference between the appropriate thermocouple and the reference thermocouple junction and calculating the temperature (relative to that of the ice-water which was measured with a mercury thermometer to be at 0 degrees Celsius $\pm$ 0.5 °C) by making use of a calibration function that was obtained from a fit on the data in standard Ni-Cr/Ni-Al thermocouple data tables. The temperature is accurate to about 1 °C but it must be noted that these temperatures were measured on the outside of the stainless steel wall and are expected to be lower than the actual temperature inside the heat pipe by a few degrees due to the temperature gradient in the stainless steel wall. For a qualitative study of the temperature profiles this setup was acceptable.

The following experimental results illustrate the properties of the sodium-argon heat pipe oven. Figure 4-3 shows temperature profiles along the length of the heat pipe oven for different values of the heating power. A homogeneous temperature plateau stretches up the heat pipe oven as far as the sodium vapour column stretches, due to the phase equilibrium existing in this volume. The heating power determines the length of the vapour column: the higher the heating power the longer the column so that the extra energy losses over the extended surface balance the extra heating power. The second observation is that heating power does not influence the equilibrium temperature measured in the vapour column - all three curves show a maximum temperature of about 740 degrees Celsius in the zone near to the heating element[3]. The conclusion is that the equilibrium temperature of the sodium vapour is not influenced by the power of the energy supply.

Note that, as illustrated in figure 4-2, the argon in the heat pipe oven is connected to a large reservoir volume of argon at the chosen pressure so that changes in the column length due to changes in the heating power will not cause a significant change in the total volume filled by

[3]Small discrepancies can be related to the fact that the thermocouples are measuring on the outer surface of the heat pipe.

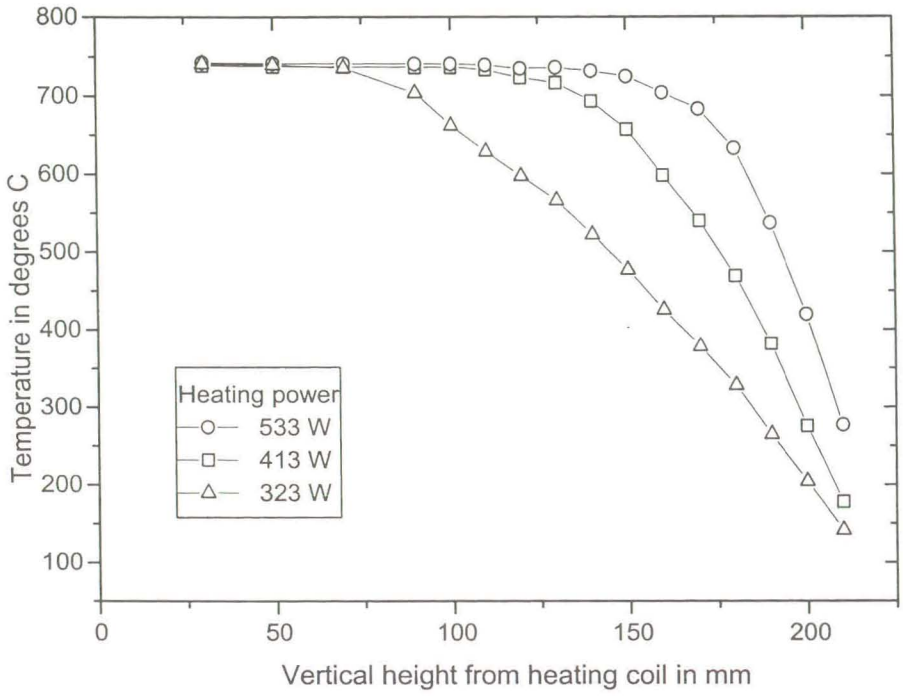

Figure 4-3: Temperature profiles in the vertical sodium argon heat pipe for different heating power values.

the argon and therefore in the pressure of the argon gas.

It is expected that the temperature of the vapour column is dependent on the pressure in the system. The relation between the equilibrium temperature and the vapour pressure is given by the sodium vapour pressure curve. Figure 4-4 illustrates temperature profiles of the heat pipe oven for different argon pressures (corresponding to the same sodium vapour pressures.) It can clearly be seen how the equilibrium (boiling) temperature of sodium depends on the sodium vapour pressure (which is equal to the external argon pressure). This data yields an experimental vapour pressure curve for sodium as illustrated in figure 4-5. The curves of figure 4-4 do not seem to agree with the statement of Vidal and Cooper [42] that the boundary layer becomes narrower at higher pressures due to a shorter mean free path for neutral-neutral collisions. In this experiment the time allowed for the heat pipe oven to stabilise after each adjustment of the external argon pressure was chosen as the minimum time needed for the equilibrium temperature of the vapour column to stabilise (about 20 minutes). This

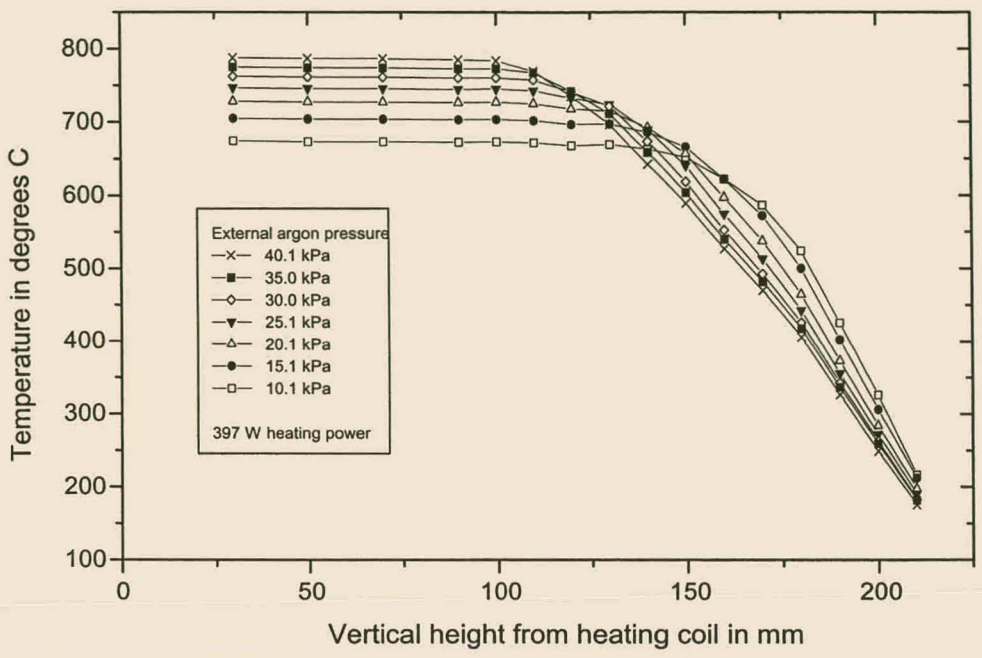

Figure 4-4: Temperature profiles in the vertical sodium argon heat pipe at different external argon pressures.

was possibly too short to allow the boundary zone that was disturbed by the large adjustment of the pressure to reach its equilibrium state at the higher pressure.

In figure 4-5 the experimental vapour pressure data for sodium is compared to existing data from literature. This data, acquired in different manners, show some variation and the experimental values fit the mean of this variation well, in spite of the fact that the temperature was measured on the outside surface of the heat pipe. This indicates that the temperature difference between the in- and outside of the wall is not more than a few degrees Kelvin. This shows a heat pipe to be a useful instrument for easy and accurate vapour pressure curve measurements as originally done by Bohdansky and Schins [4].

For the application of the heat pipe as part of a crossed concentric heat pipe for the generation of a medium for four-wave frequency mixing as a source of vacuum ultraviolet, it is not so important to know the absolute temperature to great accuracy, but it is important that the temperature is constant along the length of the vapour column, stable and reproducible. From the results illustrated in figures 4-3 and 4-4 it is clear that the temperature is constant along

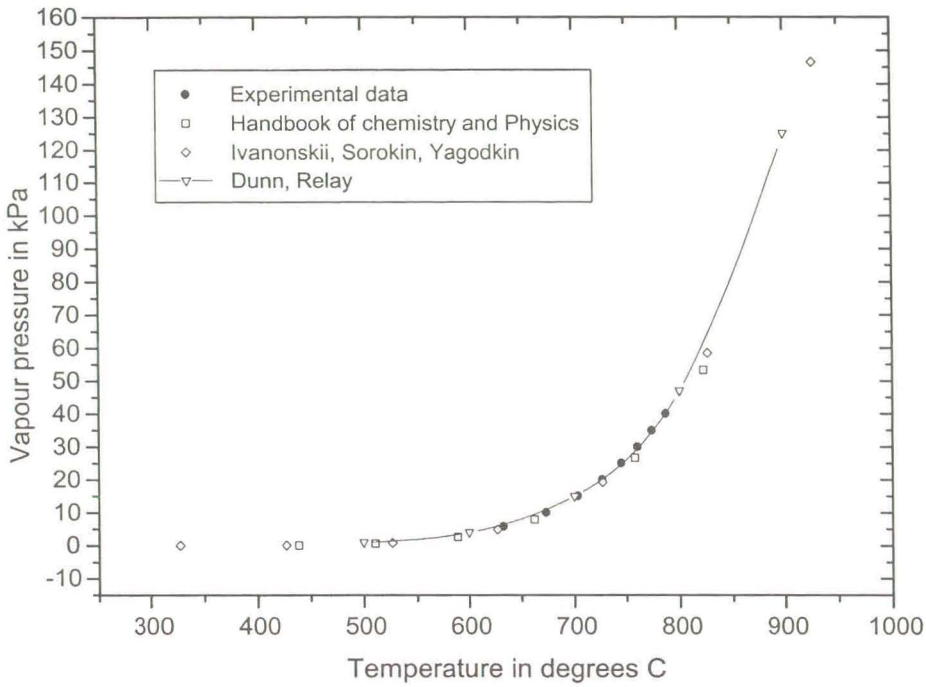

Figure 4-5: Experimental vapour pressure curve for sodium compared with values from literature.

the length of the vapour column in spite of the fact that the empty horizontal pipe running through the vertical one 100 mm above the heating element causes large heat losses from the vertical heat pipe at that position. Because the equilibrium temperature is determined only by the pressure of the sodium vapour via the vapour pressure curve of sodium, the stability and reproducibility of the temperature depend on that of the external argon pressure. The stability of the pressure is ensured by connecting the argon inlet to a large reservoir volume of argon gas. A rise in the heating power will cause the volume of the sodium vapour column to increase (due to more sodium in the vapour phase), but if the total volume of the system is large enough this volume increase does not change the pressure in the system significantly. It can be shown by calculation that if the length of the vapour column in the sodium-argon heat pipe used in this experiment increases with 50 mm, corresponding to doubling of the normal heating power, the argon pressure changes only by 0.8 percent. Practice shows that the conditions inside the heat pipe oven are reproducible from one warm up to the next.

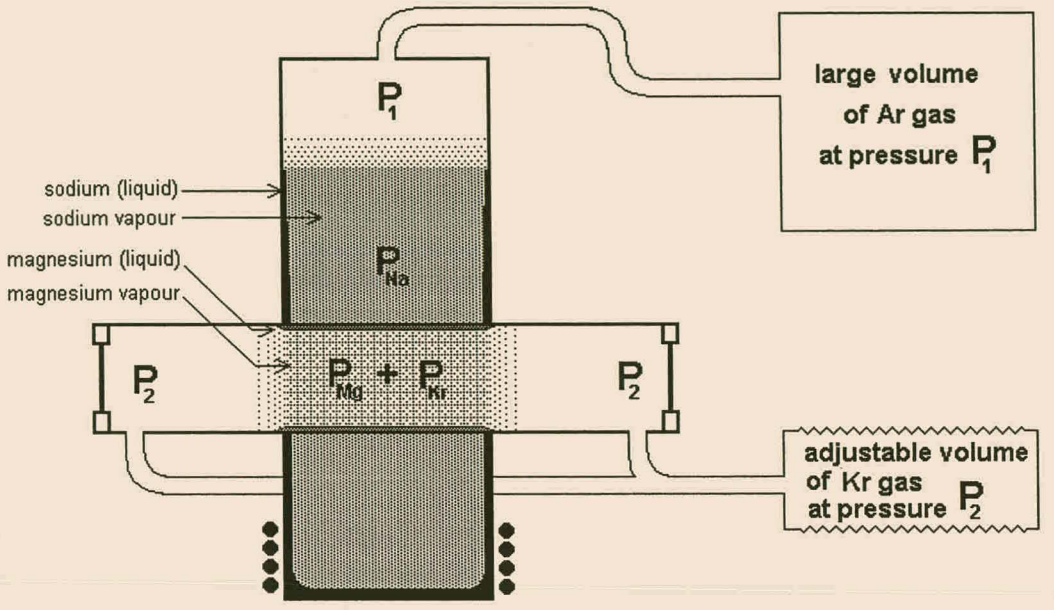

Figure 4-6: Schematic illustration of a crossed concentric heat pipe oven.

4.3 The crossed concentric heat pipe oven

4.3.1 Operation and properties

The modified heat pipe oven used to generate the medium for four-wave frequency mixing is called a crossed concentric heat pipe oven illustrated in figure 4-6. It consists of two separate heat pipes - a horizontal heat pipe inserted into a vertical one with a larger diameter as illustrated in figure 4-6 - with only thermal contact between them. The vertical heat pipe has sodium as working material and is loaded with argon gas to an external argon pressure P_1 that determines the temperature of the oven as discussed in section 4.2. The horizontal heat pipe has magnesium as working material and krypton as buffer gas at an external krypton pressure P_2.

The reasons for choosing sodium and argon for the vertical heat pipe are purely practical: sodium has a higher vapour pressure than magnesium at the same temperature which is favourable for stable operation of the heat pipe oven and to avoid start-up problems [49], and

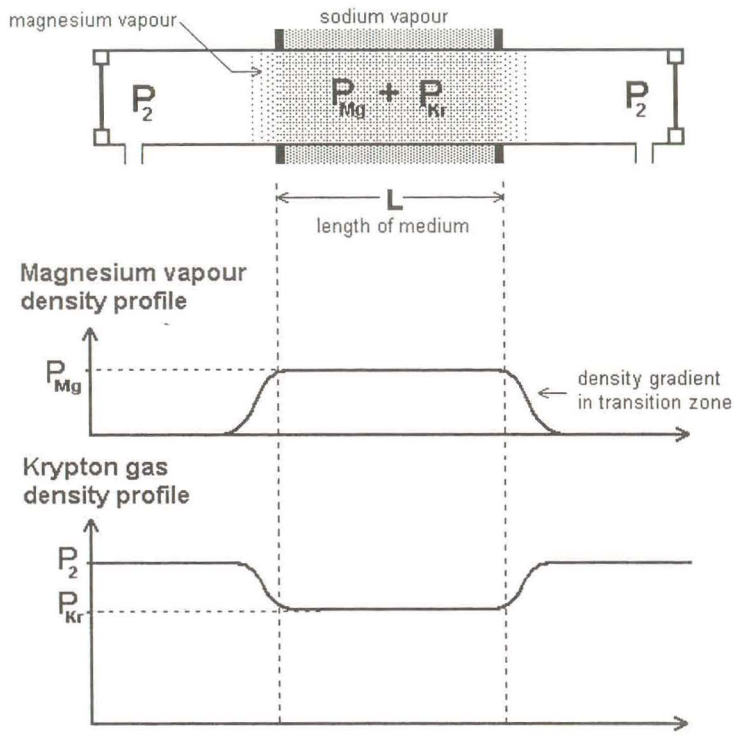

Figure 4-7: Schematic illustration of the density profiles of the magnesium vapour and krypton gas in the horizontal heat pipe.

argon is a noble gas that is readily available and inexpensive. The magnesium and krypton in the horizontal heat pipe are the two constituents of the nonlinear medium that is generated and are chosen for their optical properties.

The vertical heat pipe functions as discussed in section 4.2 with a heating element providing a constant heating power. The external argon pressure P_1 determines the sodium vapour pressure: $P_{Na} = P_1$. The sodium vapour pressure determines, according to the sodium vapour pressure curve, the temperature of the system: $T = T_{Na}$ where T_{Na} is the boiling temperature of sodium at pressure P_{Na}. The vertical heat pipe functions as an isothermal oven for the middle section of the horizontal heat pipe.

The main consideration in the functioning of the horizontal heat pipe is the fact that the middle section has a constant temperature $T = T_{Na}$. The value of this temperature determines, according to the magnesium vapour pressure curve, the partial vapour pressure of magnesium $P_{Mg}(T)$ in the middle section. The external krypton pressure P_2 is chosen to be higher than the expected value of $P_{Mg}(T)$. The middle section therefore contains a homogeneous mixture of magnesium vapour and krypton gas with the partial krypton pressure P_{Kr} equal to the difference between the external krypton pressure P_2 and the partial pressure of the magnesium vapour $P_{Mg}(T)$.

$$P_{Kr} = P_2 - P_{Mg}(T)$$

Both the magnesium vapour pressure $P_{Mg}(T)$ and the partial krypton pressure in the two-component medium P_{Kr} can be adjusted independently: The magnesium vapour pressure by adjusting the external argon pressure P_1 and thus the temperature in the vertical heat pipe, and the partial krypton pressure by adjusting the external krypton pressure P_2. In practice a suitable value for the partial magnesium vapour pressure is chosen by choosing the correct external argon pressure and the krypton pressure is then adjusted until the exact pressure ratio resulting in phase matching is reached. An accurately mechanically adjustable volume, as part of the krypton gas system, facilitates the fine-tuning of the krypton partial pressure without disturbing the closed system.

At both ends of the homogeneous medium in the heated middle section of the horizontal heat pipe a transition zone exist. Over the width of the transition zone the temperature, and therefore also the magnesium vapour pressure decreases with a certain gradient - see figure 4-7.

The crossed geometry of the crossed concentric heat pipe offers the advantage that the length of the magnesium krypton medium is well defined and constant being dictated by the diameter of the vertical heat pipe. The only uncertainty is the density profile in the transition zones. Fluctuations in the length of the sodium column in the vertical heat pipe due to fluctuations in the heating power do not influence the stability of the conditions in the magnesium krypton medium as long as the sodium vapour column extends well beyond the horizontal pipe. A stable medium can also be established long before the vapour column in the vertical heat pipe has reached its equilibrium position, thereby shortening the warm-up time of the crossed concentric heat pipe oven in comparison to the preceding concentric heat pipe oven models [37].

The noble buffer gas solves the problem of vaporised material being deposited on the windows as is encountered in many other experimental setups. In the crossed concentric heat pipe oven the inert gas confines the magnesium vapour and protects the windows from it. Traces of magnesium vapour may reach the windows carried by convection of the confining gas, but this can be prevented by (even rather large) apertures inserted in the horizontal heat pipe between the vapour column and the windows.

4.3.2 Influence of the density profile on phase matching

The asymmetry in the phase matching curve can now be explained in more detail, by considering the true density profile of the magnesium vapour in the heat pipe oven. In the central part of the medium volume the partial pressure of the magnesium vapour is fixed by the constant temperature provided by the vertical heat pipe. The phase matching condition $\triangle k = 0$ is met when a certain ratio P_{Kr}/P_{Mg} (about 12/1) is reached in the central region. With a lower P_{Kr} a phase mismatch $\triangle k < 0$ exists and with higher P_{Kr} a phase mismatch of $\triangle k > 0$. When a rectangular density profile is assumed, the phase matching curve is symmetrical around $\triangle k = 0$, but in practice the magnesium vapour pressure decreases with a certain gradient in the transition regions. In these regions volume elements of medium exist where P_{Mg} has some value lower than in the central part. For a buffer gas pressure below the pressure needed for phase matching in the central region (meaning that $\triangle k < 0$ in the central region), there must always be a small volume in both the transition zones where the phase matching condition is met due to the proportionally lower value of P_{Mg} in those volume elements. These small phase

matched volumes in the transition zones contribute significantly to the harmonic output in the (lower krypton pressure) region of the phase matching curve where $\triangle k < 0$ for the central region. For a buffer gas pressure higher than the pressure needed for phase matching in the central region (meaning that $\triangle k > 0$ in the central region) the phase matching condition is met nowhere in the medium and the phase matching curve decreases much more rapidly towards positive values of $\triangle k$ (higher krypton pressure).

4.4 Conclusions

In the vertical heat pipe of a crossed concentric heat pipe oven the physical properties of a phase equilibrium in a constant pressure system is employed to provide an extremely stable isothermal oven. Its temperature stability does not depend on a stabilised heating supply or any electronic control. Inside this isothermal oven (inside the middle section of the horizontal heat pipe) a second phase equilibrium ensures that the homogeneous temperature of the oven gives rise to a homogeneous magnesium vapour pressure throughout the bulk of the medium. The krypton gas has a double function: to facilitate phase matching of the medium and to confine the metal vapour, solving the problem of window contamination.

The two experimental variables in the generated medium - the temperature dependent magnesium vapour pressure and the partial pressure of the krypton gas in the medium volume - are controlled by the external pressures of the argon in the vertical heat pipe and krypton in the horizontal heat pipe respectively. These external pressures are easily adjustable, not subject to large or rapid fluctuations. They can be measured accurately to ensure reproducibility of the experimental conditions in the system. The external argon and krypton pressures are independent of each other, facilitating the independent adjustment of the magnesium vapour pressure and the krypton partial pressure in the two-component medium.

The homogeneity and stability of the medium generated in the crossed concentric heat pipe oven satisfy the requirements for efficient four-wave frequency mixing, and the adjustability of the well defined magnesium and krypton partial pressures facilitates phase matching.

Some aspects of the operation of a heat pipe oven have to be determined experimentally. The sodium vapour pressure is known with good accuracy, but to obtain the magnesium vapour

pressure vapour pressure curves have to be relied on, and therefore the fine tuning of the krypton pressure for phase matching is done experimentally. It is not easy to predict the changes during the warm-up time of the crossed concentric heat pipe oven and therefore to know from calculation what the heating power should be to obtain a certain column length, or what the argon and krypton pressures in the cold heat pipe oven must be to obtain phase matching when it is warmed up. These properties of the heat pipe oven must be determined experimentally, but once determined the system is stable and insensitive to normal changes in the laboratory environment.

The last statement can be motivated by calculation. If the temperature of the argon in the reservoir volume rises for some reason from 20 to 30 degrees Celsius it would cause a rise in the argon pressure in the vertical heat pipe of approximately 0.9 kPa at an operating pressure of 28.0 kPa. Making an approximation with the help of the gradient of the sodium vapour pressure curve in this pressure region, this rise in pressure will cause a rise in the sodium boiling temperature of approximately 2.5 Kelvin. At a temperature of 1025 K this rise in temperature will cause a rise in the magnesium vapour pressure of the order 0.07 kPa according to the magnesium vapour pressure curve. To re-establish phase matching under the new conditions the Kr pressure must be increased by an amount of the order 0.7 kPa. This simply requires adjusting the adjustable volume in the krypton gas system by a few turns of the winching mechanism. With the adjustable volume the Kr pressure can be adjusted by ± 7 kPa around 28.0 kPa.

These results illustrate how the stringent requirements for phase matching for third-harmonic generation can be met in a quite simple setup.

4.5 Limitations of the spectroscopic heat pipe

In spectroscopy modified heat pipes (heat pipe ovens) are not used primarily for heat transfer but for the stable temperature and well defined pressure conditions generated inside the operating heat pipe. In order to have the required homogeneous vapour column with well known density and temperature the heat pipe oven must be operated carefully within its limitations.

The first important practical consideration is that the heat pipe must be constructed using

stainless steel, for the parts as well as the welds, which is not attacked by the metals used as working material.

The circulation of the liquid phase of the working material back to the evaporation zone by capillary forces must be efficient to prevent the formation of "hot spots" where the wick in the evaporation zone becomes depleted of liquid. These "hot spots" not only disturb the stable operation of the heat pipe oven but may cause damage to the heat pipe oven due to overheating. In order to prevent this the wetting properties of the wick material must be compatible with the surface tension of the specific working material and the heat pipe oven must be loaded with a sufficient quantity of the working material to wet the wick structure. (A small excess of working material does not matter.) On the contrary it is advisable in the crossed concentric heat pipe to have a mechanism preventing the condensate to drip from the upper part of the condensation zone onto the horizontal heat pipe causing temporary cooling.

Under conditions of normal heat pipe operation the input heating power determines the length of the vapour column in the heat pipe oven. The heating power must in the first place be regulated to keep the vapour column inside the usable zone of the heat pipe away form water cooled parts where the working material will solidify. Both Boyd et al [6] and Vidal [45] found, by different ways of analysis, that high vapour flow velocities due to excessive heating power at a small vapour pressure disturb the homogeneous temperature and vapour pressure in the vapour column. It is therefore advisable to operate the vertical heat pipe of the crossed concentric heat pipe with a working material like sodium that has a relatively high vapour pressure at the required temperature, and to use the minimum heating power providing a vapour column of adequate length.

The spectroscopic heat pipe oven is designed for moderate heat transfer. If used with the correct quantity of working material and heating power to generate a vapour column of just adequate length, none of the limitations and optical conditions listed in heat pipe literature such as Faghri [10] cause problems.

Chapter 5

Experimental VUV laser source: results and discussion

The experimental work done as part of this study consists of two complementary parts: (I) the development of a vacuum ultraviolet laser source and the supplementary apparatus for use in molecular spectroscopy in the laser laboratory of the Physics Department of the University of Stellenbosch and (II) the experimental investigation of the characteristics of a similar system in the molecular spectroscopy laboratory of the Max Planck Institut für extraterrestrische Physik in Garching (near München) in Germany during a study visit of six weeks to the institute.

The experimental setup and procedures followed in the development of the apparatus in Stellenbosch are discussed in sections 5.1 and 5.2. The experimental setup and results obtained in Garching are discussed in sections 5.3 and 5.4. In chapter 6 the results of both parts of the experimental work are considered to draw conclusions on the optimal conditions for efficient generation of tunable vacuum ultraviolet in such an experimental setup.

5.1 Experimental setup in Stellenbosch

The experimental setup for generating tunable vacuum ultraviolet by four-wave frequency mixing was developed in Stellenbosch as a source for experimental work in the field of molecular spectroscopy. Photon energies in the vacuum ultraviolet spectral region are frequently needed for the first electronic excitation step of smaller molecules or one-step ionisation of larger or-

ganic molecules. The tunability is needed in order to make optimal use of the state selectivity offered by laser spectroscopy.

The systematic steps in the development of the experimental setup is:

1. Constructing the heat pipe oven system and vacuum system and connecting it to the existing linear time of flight mass spectrometer; setting up the diagnostic instrumentation and developing a customised computerised instrument control and data acquisition system. Testing and calibration of the various components of the setup.

2. Obtaining third-harmonic generation of a single incoming laser beam - the setup is illustrated in figure 5-1. In order to obtain third-harmonic generation in a newly built heat pipe oven it is important to meet the two critical conditions for efficient third-harmonic generation, namely the correct incident wavelength of 431 nm for two-photon resonance with the $3s^2 - 3s3d$ energy levels of atomic magnesium and the correct krypton magnesium pressure ratio in the medium for phase matching. In section 5.1.1 the practical aspects of phase matching of the medium in the crossed concentric heat pipe are discussed and in section 5.1.2 the calibration of the dye laser wavelength. The calibration was done in order to ensure beforehand that the laser wavelength is accurately tuned to the two photon resonance.

   After third-harmonic generation is achieved a systematic study of the influence of different experimental parameters does not only yield the optimal conditions for third-harmonic generation in the specific setup, but also serves as an experimental characterisation of the medium from which medium parameters such as optical depths and the density gradients can be derived.

3. Modification of the experimental setup (see figure 5-3) for the generation of tunable vacuum ultraviolet by non-degenerate sum-frequency generation, as described theoretically in section 3.7 and the experimental determination of the properties and limitations of the tunable vacuum ultraviolet source.

In this thesis the experimental work up to the second development step of the apparatus in Stellenbosch is covered. The experimental characterisation of the tunable vacuum ultraviolet

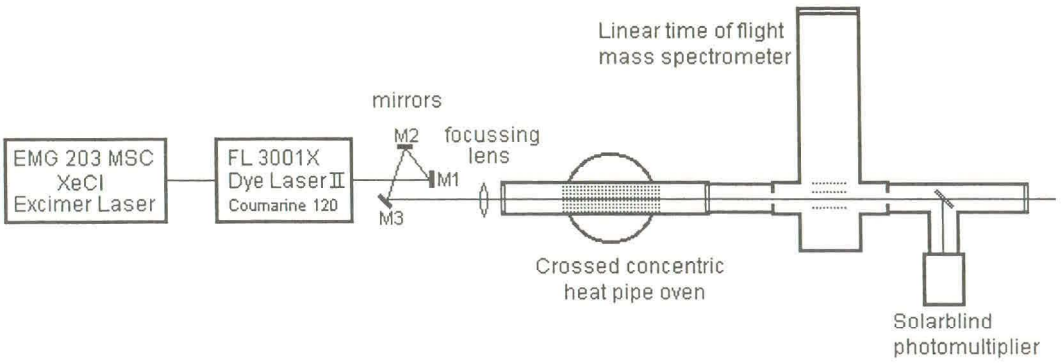

Figure 5-1: Experimental setup for third harmonic generation in Stellenbosch.

source presented in section 5.4 was obtained with an experimental setup in Garching that is similar to the final setup planned in Stellenbosch, and should therefore give an indication of the results that can be expected when the experimental setup for Stellenbosch is completed up to the third step of development.

The experimental setup for third-harmonic generation, that is illustrated schematically in Figure 5-1, is very simple. The single incident dye laser beam is aligned through the magnesium krypton medium in the crossed concentric heat pipe oven by means of mirrors. The beam should be focussed slightly to compensate for the divergence of the dye laser beam, but no polarising optics are needed since the angular momentum selection rule allows third-harmonic generation of the plane polarised dye laser beam.

The detail of the heat pipe system will be discussed in detail in section 5.1.1 and is therefore not shown in this diagram. The detail of the vacuum system and power supplies are also omitted for the sake of simplicity. The system for instrument control and data acquisition is discussed in section 5.1.3.

The single Lambda Physik FL 3001X dye laser providing the incident laser beam is pumped by a Lambda Physik EMG 203 MSC XeCl excimer laser with an output at 308 nm with maximum energy of ca. 300 mJ per 20 ns pulse at a 25 kV discharge voltage. To provide the two-photon resonant wavelength of 431 nm the dye laser is operated with Coumarine 120 (LC 4400) dissolved in methanol. When the prescribed concentration of 0.82 g/l for the oscillator cuvette

(diluted by a factor 3 for the main amplifier) is used the lasing peak is at 440 nm, giving about 80 percent of the peak energy at 431 nm. The lasing peak can be shifted to shorter wavelengths by using a lower concentration of the dye - about half the prescribed concentration in the oscillator cuvette to have the peak at about 430 nm. The dye laser beam is polarised linearly in the vertical direction and can be used directly for third-harmonic generation according to the selection rules as discussed in section 2.3.2.4. The three laser mirrors directing the laser beam before it enters the heat pipe oven are needed to bring the incident laser beam on the correct height and to align it through the heat pipe oven and time of flight mass spectrometer, because these two instruments are mounted on an optical table and cannot easily be aligned to the laser beam. The dye laser beam is focussed with a lens to have the beam waist approximately in the centre of the magnesium vapour krypton gas medium in the heat pipe oven. In the medium the third harmonic of the incident frequency is produced by the nonlinear interaction between the incident photons and the atomic magnesium, whereas the krypton facilitates phase matching. The outgoing beam, consisting of the fundamental as well as the generated third harmonic, leaves the heat pipe oven through a MgF_2 window and enters directly into the evacuated ionisation region of the time of flight mass spectrometer where the generated vacuum ultraviolet could be used for excitation or ionisation. In order to detect the generated vacuum ultraviolet, a part of the beam is split off by a reflector towards a solarblind photomultiplier (EMR Photoelectric model 542G-08-18, with sensitivity range $105-220$ nm) that is sensitive to the generated third-harmonic frequency, but insensitive to the fundamental frequency. The current signal of the generated third harmonic on the solarblind photomultiplier is large enough to be read by an oscilloscope or SR 250 boxcar over 50 Ω input impedance without any amplification. The circuit of the solarblind photomultiplier for measuring nanosecond pulses is illustrated in figure 5-2.

In order to have data on the pulse to pulse variation of the incident laser intensity that can be used to normalise the signal, a small fraction of the incident beam can be split off by the reflection from a thin glass window (a glass microscope slide) onto a photodiode to obtain a relative pulse to pulse intensity measurement. Care must be taken to avoid the saturation of the photodiode response by the intense pulses. In experiments where the wavelength of the incident beam is scanned, a window can also be used to split off a fraction of the incident beam to record an optogalvanic spectrum of neon simultaneously for wavelength calibration of

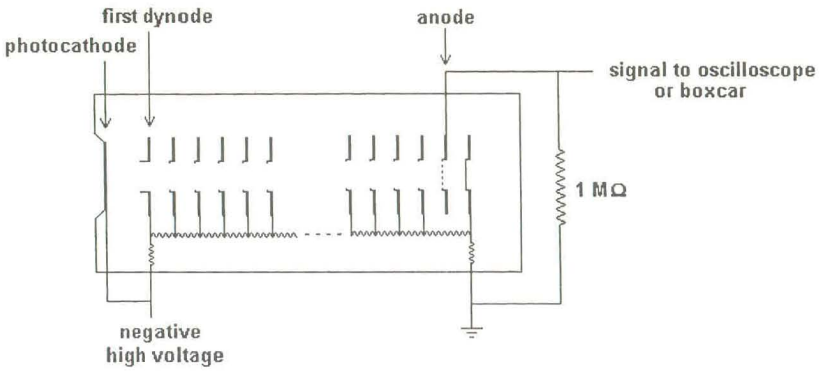

Figure 5-2: Circuit used with the EMR Photoelectric solarblind photomultiplier tube model 542G-08-18 for the detection of short pulses (of the order of 10 ns) such as the third harmonic signal.

the scan (see section 5.1.2). The third-harmonic signal, incident laser intensity, optogalvanic spectrum and external krypton pressure are finally all registered by boxcars and digitalised by a SR245 computer interface, from where the data is transferred via a HP-IB bus to a personal computer where it is processed and displayed in real time by the customised control program (see section 5.1.3 for more detail).

The planned experimental setup in Stellenbosch for generating tunable vacuum ultraviolet radiation by generation of the sum-frequency $\omega_s = 2\omega_1 + \omega_2$ is illustrated in figure 5-3. This requires a more complicated optical setup since the two incident pulsed laser beams must be (i) well synchronised in time in order to have good temporal overlap, (ii) combined colinearly and aligned as colinear beams through the heat pipe and (iii) left-hand and right-hand circularly polarised respectively. The purpose of the opposite circular polarisation of the incident laser beams is to make the generation of the third harmonics of either of the incident frequencies forbidden by angular momentum selection rules while the generation of the sum-frequency is allowed (see section 3.7). This optimises the efficiency of the sum-frequency generation by minimising the competing third-harmonic generation process.

Both FL 3001X dye lasers - dye laser I providing the two-photon resonant beam and dye laser II the nonresonant beam - are pumped by the same EMG 203 MSC XeCl excimer laser.

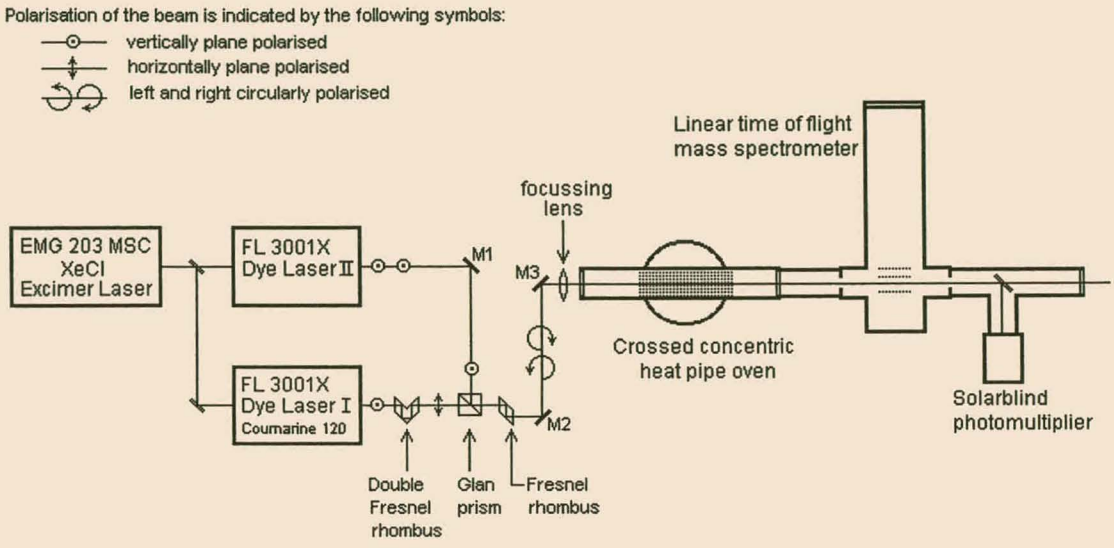

Figure 5-3: Planned experimental setup for four-wave frequency mixing with two laser beams in Stellenbosch.

This ensures good temporal synchronisation, without the problems of electronic jitter which is of the order of at least 5 ns when trying to synchronise two excimer lasers. Care must be taken to keep the optical path length, from the excimer laser outcoupling window through the dye laser up to the beam combiner, equal for the two dye lasers in order to maintain good temporal overlap of the 20 ns laser pulses from the two dye lasers in the medium. (A path length difference of 1.5 m will cause a delay of 5 ns which is a quarter of the total pulse length.) Therefore figure 5-3 shows the beam combiner at the output aperture of dye laser I although the heat pipe is nearer to the output aperture of dye laser II.

As discussed theoretically in section 3.7 the incident laser beams must be left- and right-hand circularly polarised to suppress third-harmonic generation of the incident frequencies. This is done by first changing the polarisation of the incident beam coming from dye laser DL I by 90 degrees by a double Fresnel rhombus. After combining the two beams colinearly the two internal reflections in a single Fresnel rhombus are used (instead of a quarter-wave plate) to change the polarisation from two perpendicularly plane polarisations to left- and right-hand circular polarisations.

When the generated vacuum ultraviolet is in the future applied for doing spectroscopy it will be better to measure the vacuum ultraviolet energy, that is needed in order to normalise the measurements made, before the radiation enters the region where the spectroscopic process takes place (for example in the ionising region of the time of flight mass spectrometer.) A MgF_2 window, reflecting a fraction of the beam towards the solarblind photomultiplier and transmitting the rest of the beam, can be positioned between the output window of the heat pipe and the application. In this setup no provision is made to separate the generated vacuum ultraviolet from the fundamental beams or to focus the generated vacuum ultraviolet beam onto a sample volume. Whether it is necessary to do so will depend on the specific application of the vacuum ultraviolet radiation.

5.1.1 Construction and operation of the heat pipe oven system

The crossed concentric heat pipe oven used in Stellenbosch, illustrated in figure 5-4, is the heat pipe oven described by Scheingraber et al [37]. This heat pipe provides a well defined optical path length in the active medium of about 60 mm as well as a short warm-up time. It was designed for the generation of a nonlinear medium of strontium and xenon. Due to the relatively high two-photon absorption cross-section of strontium vapour, the conversion efficiency in a strontium vapour medium does not benefit from a much longer medium (see the discussion of equation 3.17 for an explanation). This heat pipe oven can also be used to generate a magnesium krypton medium although the conversion efficiency, in the case of a magnesium vapour medium, can be increased by the use of the modified concentric heat pipe described by Steffes et al [38], providing a longer optical path length in the active medium (about 300 mm). Such a heat pipe oven is presently under construction in Stellenbosch.

Preliminary experiments were done with a smaller prototype of the crossed concentric heat pipe oven to determine operational considerations such as heating power, warm-up time, pressure stability, and to verify the thermodynamic characteristics of the heat pipe oven. The results of these experiments were discussed in section 4.2.1. These results confirmed that the vertical heat pipe of the crossed concentric heat pipe oven has the following properties:

- The temperature in the heat pipe is constant for all practical purposes as far as the pure sodium vapour column extends up the heat pipe. Between the sodium vapour column

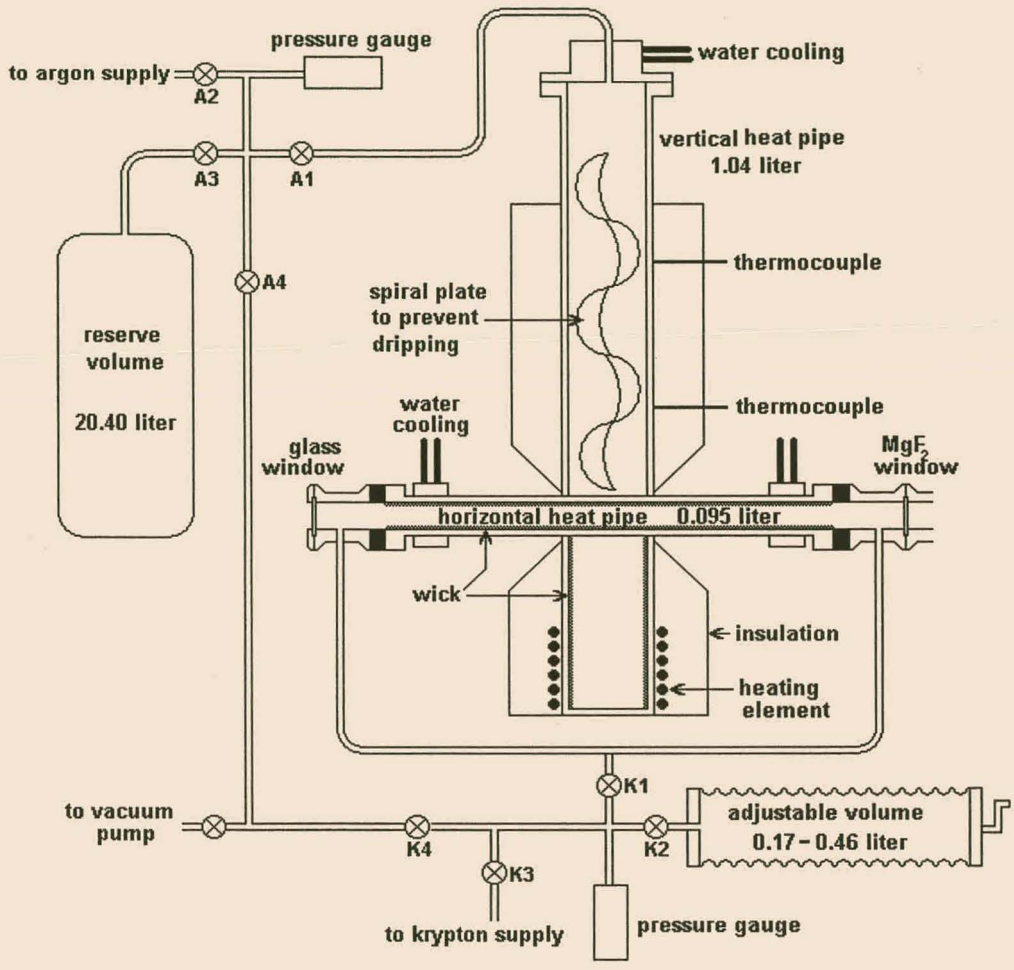

Figure 5-4: Schematic illustration of the crossed concentric heat pipe and the vacuum system.

and the confining argon gas a narrow transition zone exists over which the temperature decreases with a certain gradient.

- The heating power of the heating element determines the height of the sodium vapour column in the heat pipe (see figure 4-3, page 90), but does not have any direct influence on the temperature of the column, making the heat pipe an ideal isothermal oven for the central part of the horizontal heat pipe as soon as the vapour column has surpassed the crossing of the two heat pipes.

- The temperature of the sodium vapour column of the heat pipe is determined by the vapour pressure of the sodium according to the sodium vapour pressure curve as expected. This is illustrated in figures 4-4 and figure 4-5. Because of the net flow of vapour atoms in the dynamic equilibrium, the sodium vapour and argon gas do not mix (except for the transition zone) and the vapour pressure of the sodium is equal to the external pressure of the argon which can easily be adjusted and stabilised.

In sections 4.3 and 4.4 the functioning and advantages of the crossed concentric heat pipe oven are discussed. The most important aspect of the functioning of the crossed concentric heat pipe is the relation between the two externally regulated noble gas pressures and the composition of the magnesium krypton medium. The external argon pressure in the vertical heat pipe determines the sodium vapour pressure that determines - according to the sodium vapour pressure curve - the temperature of the middle section of the horizontal heat pipe, and the temperature determines the vapour pressure of the magnesium, $P_{Mg}(T)$, in the two-component medium in the middle section of the horizontal heat pipe. The external krypton pressure determines the partial krypton pressure in the medium according to the relation $P_{Kr} = P_{Kr(external)} - P_{Mg}(T)$. For good performance and reliability of the heat pipe oven these two externally regulated gas pressures must be stable and not subject to fluctuations (especially the argon pressure on which the equilibrium in the vertical heat pipe depends), they must be easily and accurately adjustable (especially the krypton pressure that must be carefully adjusted to obtain phase matching) and they must be accurately measurable.

Figure 5-4 is a schematic illustration of the crossed concentric heat pipe oven with its gas supply system. The heating element of the vertical heat pipe is a simple rod-shaped oven

element (specified to take power up to 1000 W) wound into a coil that fits tightly around the heat pipe. The vertical heat pipe is insulated to reduce energy losses, but the insulating material is cut away around the horizontal heat pipe in order to keep the temperature gradient in the transition zones both sides of the heated middle zone as steep as possible. In the vertical heat pipe gravitation can be relied on to return the liquid sodium to the heating zone at the bottom, and a wick is only applied to the inner walls of the heating zone itself to ensure an even distribution of liquid sodium in the heating zone and avoid the formation of "hot spots" (see section 4.5.) The spiral plate inserted into the vertical heat pipe from the top avoids that liquid sodium from the upper part of the vertical heat pipe drips directly onto the horizontal heat pipe causing temporal cooling. In the horizontal heat pipe a wick is essential to avoid depletion of the magnesium in the middle section by returning the liquid magnesium from the outer regions where it condenses to the heated middle section where evaporation takes place. The wick consists of a stainless steel mesh pressed to the inside of the vertical heat pipe by a stainless steel spring, and extends up to the region at both ends that are water cooled.

To ensure the stability of the argon pressure, also in the case of fluctuating heating power, the vertical heat pipe is permanently connected to a large reservoir volume of argon at the chosen pressure. The external krypton pressure must be easily adjustable and therefore the horizontal heat pipe is connected to bellows of thin stainless steel of which the volume can be adjusted slowly and accurately by turning a crank-handle. The volume of the bellow was chosen to be larger than the volume of the rest of the krypton system including the horizontal heat pipe so that its range of adjustment provides a significant pressure tuning range. It is obvious, but important that the two ends of the horizontal heat pipe must be permanently connected by a bypass to avoid pressure differences between the two ends that could force the magnesium vapour out of the centre. The external argon and krypton pressures are measured by commercial absolute pressure meters (Keller PAA-23/8465-1 censor and Instrotech readout for the argon and a Sensotech STJE/1834-02 censor and readout for the krypton). Two thermocouples are clamped into small stainless steel blocks welded onto the outer surface of the vertical heat pipe at heights of 7 and 18 cm above the horizontal heat pipe. The temperature readings obtained from them are definitely not a very accurate measure of the temperature inside the heat pipe, due to the poor heat conductivity of stainless steel as well as the influence of the heat reaching

them by the hot air that rises from the heating element, making the temperatures measured by the thermocouples to an extent dependent on the heating power, which is not true for the temperature inside the heat pipe. The function of these thermocouples is only to give an indication of how far the sodium vapour column extends up the heat pipe. The heating power must be controlled to keep the sodium column higher than the lower thermocouple, but lower than the upper one.

The lid of the vertical heat pipe and brass blocks clamped around the horizontal heat pipes near its ends are water cooled. This is needed to protect the rubber o-rings used for vacuum sealing as well as the windows at the ends of the horizontal heat pipe from high temperature conducted by the stainless steel. The windows are further protected from temperature shock by a plastic fitting (darkly coloured in diagram). Each window is protected from traces of magnesium vapour carried by convection in the argon gas, by fitting a cylindrical piece into the end of the heat pipe that confines the aperture between the window and the central part of the heat pipe to about 4 mm diameter.

The heat pipe system was constructed, leak tested with a helium leak tester and then loaded with 100 cm^3 sodium and 23 g = 13 cm^3 magnesium respectively. The procedure of loading and starting up the heat pipe for the first time was taken from the communication of Steffes [39] and adapted for the specific experimental setup (see "Manual for Construction and Use of the Crossed Concentric Heat Pipe Oven System" [40]). The first few times the sodium heat pipe was heated, the pressure increased considerably due to evaporation of the low boiling paraffin in which sodium was stored. In order to purify the system from the paraffin the heat pipe was heated up to 300 - 500 °C, left to cool down and then evacuated as soon as the temperature (as indicated by the lower thermocouple) was near the melting point of sodium (about 98 °C). At that temperature the sodium vapour pressure is already close to zero, but most of the lower boiling paraffin is still in vapour phase. The procedure was repeated about 5 times until the pressure rise during heating was not more than two or three kPa. After the vertical heat pipe was functioning the magnesium was loaded into the horizontal heat pipe, taking care to place it in the middle of the pipe. The same procedure was followed for purifying the horizontal heat pipe, using argon, before finally filling the horizontal heat pipe with krypton.

Once the heat pipe oven is purified of low boiling impurities the changes during heating are

predictable and once warmed up, the pressures and temperature are stable. This heat pipe oven takes about 2 hours for heating with a heating power initially adjusted to about 800 W and after 2 hours turned down to between 600 and 700 W. During the heating process the external argon pressure rises by about 2 kPa and the external krypton pressure rises by about 2.5 kPa (both from an initial pressure of about 20 kPa). The heat pipe oven is considered to be in a condition of stable operation once the temperature at the lower thermocouple does not increase any more with time. The temperature at the upper thermocouple has to be monitored from time to time during operation and the heating power may need to be adjusted between 600 and 700 W to keep the vapour column below the upper thermocouple (indicated by a temperature at the upper thermocouple of about 200 degrees lower than at the lower one).

During operation magnesium crystals slowly form at both sides of the magnesium vapour column just outside of the heated section of the horizontal heat pipe, eventually blocking the optical path. The crystals are removed by heating the horizontal heat pipe at both sides where it protrudes from the vertical heat pipe with a commercial hand-held gas burner.

In this crossed concentric heat pipe oven setup the external pressures of the argon and krypton are externally regulated and known to the accuracy given by the pressure meters. The temperature of the oven and the magnesium vapour pressure are physically well-defined by the relation between the external argon pressure and these two quantities via the vapour pressure curves of sodium and magnesium, but the values of these two parameters are not well known because in this setup no provision is made to measure them independently. Relying on the vapour pressure curves, both the temperature and magnesium vapour pressure can however be estimated and for the use of the heat pipe oven for vacuum ultraviolet generation this is sufficient. In figure 5-5 the external argon pressure, the magnesium vapour pressure as estimated from the vapour pressure curves, and the external krypton pressure needed for phase matching according to the pressure ratio of 12.7 given by Junginger [21] are plotted against the temperature in the heat pipe oven. In practice the argon pressure is chosen to give - via the temperature - the desired magnesium vapour pressure and the krypton pressure is adjusted to obtain phase matching taking the values of figure 5-5 as a first guess. With the help of the bellow and taps in the system the external krypton pressure can be lowered or raised in a slow and controlled way, even beyond the adjusting range of the bellow volume (see the manual [40]).

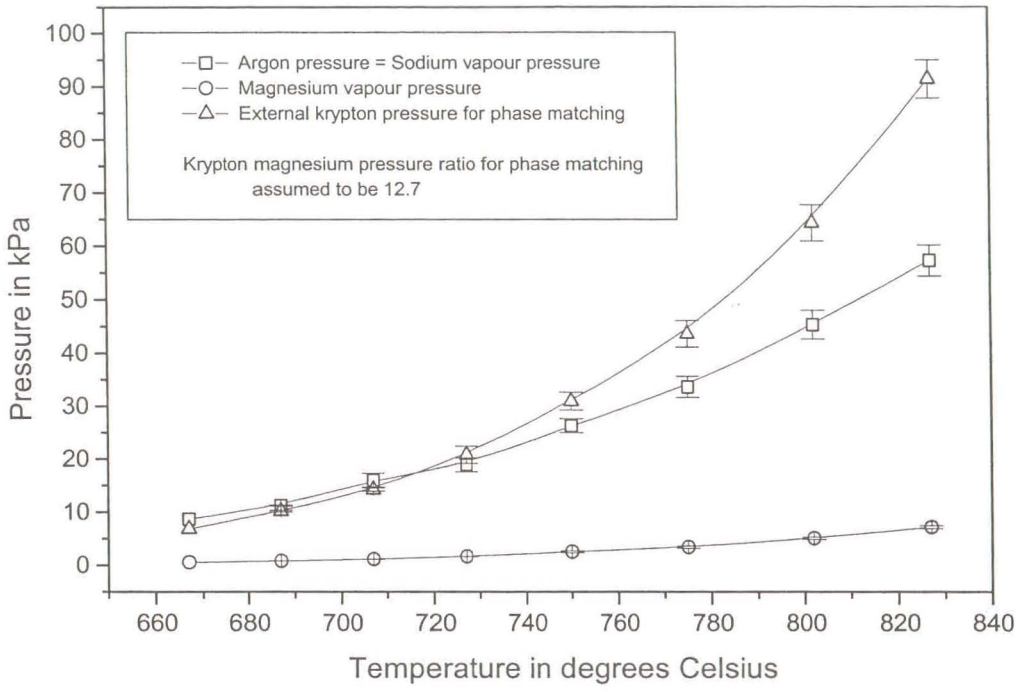

Figure 5-5: External argon and krypton pressures and estimated magnesium vapour pressure for different temperatures in the vertical heat pipe. (The true independent variable is the external argon pressure by which the temperature is determined according to the sodium vapour pressure curve.)

5.1.2 Optogalvanic wavelength calibration of the dye laser

One of the most important conditions for the observation of third-harmonic generation is the correct incident wavelength at 431 nm to obtain enhancement of the nonlinear susceptibility by two-photon resonance. In order to ensure that the laser is exactly tuned to two-photon resonance it was considered to be necessary to calibrate the wavelength of the incident laser beam correctly to an accuracy of 0.02 nm, which is the linewidth of the resonance according to experimental results obtained in the Garching heat pipe oven. The optogalvanic method was chosen to do the calibration of the dye laser frequencies in the region around 431 nm.

5.1.2.1 Optogalvanic spectroscopy

The optogalvanic effect can be described as a change in the electrical properties of a discharge caused by illuminating the discharge volume with radiation of a wavelength corresponding to an atomic or molecular or ionic transition of an atomic or molecular species in the discharge [12].

In a hollow cathode lamp a sustained discharge with a relative high electron temperature (about 3×10^4 K [24]) exists. The discharge volume therefore contains significant populations - of both the filler gas (generally Ne or Ar) and sputtered cathode material - in excited atomic as well as ionic energy levels. The electric properties of the discharge (such as the discharge current) are determined by the electron density in the discharge. The electron density is determined by the total ionisation rate from all atomic energy levels. Different collisional ionisation processes contribute to the total ionisation rate [11]. When the discharge volume is irradiated by a laser tuned to the wavelength corresponding to any transition between two populated levels of the atomic or ionic species present, the optical pumping causes a perturbation of the steady state populations of two or more levels. In general the collisional ionisation rates from different atomic levels are unequal so that a perturbation of the populations of the levels produce a perturbation of the ionisation balance and a temporal change in the electron density in the discharge. A change (say decrease) in the electron density causes a change (decrease) of the discharge current that can be measured as a change in voltage over a resistor in the lamp circuit. The optogalvanic effect can correspond to a decrease or increase in the discharge current depending on the ionisation rates and other processes coupling the levels of which the

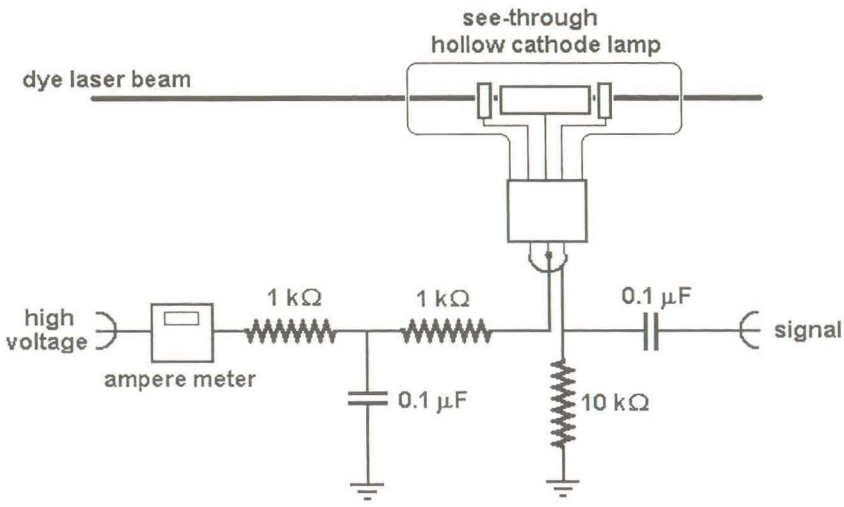

Figure 5-6: Diagram for the circuit used to record the optogalvanic spectra.

populations are perturbed by the laser radiation. It must be taken into account that, due to the large Coulomb cross-sections, the coupling of neighbouring energy levels in a discharge plasma is very efficient and a laser induced population change in one level is immediately transferred to a number of neighbouring levels too [50].

The optogalvanic effect was first reported by Penning in 1928 but it only became a widely used spectroscopic technique after 1976 when Green et al [12] demonstrated the high sensitivity of this technique in combination with tunable lasers. The optogalvanic effect is applied in many ways as a spectroscopic technique although the quantitative description of the process by means of rate equations is difficult and offers limited results [11]. Optogalvanic spectroscopy has however been proved to be extremely convenient for wavelength calibration of tunable laser sources [2] with the advantages of sensitivity, reproducibility and experimental simplicity - the components needed are readily available.

5.1.2.2 Experimental method

The optogalvanic spectra used for the calibration were recorded using the circuit illustrated diagrammatically in figure 5-6 for the zirconium and neon see-through hollow cathode lamp. The dye laser beam is aligned through the centre of the cylindrical cathode and anode of the

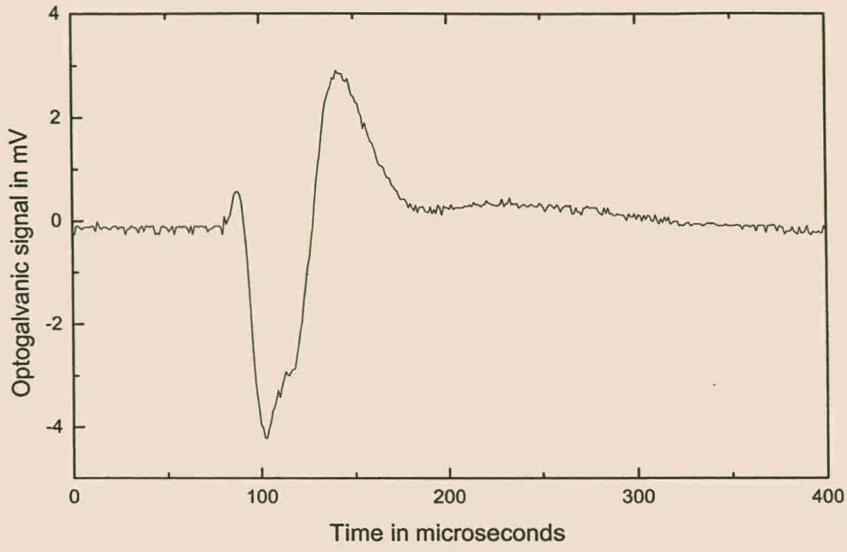

Figure 5-7: Optogalvanic signal of strong 588.233 nm line of neon as observed on the oscilloscope. With the circuit that was used a negative value of the signal corresponds to an increase in discharge current.

lamp without impinging on the electrodes in order to avoid noise caused by the photo-electric effect. The change in the lamp current, caused by excitations by the laser pulse, was measured as a change in voltage over a 10 kΩ resistor. The high voltage for the lamp was provided by a DC lamp source. The AC-coupled signal could be viewed directly on a Hewlett Packard 54616B oscilloscope. Figure 5-7 shows the typical form of an optogalvanic signal. The signal shown in figure 5-7 is a very strong optogalvanic signal belonging to the strong absorption line of neon at 588.233 nm. The signals in the spectral region used for the calibration were smaller; except for the strongest signals often not easily observable on the oscilloscope. For recording the spectra needed for calibration in the region 423 - 435 nm the signal was sent to a SR 250 boxcar gated integrator. The gate, 5 μs wide, was positioned over the first (negative) peak of the signal requiring a delay of about 3.5 μs after the trigger coming from the excimer laser pumping the dye laser. The dye laser and data acquisition were controlled by a personal computer running a customised HPVEE (Hewlett Packard Visual Engineering Environment) program that records for each position of the laser grating the wavelength and the mean of the signal over ten laser pulses with a repetition rate of 19 Hz. The laser wavelength was adjusted in steps of 0.005 nm.

Lamp	Lamp current (mA)	Wavelengths scanned (nm)
Zr-Ne (see-through)	11	422.8-435.0
Zr-Ne (see-through)	9	422.8-435.0
Ca-Ne	6	422.5-434.9

Table 5.1: Optogalvanic spectra recorded for calibration of the dye laser.

The spectra recorded for the calibration are summarised in table 5.1. The spectra of the see-through zirconium-neon (Zr-Ne) lamp, as illustrated in figure 5-8, have a good signal to noise ratio because the geometry of the see-through lamp allows the laser beam to pass through the main discharge volume without impinging on either the anode or cathode and thus a pure optogalvanic signal is produced. In the case of the calcium-neon (Ca-Ne) lamp with the regular lamp geometry it cannot be prevented that the beam impinges onto the cathode producing a strong, but wavelength insensitive photo-electric signal, on the wing of which the true optogalvanic signal has to be detected. This yields a spectrum with a poor signal to noise ratio. In spite of this the spectra of the calcium-neon lamp could be used to identify a number of lines in the zirconium-neon spectra unambiguously as neon lines on ground of the fact that they occur in the spectra of both lamps.

First it was tried to identify the lines observed in the optogalvanic spectra with the help of standard wavelength tables based on atomic emission of neon, zirconium and calcium; comparing the three spectra with each other to decide which lines belong to which element. This proved to be a very difficult task due to the complexity of the optogalvanic spectra - each containing lines belonging to several possible excited states of two different atomic species - and the lack of any very strong line that could be identified unambiguously with a line in the tables. The intensity patterns of neighbouring lines could not be used in the comparison between the optogalvanic spectra and the tables since a strong emission line may not give a strong optogalvanic signal and vice versa. No convincing fit between the spectra and the emission wavelength tables could be found in this way. The publication "An Atlas of Optogalvanic Transitions in Neon" by Ashworth and Brown [2] was obtained. Comparison of the measured spectra with the calibrated spectra in the atlas immediately showed an obvious and excellent agreement, and the identification of individual lines was easy. The wavelengths of 33 lines identified in this way were used to fit a polynomial calibration function for the dye laser wavelength readout in the

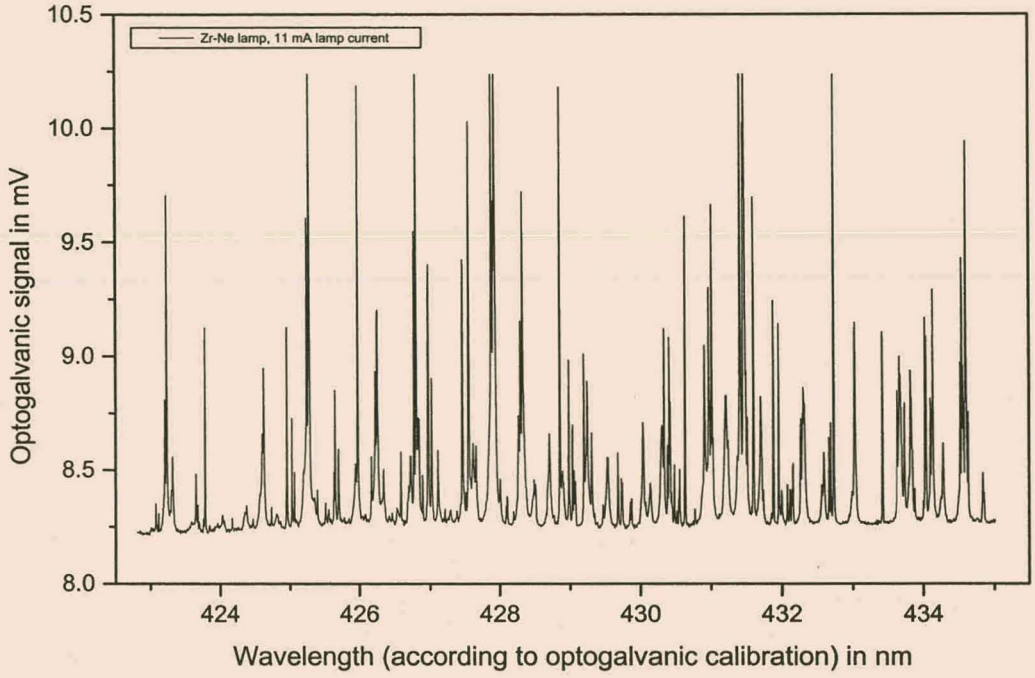

Figure 5-8: Optogalvanic spectrum used for the calibration of the dye laser wavelength. This optogalvanic spectrum, showing primarily neon lines, was obtained with the see-through zirconium hollow cathode lamp in the region 422.8 nm to 435 nm.

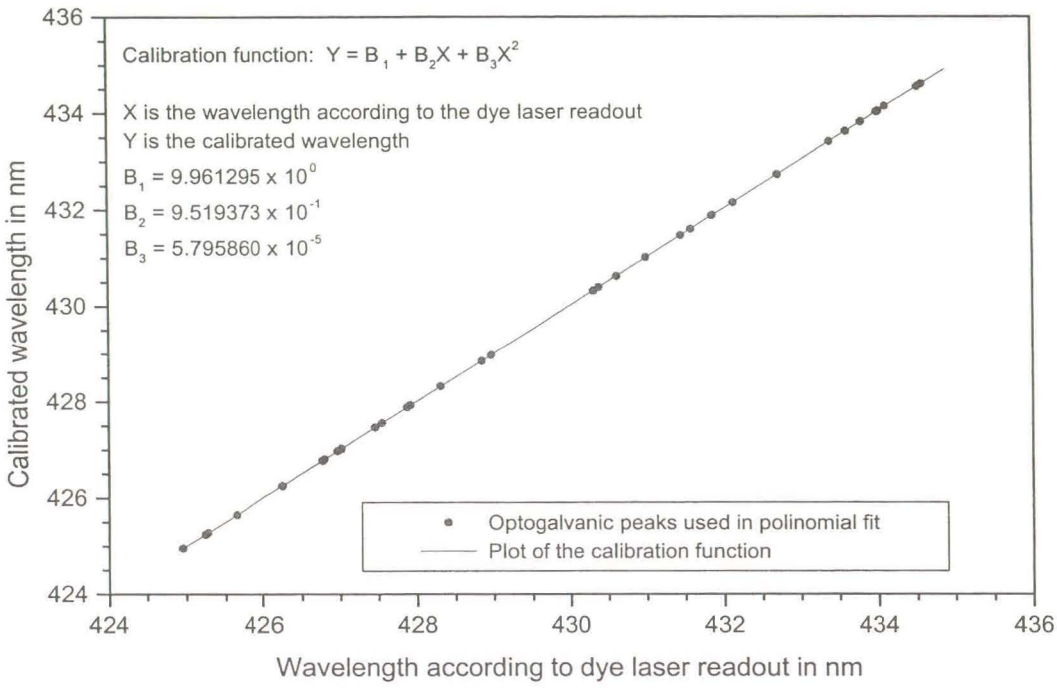

Figure 5-9: Plot of the optogalvanic data used for the wavelength calibration as well as the calibration function obtained by the least squares fit.

spectral region 423 - 435 nm by means of a least squares fitting program running in Fortran 77.

5.1.2.3 Results

In the atlas a distinction is made between lines to which wavelengths (to 7 significant figures) were assigned using the MIT wavelength tables [30] and lines the wavelengths of which were found by linear interpolation (to 6 significant figures). In the region 423 to 435 nm the atlas spectra contain 34 of the lines in the first category of which all 34 could be identified in the optogalvanic spectra of the zirconium lamp. The measured peak wavelengths and the corresponding peak wavelengths given in the atlas for 33 of these lines were used to fit the polynomial calibration function. Of the 34 interpolated lines in this spectral region 32 were identified in the experimental optogalvanic spectra but were not used in the calibration.

The results of the fit is the second order polynomial calibration function given in figure 5-9. The wavelengths calculated for the 33 calibration lines by means of this calibration function agree with the wavelengths given in the atlas with a standard error of 0.002 nm. The accuracy

of the calibration is therefore limited by the uncertainty of about 0.005 nm in the experimental peak positions.

5.1.2.4 Conclusion

The optogalvanic method is a convenient method for wavelength calibration of a dye laser in the spectral region studied. Using a see-through hollow cathode lamp, the method is experimentally simple and gives reproducible spectra with a high signal to noise ratio and a sufficient number of known neon lines for accurate function fitting.

The accuracy of the calibration function obtained in this experiment is sufficient for the purpose of finding the two-photon resonance of atomic magnesium.

The accuracy of the calibration is limited by the uncertainty in the experimental peak positions. This can be improved (possibly over smaller spectral regions of interest) by recording the optogalvanic spectra with smaller wavelength intervals. The smallest wavelength steps possible with the dye laser in this spectral region is 5.25×10^{-4} nm. The interpolation between the peaks can be improved by simultaneously recording the interference pattern produced in a quartz etalon.

5.1.3 Instrument control and data acquisition

A personal computer is used to control the lasers and record the data while scanning either the laser wavelength or another experimental variable such as the external krypton pressure. In figure 5-10 the system for instrument control and data acquisition is illustrated schematically.

The computer, with a HP 82335 interface card installed, is connected by HP-IB bus to the dye laser of which the wavelength is scanned, the SR 245 computer interface as well as the oscilloscope (Tektronix TDS 520 or Hewlett Packard 54616B). The oscilloscope is used to observe the signals in time and to adjust the gate of the boxcar for measuring each signal. Where the position of the boxcar gate is important its optimal position was determined by adjusting the delay while observing the measured signal. The oscilloscope setup can be controlled and the trace stored as an ASCII file by means of the computer and the corresponding driver software. In order to record scans customised programs were written in HPVEE controlling the dye laser in burst mode, where the number of pulses per burst and repetition rate are chosen by the user, either for a single wavelength or while scanning the wavelength over a user defined interval in

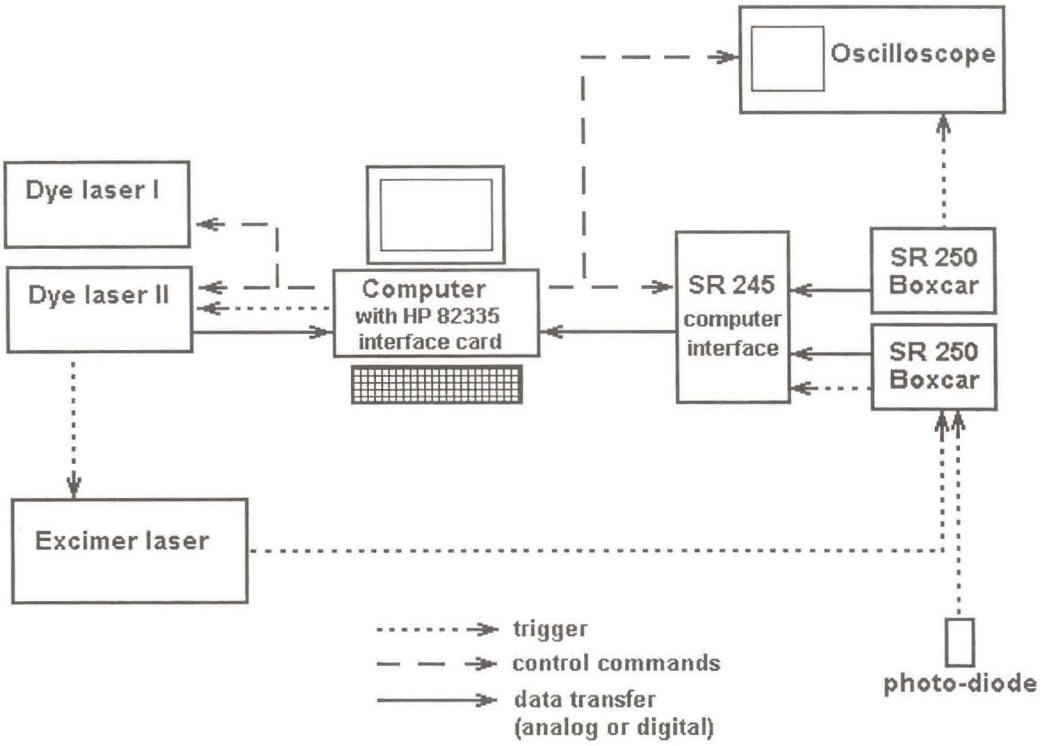

Figure 5-10: Schematic illustration of the computerised system used for instrument control and data acquisition in the experimental setup in Stellenbosch.

user defined wavelength steps. The dye laser triggers the excimer laser to release each pulse. Either the synchronous output signal of the excimer laser or a signal from a photodiode receiving radiation split off from the dye laser beam is used to trigger the data acquisition system (boxcars and SR 245 computer interface). The signals that are recorded in the scan are brought to the input ports of the SR 245 computer interface, via a boxcar integrator if necessary. For each[1] laser pulse the value of all the signals are stored by the computer interface. After the burst is finished the data is transferred as a matrix to the computer. The program processes the data, calculates the mean value and standard deviation for each burst that are plotted and saved to a file before the next burst is released. The detail of each of the programs for recording wavelength scans and phase matching curves can be obtained from the description that is part of the program.

The diagnostic instruments were tested and calibrated as far as possible. The two pressure gauges measuring the external argon and krypton pressures (Keller PAA-23/8465-1 censor and Instrotech readout for the argon and a Sensotech STJE/1834-02 censor and readout for the krypton) were calibrated together until repeatedly giving the correct values at 10^{-2} kPa (the typical pressure reached by a rotation vacuum pump) and the atmospheric pressure as obtained from a mercury barometer. The Sensotech has a DC current output that could be terminated on 1 kΩ to obtain a voltage signal that could be recorded by the computer interface. Calibration of this voltage value against the readout of the gauge yielded a linear calibration function used in the HPVEE programs to calculate the external krypton pressure.

In case of the thermocouples the standard data tables for NiCr/NiAl thermocouples were used to obtain a calibration function that could be used to calculate the temperatures relative to the reference thermocouple from the voltage readout. In the third-harmonic generation setup the absolute temperatures were not considered important and a block of aluminum at room temperature was used as reference. As mentioned in section 5.1.1 these thermocouples are only used to monitor the height of the sodium vapour column in the heat pipe. All absolute temperatures given in the experimental results were calculated from the measured sodium vapour pressure using the sodium vapour pressure curve, without using the thermocouple measurements.

[1]It was found that errors are avoided by making the number of actual laser pulses at least 2 more than the number of triggers that the SR 245 computer interface is programmed to record.

The power supply for the solarblind photomultiplier was calibrated and the photomultiplier was tested by focusing the emission of an arsenic hollow cathode lamp with strong emission lines at 193.7, 197.2 and 189.0 nm onto the photomultiplier, chopping the light to observe the difference. The signal of the photomultiplier could not be calibrated with the available apparatus. Therefore all signals are relative values given in millivolt. It can be noted that, when the emission of the arsenic hollow cathode lamp operating near its maximum lamp current is focussed (in air) onto the solarblind photomultiplier cathode, the maximum signal amplitude obtained was about 1 mV. The fraction of the generated vacuum ultraviolet reaching the solarblind photomultiplier cathode after scattering from the glas window gives a signal of about 500 mV. This gives some indication of the relative power of the generated vacuum ultraviolet although these values cannot be used for any quantitative purposes.

In most of the scans done a small percentage of the incident dye laser beam was split off by a glass window (microscope slide) onto a photodiode and the signal used as a trigger for the boxcars and computer interface to avoid the ca. 1 μs delay between trigger and signal if the excimer synchronous output is used as trigger. The signal of the photodiode was found unfit for use as a measure of the dye laser energy since even by significant attenuation of the reflected beam no intensity region could be found where the photodiode signal showed linear dependence on the beam energy. The third-harmonic signal measured in the experimental scans was therefore not normalised with regard to the energy of the fundamental wave.

5.2 Experimental results for third-harmonic generation

The aim of the experimental work was to construct the apparatus in which a suitable magnesium krypton medium could be prepared, to obtain third-harmonic generation and to investigate the characteristics of the specific experimental setup with regard to vacuum ultraviolet generation by third-harmonic generation. The experimental results are compared qualitatively with similar results from literature and with the theory as far as the experimental conditions permit, in order to characterise the magnesium krypton medium[2].

[2]When comparing the results obtained with that of Junginger et al it must be taken into account that a nitrogen laser was used as pump laser in their experiments resulting in pulses that are shorter by a factor of 10 compared to the excimer pumped system. This has an influence on the behaviour of the optical system.

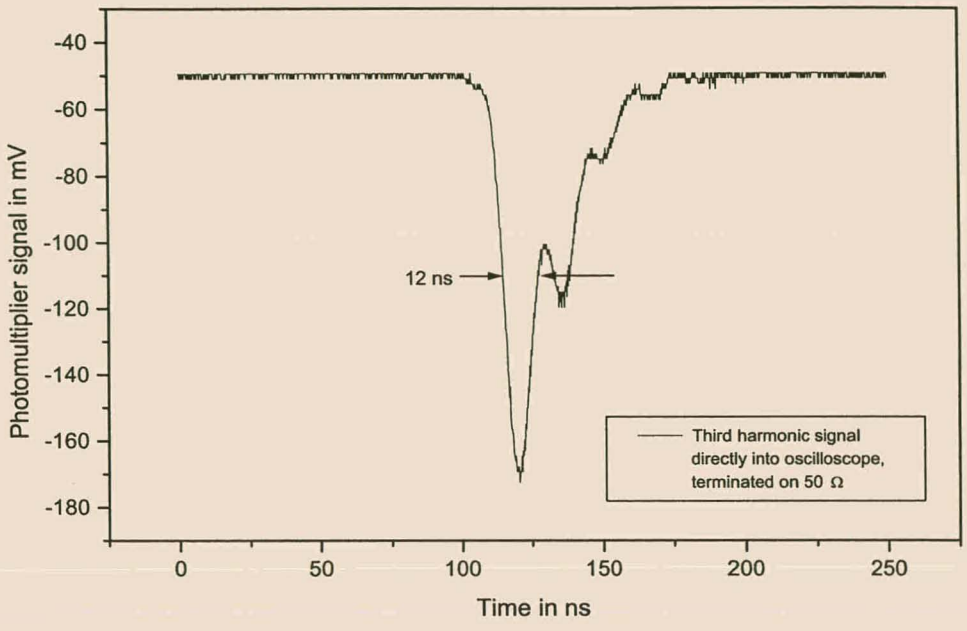

Figure 5-11: The third harmonic signal from the solarblind photomultiplier as observed on the oscilloscope. The smaller peaks following the main peak are artifacts of the electronic circuit.

A reproducible vacuum ultraviolet third-harmonic signal was observed for the first time under the following conditions: laser wavelength 431.0 nm, external argon pressure 23.5 kPa, external krypton pressure 24.0 kPa, excimer laser energy 220 mJ per pulse at 21 kV and 2 Hz, dye laser energy 5.2 mJ per pulse at 431 nm, the laser beam focussed by a $f = 20$ cm lens positioned 29 cm from the centre of the horizontal heat pipe to have the beam focussed in the center of the medium. Without the focusing lens no third-harmonic generation could be observed. Due to the divergence of the laser beam over the path length of about 2 m from the dye laser to the heat pipe the peak intensity of the unfocussed beam is not sufficient for observable third-harmonic generation.

In figure 5-11 a typical third-harmonic signal as observed directly on the oscilloscope is shown. The first highest peak is the true signal and the reflection-like peaks following with intervals of about 15 ns are electronic artifacts of which the origin is still uncertain[3]. The

[3]Changing the length of the co-axial cable from the photomultiplier to the oscilloscope, terminating the co-

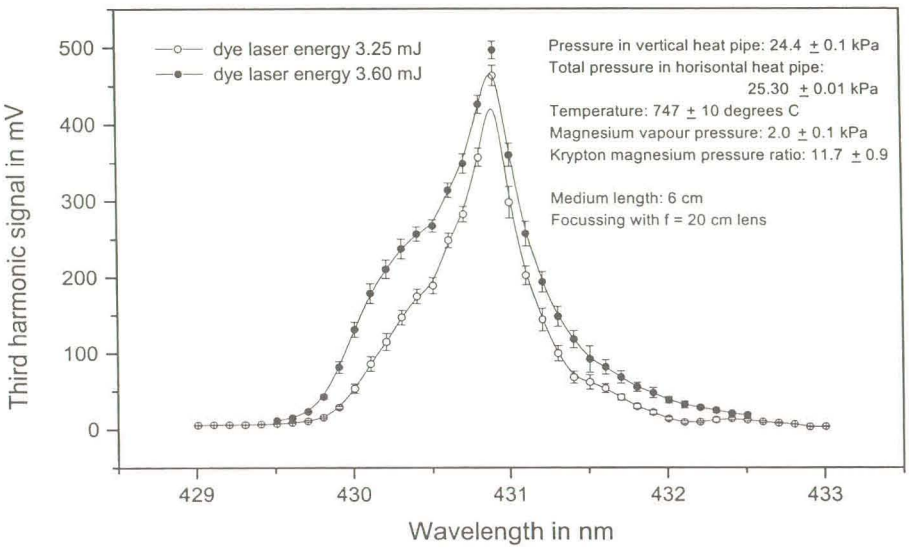

Figure 5-12: An experimental plot showing the dependence of the third harmonic signal on the wavelength of the incident beam, i.e. on the two-photon resonance, for a rather tightly focussed incident beam. The two curves, obtained with two different energies of the incident laser beam, shows a higher energy to cause broadening of the peak.

true signal has a full width at half maximum of 12 ns and an amplitude of more than 100 mV with the high voltage on the photomultiplier 2500 V. The dependence of the signal on the two-photon resonant wavelength and the krypton magnesium pressure ratio served as evidence that the observed signal was the third-harmonic signal and that the solarblind photomultiplier is indeed insensitive to the visible incident beam.

The fundamental experiments in the investigation of the characteristics of the system as vacuum ultraviolet source are to determine the wavelength and the pressure ratio that gives optimal conversion by measuring the wavelength dependence and phase matching curve.

5.2.1 Two-photon resonance

The dependence of the third-harmonic signal on the wavelength of the incident beam is

axial cable with a different impedance and changing the impedance in the photomultiplier circuit did not change these reflections or the period of 15 ns at all.

illustrated in figure 5-12 for two different incident beam energies.

For these measurements the medium was phase matched for 431 nm, but since the wavelength is only tuned over a narrow region and the phase matching peak is broad (see figure 5-15), phase matching is not expected to have a significant influence on the signal. The observed peak is therefore a direct result of the enhancement of the third order susceptibility responsible for third-harmonic generation by two-photon resonance of the incident frequency. The experimental peak occurs at a wavelength of 430.88 ± 0.005 nm that corresponds exactly with the two-photon resonant wavelength of 430.88 nm given by Wallace et al [51], and differs by 0.12 nm from the 431.00 nm tabulated for the $3s^2 - 3s3d$ transition of magnesium by Moore [28]. Figure 5-12 shows a peak at the two-photon resonance wavelength that is much wider (full width at half maximum of about 0.5 nm) than the 0.02 nm peak width expected for the two-photon absorption linewidth according to results that have been obtained with the heat pipe in Garching. Pressure broadening or Doppler broadening of the linewidth cannot be the cause since the result was obtained at roughly the same total pressure and temperature as the results in Garching. Power broadening is a possible explanation. This is confirmed by the observation that the width of the peak increases as the energy of the incident beam is increased. It is however unlikely that power broadening alone could be responsible for such a large line broadening effect without causing saturation behaviour. An intensity profile similar to figure 5-12 obtained by Steffes et al [38, figure 4] shows typical saturation behaviour - a dip in the centre of the peak caused by changes in the medium due to a significant population of the two-photon resonant level - with a peak width of only about 0.03 nm. The single peak in figure 5-12 indicates that the intensity region of saturation has not yet been reached.

The remaining factor that could influence the line profile is the focussing condition. This was investigated by replacing the $f = 20$ cm lens with a $f = 80$ cm lens to obtain a less tightly focussed incident beam. The result for the wavelength dependence of the less tightly focussed beam is showed in figure 5-13. The decreased focussing (or progression towards the parallel beam limit) does not only result in a much narrower peak at 430.88 nm (full width at half maximum of about 0.1 nm), but also shows that the unsymmetrical broadening observable on the short wavelength side of the peak in figure 5-12 is caused by two reproducible, evenly spaced "side bands".

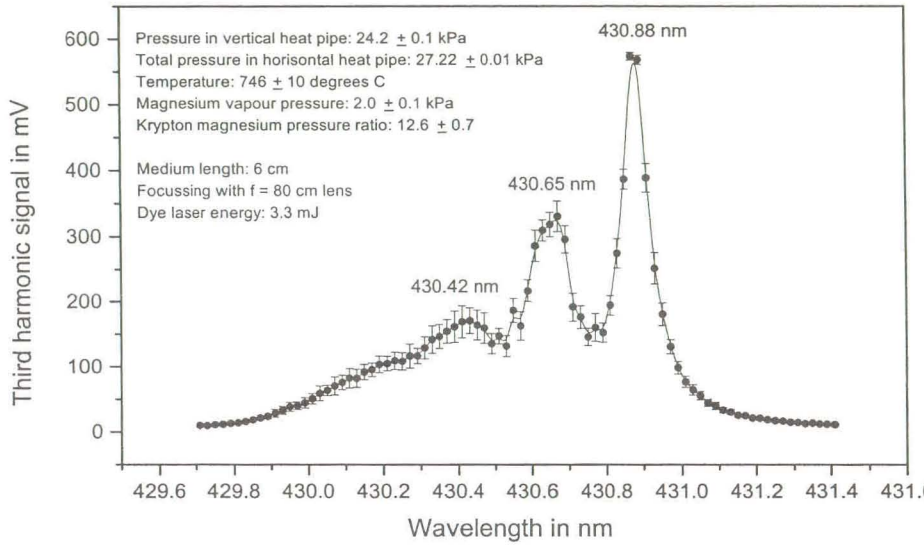

Figure 5-13: The dependence of the third harmonic signal on the incident wavelength around two-photon resonance for a less focussed incident beam. The curve yields the two-photon resonance peak at 430.88 nm as well as two additional smaller peaks at intervals of 0.23 nm - probably due to imperfect alignment of the dye laser cavity and grating allowing more than one frequency to exist in the laser cavity.

These side bands were thought to be caused by frequency side bands occurring in the output of the dye laser at certain positions of the grating as it is rotated to scan the wavelength. It was tested by repeating the experiment: once after having made small adjustments to the alignment of the dye laser resonator and a second time using the seventh grating order instead of the sixth order (as used in all previous experiments). As illustrated in figure 5-14 the adjustment of the laser resonator resulted in one side band occurring closer to the main peak, and in using the seventh grating order the side bands vanished. It shows that these side bands are artifacts caused be imperfect aligning of the dye laser that can be eliminated by fine-tuning the dye laser alignment or the use of an etalon.

Comparing the curves of figures 5-12, 5-13 and 5-14 it is clear that the line broadening can be reduced to the values measured in Garching by adjusting the focussing condition to obtain a parallel beam and by reducing the laser bandwidth.

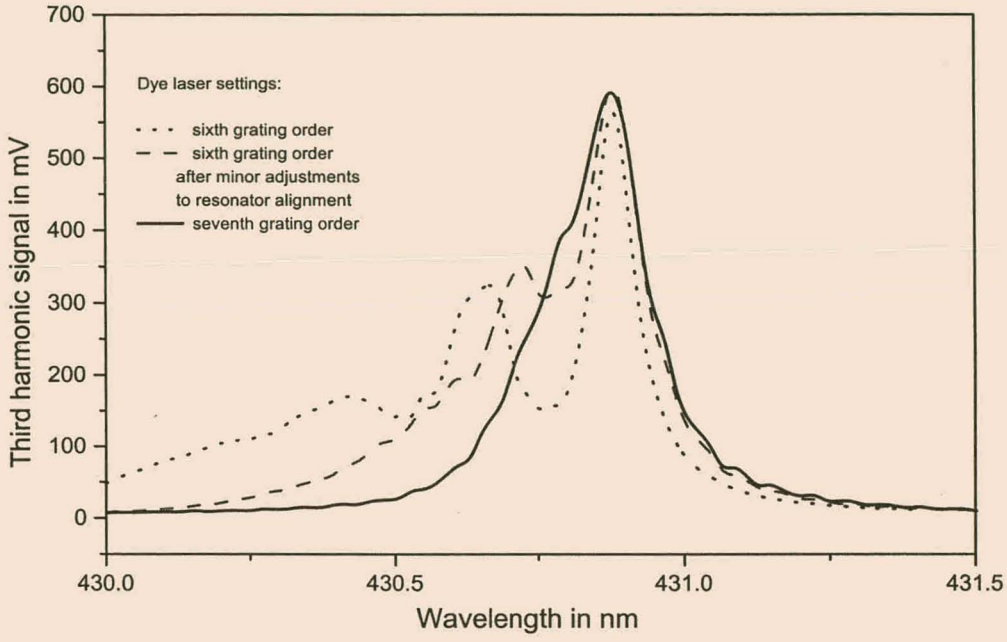

Figure 5-14: The influence of adjustment to the dye laser resonator on the artificial side bands observed in the two-photon resonance profile of the third harmonic signal. The dotted line represents the original observed profile with two side bands, the dashed line a profile measured after small adjustments to the resonator alignment were made and the solid line a profile measured using a different grating order. The other experimental conditions were the same for all three curves.

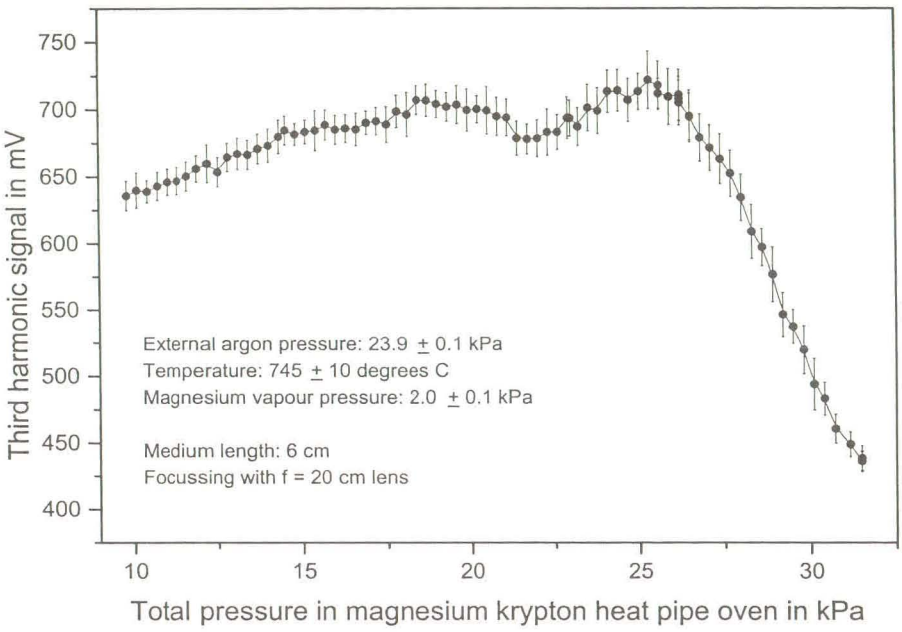

Figure 5-15: An experimental phase matching curve, showing the dependence of the third harmonic signal on the krypton magnesium pressure ratio, for a tightly focussed incident beam. The curve was obtained by slowly lowering the krypton pressure while the magnesium vapour pressure remains constant.

5.2.2 Phase matching

The first experimental phase matching curve, figure 5-15, illustrates the dependence of the third-harmonic generation process on pressure ratio of the magnesium krypton medium for an incident beam tightly focussed by a $f = 20$ cm lens. The curve was obtained by decreasing the external krypton pressure from 32 to 10 kPa at a rate of about 0.8 kPa per minute at a constant magnesium vapour pressure of about 2.0 kPa. The third-harmonic signal value measured at each pressure step is the average of 30 laser pulses with the laser operating at a repetition rate of 3 Hz. The low repetition rate and the averaging were necessary to reduce the large pulse to pulse variation of the excimer laser energy at higher repetition rates that is amplified by the cubic dependence of the third-harmonic signal on the input intensity, resulting in large fluctuations of the measured signal.

The experimental phase matching curve in figure 5-15 resembles the typical phase matching curve obtained with a tightly focussed beam. As discussed at the end of section 3.3 and illustrated in figure 3.3 of [47], focussing of the incident beam does not only shift the peak towards negative values of $\triangle k$, but also smears out the oscillatory structure, yielding a smooth asymmetrical curve in the tightly focussed limit as illustrated in 3-6. The third-harmonic signal shows a peak at the krypton magnesium pressure ration of 11.8 ± 1.

In figure 5-16 the phase matching curve of an incident beam, less tightly focussed by a lens with 80 cm focal length, is illustrated. The same experimental conditions as for the measurement on the tightly focussed beam apply. The asymmetry of the curve, decreasing much more rapidly towards higher krypton pressures due to the magnesium vapour density gradient in the transition zones (discussed in section 4.3.2 on page 96) is clearly visible. On the small pressure side of the maximum the oscillatory structure of the phase matching curve as predicted by the theory for parallel beams (see figure 3-4) is prominent. The phase matching peak for this curve is measured at a krypton magnesium pressure ratio of about 12.9 ± 0.7, that corresponds well with the value of 12.7 obtained by Junginger et al [21] and is significantly higher than the value of 11.8 for the tightly focussed beam of figure 5-15. This observation agrees with the theoretical prediction (section 3.3) that focussing of the (Gaussian) incident beam shifts the condition for phase matching towards negative values of the phase matching factor $\triangle k$, which is found at lower krypton magnesium pressure ratios. Junginger's results confirm this observation [21].

The intervals between the successive minima of the oscillations can be used to determine the effective length of the optical medium experimentally. The minima occurs when $\triangle kL = 1, 2, 3...$ where L is the length of the medium and $\triangle k$ is influenced by the absolute magnesium vapour pressure. By comparing the curve in figure 5-16 with the phase matching curve of Junginger et al measured at approximately the same magnesium vapour pressure and a medium length of 30 cm, a medium length of 5.7 cm is calculated. This confirms that the magnesium vapour is effectively confined to the heated zone in the horizontal heat pipe, the length of which is defined by the 6 cm diameter of the vertical heat pipe.

The dependence of the oscillatory structure of the phase matching curve on the optical depth for the generated frequency - as discussed in theory in section 3.2 - makes it possible to

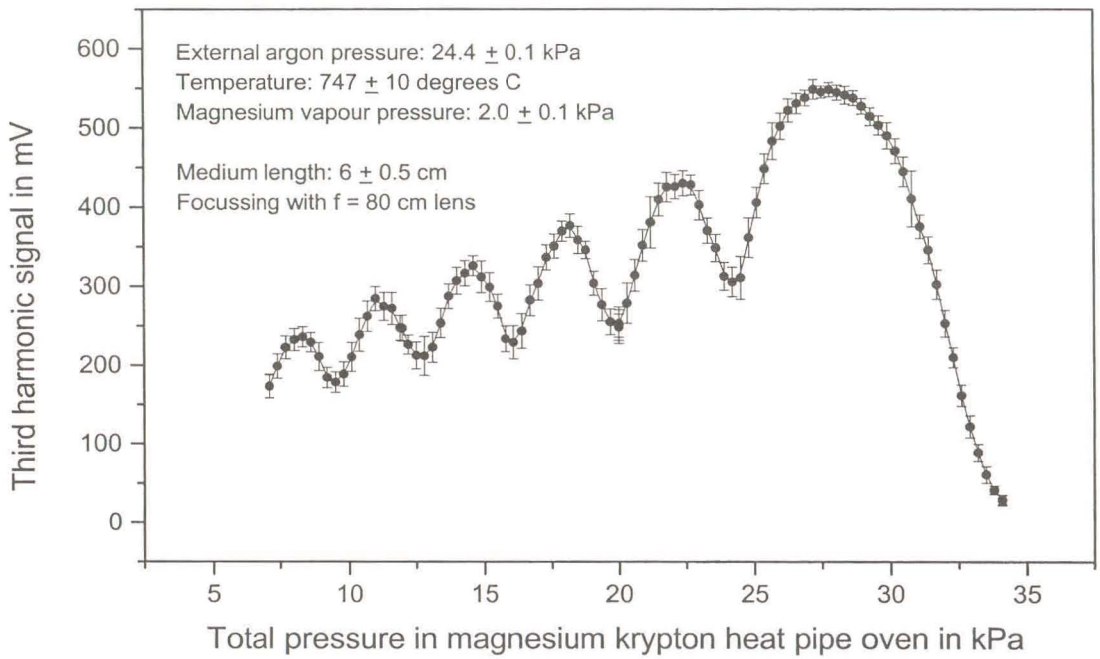

Figure 5-16: Phase matching curve for a less tightly focussed beam. The oscillatory structure of the curve as predicted by theory for the limit of a parallel beam is observable on the small pressure side of the main maximum.

deduce the optical depth of the nonlinear medium from the experimental third-harmonic phase matching curve (as long as the optical depth at the fundamental frequency is much smaller than at the generated frequency, $\tau_i \ll \tau_s$). The oscillatory structure of the phase matching curve is quantified by the modulation depth that is defined as the intensity ratio of the curves through the maxima (neglecting the main maximum at $\triangle kL = 0$) and minima of the phase matching curve respectively. The experimental phase matching curve is unsymmetrical due to the density profile of the medium in the heat pipe, but to first order the modulation depth on the side where the oscillatory structure is visible is not affected by the asymmetry [38].

The relation between the modulation depth and the optical depth $\Gamma_s = NL\sigma^{(1)}(\omega_s)$ (where $\sigma^{(1)}(\omega_s)$ is the one-photon absorption cross-section for the generated sum frequency ω_s, in this case the third harmonic) can be derived from the expression for the phase matching factor, expression 3.13. The modulation depth is the ratio of the maximum and minimum values of the phase matching factor with $\cos(\triangle kL)$ equal to -1 and $+1$ respectively. Therefore the modulation depth M can be expressed as

$$\begin{aligned} M &= \frac{F(\cos\triangle kL = -1, \Gamma_s)}{F(\cos\triangle kL = +1, \Gamma_s)} \\ &= \frac{1 + \exp(-\Gamma_s) + 2\exp(-\frac{\Gamma_s}{2})}{1 + \exp(-\Gamma_s) - 2\exp(-\frac{\Gamma_s}{2})} \end{aligned}$$

Substituting $\exp(-\frac{\Gamma_s}{2}) = z$ the relation

$$M = \frac{1 + 2z + z^2}{1 - 2z + z^2}$$

is obtained. The second order equation can be solved for z, giving the solution[4]

$$z = \frac{2(M+1) \pm \sqrt{4(M+1)^2 - 4(M-1)^2}}{2(M-1)}$$

and $\Gamma_s = -2\ln z$ can be calculated from the value of the modulation depth M.

The application of this method to obtain the modulation and optical depth for the experimental phase matching curve for sum-frequency generation is illustrated in figure 5-17. Second

[4]The smaller solution of the two, corresponding to the minus sign, is the valid one giving a positive value for τ_s.

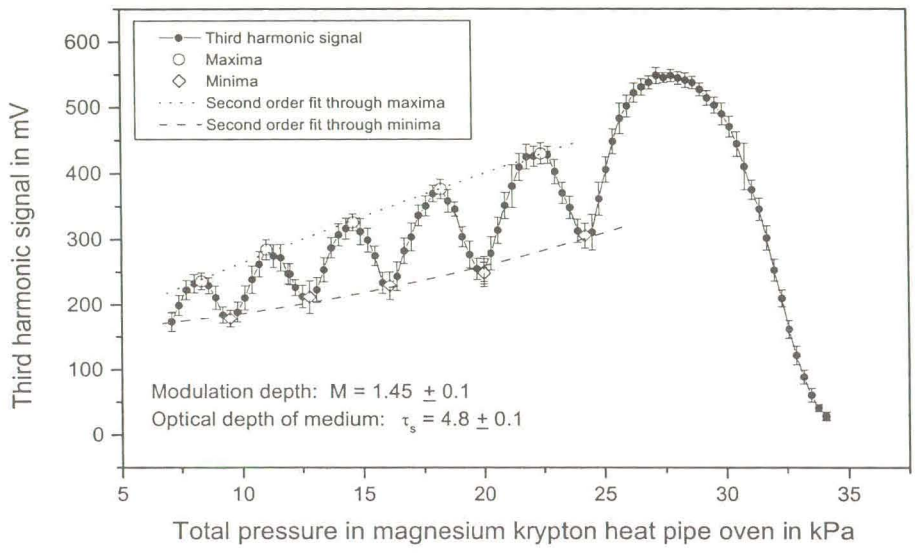

Figure 5-17: Experimental phase matching curve on which it is illustrated how the modulation depth is obtained for the calculation of the optical depth of the medium.

order polynomials were fitted through the minima and maxima of the oscillations respectively, the average ratio between the value of the two functions was taken as the modulation depth giving a value of 1.45 ± 0.1 for the modulation depth giving an optical depth $\Gamma_s = 4.8 \pm 0.3$ and an absorption cross-section $\sigma^{(1)}(\omega_s) = \sigma^{(1)}(143.6\text{nm}) = 5.6 \times 10^{-18}$ cm^2. This calculated absorption cross-section is larger than the value calculated by Junginger et al [20] and the values that can be calculated from the data of Steffes et al [38] by a factor 10. This implies that the modulation depth should be much larger for a medium of this length and density than the observed depth. This result leads to the conclusion that the focussing with the $f = 80$ cm lens is still smearing out the phase matching curve, reducing the modulation depth significantly. Much weaker focussing is needed to approach the parallel beam limit and to obtain results that can be quantitatively compared to the theory as described in section 3.2. It was not attempted to obtain the density gradient of the magnesium vapour in the transition zones from the asymmetry of the curve because the focussing that enhances the asymmetry will lead to false results.

5.2.3 Conclusions

The apparatus was successfully used to generate and detect the third harmonic at about 143 nm. The two-photon resonant wavelength and the krypton magnesium pressure ratio for optimal conversion efficiency were obtained experimentally for different focussing conditions of the incident laser beam. The advantage of the relatively short medium length (L) of this crossed concentric heat pipe oven is that the phase matching parameter $\triangle kL$ is smaller for a certain value of $\triangle k$ due to the smaller value of L. Therefore the peak maximum of the phase matching curve is broader, making the dependence of the conversion efficiency less sensitive to small deviations of the pressure ratio in the medium from the exact ratio giving phase matching. Focussing contributes to the broadening of the phase matching peak. This will make continuous tuning of the generated vacuum ultraviolet by sum-frequency generation easier. The focussing of the incident laser beam influences the form of the phase matching curve significantly, making quantitative comparison with the theory - that is valid for parallel beams - impossible. It is therefore not possible to obtain accurate values for the medium parameters such as the optical depth and density gradient of the magnesium vapour from these experimental results by the standard ways of analysis.

Some more work needs to be done to determine the focussing condition that optimises the conversion efficiency. From the results obtained already no conclusion can be drawn regarding the effect of focussing on the absolute conversion efficiency since, in the current setup, the focussing condition also influences the fraction of the output beam that reaches the solarblind photomultiplier, and the signal intensities measured with different focussing conditions cannot be compared directly.

The two-photon resonant enhanced third-harmonic generation process proved to be a very sensitive test for the quality of the dye laser beam. Fine-tuning of the resonator alignment will probably improve the results.

5.3 Experimental setup in Garching

The experimental setup for generating tunable vacuum ultraviolet by four-wave frequency mixing in Garching, as illustrated in figure 5-18, is customised as a source for molecular spectroscopy

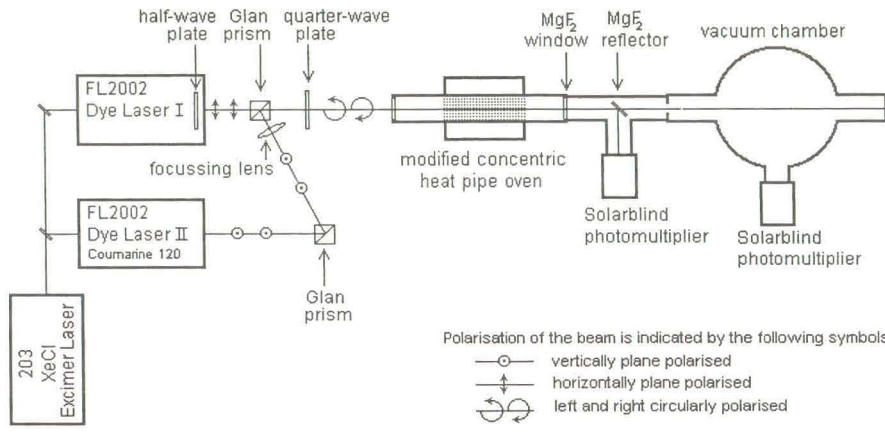

Figure 5-18: Experimental setup in Garching for the generation of tunable vacuum ultraviolet by sum-frequency generation in a magnesium krypton medium.

of primarily CO. Wavelengths of 140 to 160 nm in the vacuum ultraviolet region can be generated with this setup [25]. Such wavelengths are typically needed for the first excitation step of CO molecules. To excite the CO molecule from its $X\ ^1\sum^+$ ground state to the $a'\ ^3\sum^+$ ($\upsilon = 14$) intermediate state, from which the triplet Rydberg states of the molecule are accessible, a wavelength of 141.9 to 143.0 nm is needed. The main reason, as discussed in detail by Mellinger [26], for choosing the $a'\ ^3\sum^+$ ($\upsilon = 14$) state as intermediate state for reaching higher triplet states, is that the transition probability for the spin-forbidden transition from the singlet ground state to this specific triplet state is enhanced by the strong interaction between the $a'\ ^3\sum^+$ ($\upsilon = 14$) triplet state and the $A^1\Pi$ ($\upsilon = 4$) singlet state.

The modified concentric heat pipe oven used in Garching, illustrated in figure 5-19, is the heat pipe oven introduced by Steffes et al [38] in 1996. For a magnesium vapour krypton gas medium the conversion efficiency can be increased by the use of this modified concentric heat pipe that provides a longer optical path length (about 30 cm) in the medium. A magnesium vapour medium has a smaller two-photon absorption cross section making it favourable to have

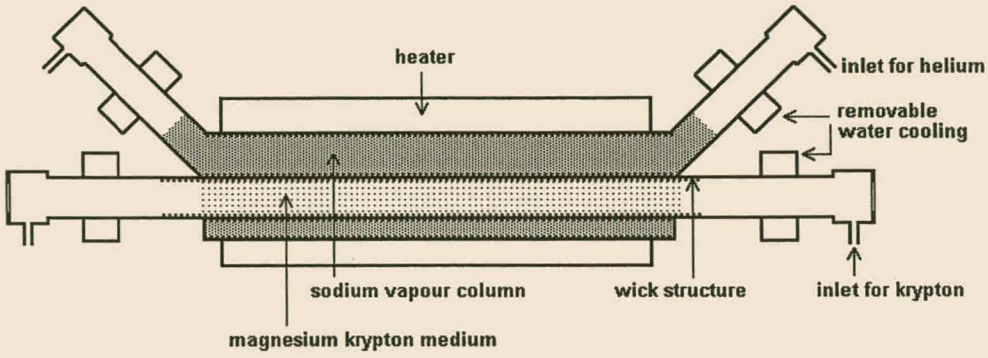

Figure 5-19: Schematic illustration of the heat pipe oven used in Garching for an optical path length of 30 cm in the magnesium-krypton medium. The outer heat pipe is operated with sodium as working material confined by helium gas.

a longer path length L in the medium so that an optical thickness $\Gamma = NL\sigma \approx 1$ can be obtained at a moderate density N, avoiding the homogeneous pressure broadening of the resonance lines. According to Steffes [38] and Mellinger [26] an optical depth of about unity is an experimental rule of thumb for optimal conversion efficiency. Except for the modified geometry of the outer heat pipe, this modified concentric heat pipe oven functions exactly like the crossed concentric heat pipe oven described in 5.1.1.

The two Lambda Physik FL 2002 dye lasers providing the incident beams are pumped by a LPX 205 XeCL excimer laser with an energy output of 300 to 400 mJ per 20 ns pulse. Sixty percent of the excimer pump beam pumps dye laser I (with Coumarin 120 dissolved in propylenecarbonate) providing the beam at the two-photon resonant frequency with an energy of about 4 - 7 mJ per pulse. Forty percent of the excimer pump beam is split off towards dye laser II (with PBBO dissolved in propylenecarbonate) providing the nonresonant beam at about 2 - 3 mJ per pulse. In this setup the mounting of the heat pipe and the rest of the vacuum system can be adjusted to align the heat pipe and vacuum system to the beam of dye laser I. The half-wave plate changing the polarisation of the resonant incident beam by 90 degrees is mounted inside dye laser I. Making use of the perpendicular polarisation of the two beams two Glan prisms are used to align the beam of dye laser II colinearly with the beam of dye laser

I by looking at the beam overlap at different distances. A quarter-wave plate mounted just before the heat pipe is responsible for the circular polarisation of the incident beams. The dye laser II beam, that has a longer optical path length to the heat pipe, is focussed slightly with a $f \approx 150$ cm lens to compensate for the divergence of the beam.

Sum-frequency generation is obtained and optimised by the following procedure: With the quarter-wave plate removed and only the dye laser I beam - tuned to the two-photon resonant frequency - unblocked, the krypton pressure is adjusted till a third-harmonic signal is observed. The two-photon resonant frequency is fine-tuned to optimise the third-harmonic signal. The quarter-wave plate is returned and rotated towards the position that minimises the third-harmonic signal due to the circular polarisation of the incident beam. The second beam from dye laser II is unblocked, the krypton pressure adjusted to phase match the sum-frequency process and the beam overlap of the two beams in the medium is optimised by monitoring the sum-frequency signal.

The dependence of the third-harmonic signals as well as the sum-frequency signals, as detected by the EMR 541-G-09 solarblind photomultiplier, on the pressure ratio as well as the polarisation of the incident beam was studied. The tuning range of the generated vacuum ultraviolet was determined experimentally.

As an application the tunable vacuum ultraviolet radiation was used to excite CO molecules, in the vacuum chamber filled with CO to a pressure of about 2×10^{-2} kPa, to different rotational levels in the $A^1\Pi\,(v = 4)$ and $a'\,^3\sum^+\,(v = 14)$ excited states. The excitation was accomplished with the output beam of the heat pipe oven containing the vacuum ultraviolet as it is without any attempt to separate the sum-frequency from the fundamental beam or additional focussing. The vacuum ultraviolet laser induced fluorescence from the excited level was detected by a EMR 541-J-08 solarblind photomultiplier mounted perpendicular to the laser beam. All signals were observed and measured on a 500 MHz Hewlett Packard oscilloscope model 54522A.

5.4 Experimental results for sum-frequency generation

The typical conditions for observing third-harmonic and sum-frequency signals were: a pressure in the outer sodium-helium heat pipe of about 28.5 kPa giving a temperature inside

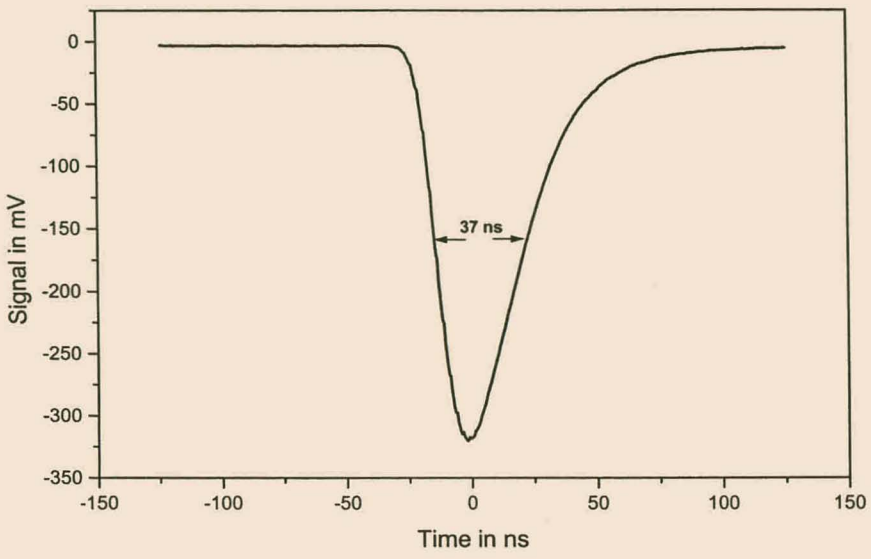

Figure 5-20: A typical sum-frequency signal as observed on the oscilloscope.

the heat pipe (measured by a thermocouple inserted into the heat pipe) of about 760 °C; the bellow allowing the external krypton pressure in the inner heat pipe to be adjusted between 20 and 32 kPa. The medium length is 30 cm. Dye laser I was tuned to the two-photon resonance between 430.88 and 431.0 nm and for most of the measurements (unless stated otherwise) the wavelength of dye laser II was about 416 nm. For these wavelengths the sum-frequency generation could be phase matched at an external krypton pressure of about 29.3 kPa. Third-harmonic generation of the resonant incident beam was also observed, but the pressure range that the bellow provides did not allow a high enough krypton pressure for phase matching of the third-harmonic generation process (expected at an external krypton pressure of about 37 kPa). At an excimer laser energy of about 330 mJ per pulse (18 kV discharge voltage) and dye laser energies of about 5 mJ and 2.5 mJ for dye lasers I and II respectively, a sum-frequency signal of about 300 mV was obtained from the solarblind photomultiplier (with 1.8 kV high voltage). Figure 5-20 illustrates a typical sum-frequency signal as observed on the oscilloscope. The true duration of the vacuum ultraviolet pulse is expected to be shorter than the 20 ns of the excimer pulses and the 37 ns half width measure on the oscilloscope is a function of the

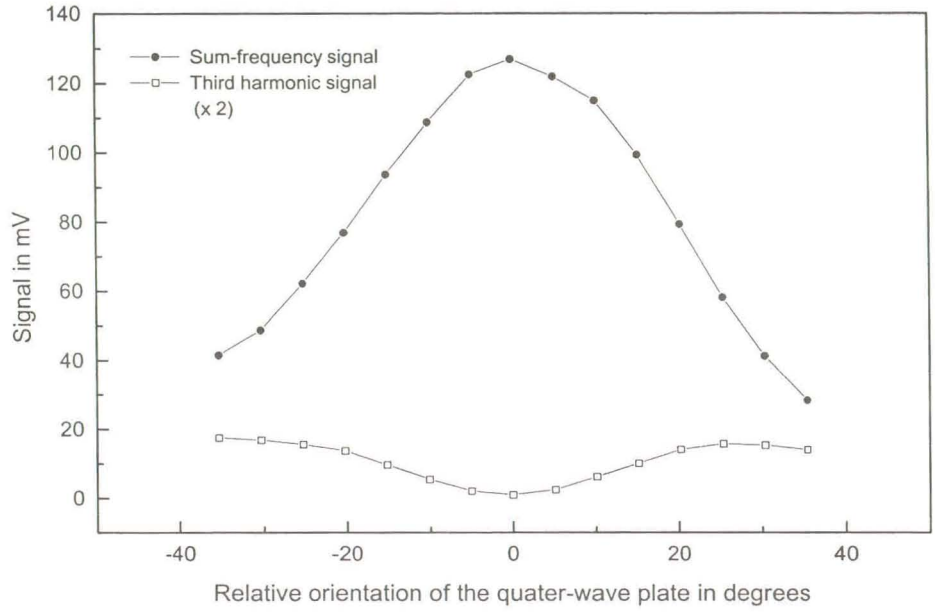

Figure 5-21: Plot of the third harmonic and sum frequency signals for different orientations of the quarter wave plate. In its zero-orientation the quarter-wave plate causes optimal circular polarisation of the incident beams.

inertia of the photomultiplier.

5.4.1 Polarisation of the incident beam

Figure 5-21 illustrates the dependence of third harmonic of the resonant frequency as well as the sum-frequency signals on the polarisation of the incident beams, as determined by the orientation of the quarter-wave plate. The third-harmonic signal was observed alternately with the sum-frequency signal by blocking the beam of dye laser II. The third-harmonic signal is much smaller than the sum-frequency signal due to the lower total power when the second dye laser beam is blocked as well as the krypton-magnesium pressure ration that is near to phase matching for the sum-frequency generation, but too low to phase match the third-harmonic generation process. (The krypton pressure was adjusted to a slightly higher value than the correct value for phase matching of the sum-frequency generation in order to enhance the third-harmonic signal). Each data point is the average of 64 laser pulses. It can clearly be seen how the third-harmonic signal decreases and the sum-frequency signal increases as the quarter-wave

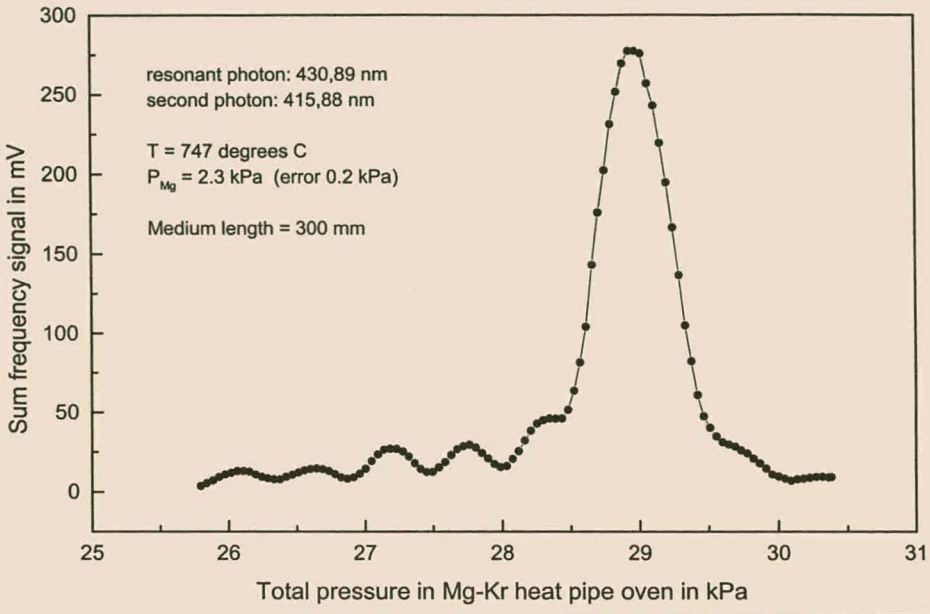

Figure 5-22: Experimental phase matching curve obtained by adjusting the external krypton pressure at a constant magnesium vapour pressure of about 2.3 kPa.

plate is rotated towards its zero position in which case it causes optimal left- and right-hand circular polarisation of the two incident beams respectively. When the incident beams have opposite circular polarisations, third-harmonic generation of either one of the incident beams is forbidden by the angular momentum selection rule as shown in section 3.7, and the sum-frequency that is allowed by angular momentum conservation, is enhanced by the elimination of the competing third-harmonic generation processes.

5.4.2 The phase matching curve

The experimental phase matching curve for the sum-frequency generation process - illustrated in figure 5-22 - was obtained by slowly lowering the external krypton pressure by means of the bellow at a rate of about 0.04 kPa per minute at a constant magnesium vapour pressure of about 2.3 ± 0.2 kPa (obtained by using the vapour pressure curves). Each data point is the average of 128 laser pulses. The pressure values were calculated from the number of turns of the crank-handle of the bellow from its initial position. This method was tested beforehand and calibrated by adjusting the bellow through its whole range (20 kPa to 32 kPa), taking pressure

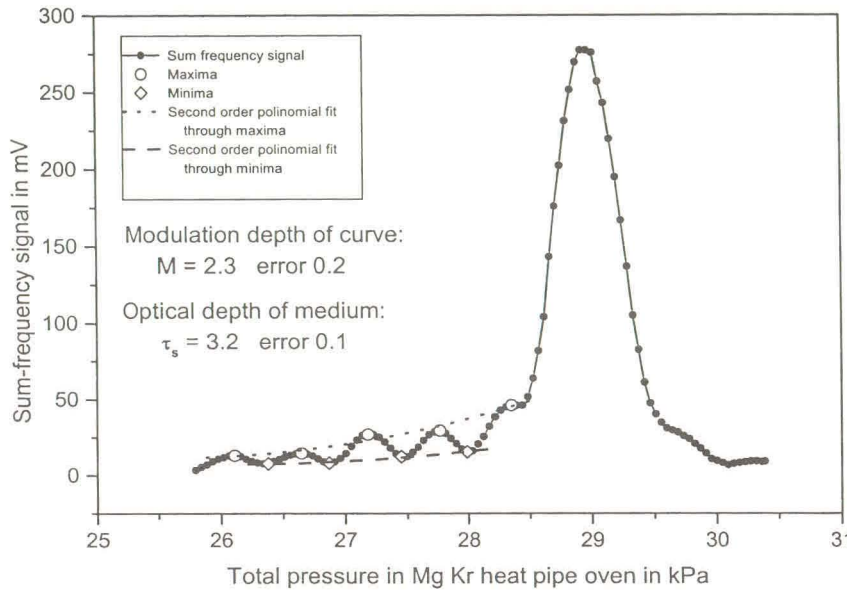

Figure 5-23: Experimental phase matching curve on which is illustrated how the modulation depth is obtain for the calculation of the optical depth of the medium.

readings on the pressure meter at intervals and doing a linear fit on the data. The focussing condition in this experiment is close to the parallel beam limit making it possible to compare the results obtained with the theory.

The experimental phase matching curve illustrates the enhancement of the macroscopic efficiency of the sum-frequency generation process when the phase matching condition is met at a total krypton pressure of 29.0 kPa (a krypton magnesium pressure ratio of about 12). The pressure ratio for the generation of the sum-frequency at the shorter wavelength, 142.0 nm, in this experiment is lower than the pressure ratio for third-harmonic generation at a longer wavelength (143.7 nm) - as expected from the dispersion curves of magnesium and krypton. Again the asymmetry in the phase matching curve due to the magnesium vapour gradients in the transition zones at both sides of the medium can be observed.

The oscillatory structure is clearly observable on the lower pressure side of the main maximum. The relation between the modulation depth of the oscillatory structure and the optical depth of the medium for the generated sum-frequency is used, as discussed in section 5.2.2, to determine the optical depth of the medium experimentally. Figure 5-23 illustrates

the second order polynomials fitted through the minima and maxima of the oscillations respectively, the average ratio between their values giving a value of 2.3 ± 0.2 for the modulation depth. This yields an optical depth $\Gamma_s = 3.2 \pm 0.1$ and an absorption cross-section $\sigma^{(1)}(\omega_s) = \sigma^{(1)}(142.0\text{nm}) = (6.5 \pm 0.4) \times 10^{-19}$ cm^2. The calculated absorption cross-section agrees well with the absorption cross-section for the third-harmonic wavelength that can be calculated for the phase matching curve given in figure 2 in the report of Steffes et al [38]: $\sigma^{(1)}(3\omega) = \sigma^{(1)}(143.7\text{nm}) = (6.6 \pm 0.3) \times 10^{-19}$ cm^2 and is larger but of the same order as the value of $\sigma^{(1)}(3\omega) = \sigma^{(1)}(143.7\text{nm}) = (4.5 \pm 0.7) \times 10^{-19}$ cm^2 obtained by Junginger. The values of the absorption cross-sections are not expected to vary strongly with wavelength in this spectral region - making it possible to compare the cross-sections at different wavelengths - in agreement with the evidence that the ionisation continuum of magnesium is structureless in this energy region, lacking discrete auto-ionisation levels that cause the absorption of different wavelengths to differ largely. The good agreement of the cross-section values shows that the focussing condition in this experiment is indeed near to the parallel beam limit, an important condition for good agreement between theory and experiment in the case of the phase matching curve.

5.4.3 Wavelength tunability of the generated vacuum ultraviolet

The last experiment with the setup for sum-frequency generation was to test the wavelength tunability of the sum frequency with and without adjustment of the pressure ratio as the wavelength of the nonresonant incident beam of dye laser II is tuned. Figure 5-24 shows two plots of the sum-frequency signal as a function of the nonresonant wavelength: curve 1 (marked by open circles) was obtained by tuning the wavelength without adjusting the krypton magnesium pressure ratio (the medium was phase matched for 416 nm) and curve 2 (marked by squares) by adjusting the pressure ratio to obtain phase matching after each wavelength adjustment. When phase matching is maintained by increasing the krypton magnesium pressure ratio as the wavelength is tuned towards longer wavelengths (curve 2), the effective tuning range was found to be limited only by the tuning range of the laser dye used in dye laser II. The intensity of the sum-frequency signal decreases around 390 nm not because of deterioration of the sum-frequency generation process, but because of the decrease in input power due to a

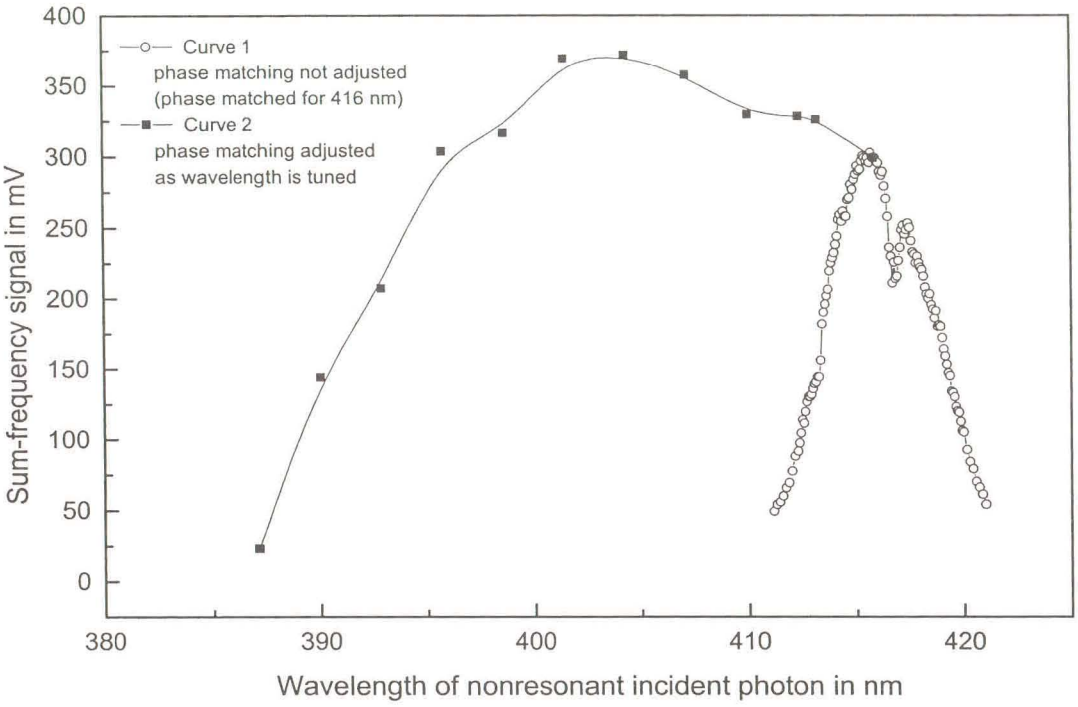

Figure 5-24: Graph illustrating the wavelength tunability of the vacuum ultraviolet generated by four-wave frequency mixing. The sum-frequency signal is plotted against the wavelength of the incident beam that is not responsible for the two-photon resonance. Curve 1 (marked by open circles) was obtained by tuning the wavelength, using a fixed krypton magnesium pressure ratio phase matching the medium for 416 nm. Curve 2 (marked with squares) was obtained by adjusting the krypton magnesium pressure ratio to maintain phase matching as the wavelength was tuned.

decrease in the effectivity of the laser dye at the limit of its usable range. The nonresonant wavelength could be tuned from about 390 to about 420 nm making the sum-frequency tunable over about 1830 cm^{-1} in the vacuum ultraviolet region. The smooth intensity profile is experimental evidence that this part of the ionisation continuum of magnesium does not contain discrete levels. When the wavelength alone is tuned (curve 1) the effective tuning range is much smaller because it is limited by the wavelength interval for which the fixed pressure ratio meets the phase matching condition sufficiently. The smaller peak to the long wavelength side of the main maximum can be explained by careful consideration of the change of the phase matching condition with wavelength in the magnesium krypton medium at these wavelengths. As it has already been observed a few times in this section a higher krypton magnesium pressure ratio is needed to phase match the generation of vacuum ultraviolet with a longer wavelength. If the system is phase matched at 416 nm and the wavelength of the nonresonant beam is tuned towards longer wavelengths the fixed pressure ratio becomes too low for phase matching at the longer wavelength and it can be expected to observe the same oscillatory behaviour as on the left-hand (small pressure) side of the phase matching curve in figure 5-22. The first minimum and first secondary maximum of this oscillatory behaviour can be seen on the right-hand side of curve 1 in figure 5-24.

5.4.4 Laser induced fluorescence of CO in the vacuum ultraviolet

The generated sum-frequency laser beam was used to excite CO molecules, in CO gas at pressures between 3.4×10^{-2} and 1.2×10^{-2} kPa, and the laser induced fluorescence of a number of lines was studied. The singlet and triplet lines of CO that were observed by tuning the nonresonant wavelength λ_2 between 415.83 and 415.95 nm are listed in table 5.2 with their observed wavelengths. The pairs of triplet lines marked by an asterisk could not be resolved with the bandwidth provided by the dye lasers without etalons. Figure 5-25 illustrates the singlet and triplet spectra of CO in this spectral region. Fluorescence from the singlet and the triplet lines, corresponding to excitation of sublevels of the $A^1\Pi$ ($v = 4$) singlet state and the $a'^3\Sigma^+$ ($v = 14$) triplet state respectively, could be distinguished by the longer lifetimes of the triplet levels giving rise to a slowly decaying fluorescence signal in contrast to the temporally narrow fluorescence signal of a singlet state. The typical laser induced fluorescence signals from

Line	J(lower)	J(upper)	N(lower)	N(upper)	λ_{VUV} in nm
Singlet lines					
$R(11)$	11	12	11	12	141.940
$P(4)$	4	3	4	3	141.944
$Q(7)$	7	7	7	7	141.950
$R(12)$	12	13	12	13	141.953
$P(5)$	5	4	5	4	141.958
Triplet lines					
${}^{R}R(0)$	0	1	0	1	141.946*
${}^{R}R(2)$	2	3	2	3	141.946*
${}^{R}Q(3)$	3	3	3	4	141.949
${}^{R}R(3)$	3	4	3	4	141.952
${}^{R}Q(4)$	4	4	4	5	141.957*
${}^{P}Q(1)$	1	1	1	0	141.957*

Table 5.2: Table of singlet and triplet lines observed by laser induced fluorescense with their associated quantum numbers. The line pairs marked with asterisks could not be resolved individually.

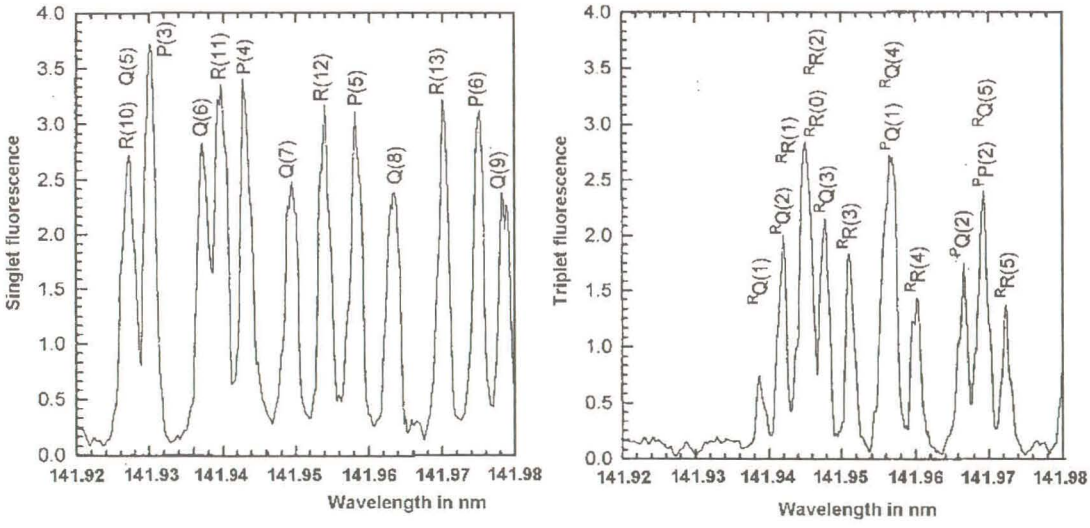

Figure 5-25: The singlet and triplet spectra of CO in the wavelength region that was investigated with the generated sum-frequency.

singlet and triplet states are illustrated in figures 5-26 and 5-27 respectively.

It was also attempted to reproduce the oscillations in the decay of the fluorescence of some of these lines observed previously in the laboratory in Garching and attributed to the quantum beat effect, by exciting the CO gas in a magnetic field, but the observation could not be reproduced in the time available.

5.4.5 Conclusions

Sum-frequency generation in a magnesium krypton medium prepared in a heat pipe oven is a reliable vacuum ultraviolet source for spectroscopy. Circular polarisation of the incident beams as well as the correct pressure ratio for phase matching is important for efficient sum-frequency generation. When the pressure ratio is adjusted to maintain phase matching as the wavelength is changed the generated sum-frequency is widely tunable. For an optically thin system the optical depth of the medium can be calculated from the modulation depth of the phase matching curve obtained with parallel laser beams. State selective spectroscopy of molecules like CO was done with the generated vacuum ultraviolet radiation. In the specific case of CO the fundamental wavelength does not interfere with the laser induced fluorescence and there is no need to separate the sum-frequency beam from the fundamental beam.

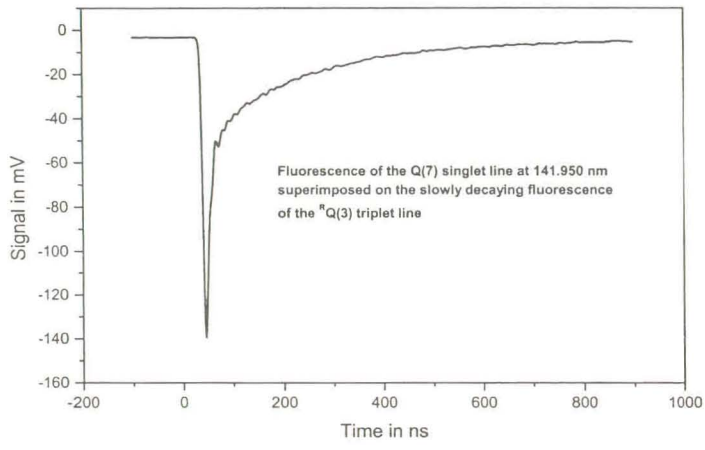

Figure 5-26: The vacuum ultraviolet fluorescence of the short lifetime Q(7) singlet state (the narrow peak) superimposed on some slower decaying fluorescence of the ^{R}Q(3) triplet state (the slowly decaying component following the peak) as observed on the oscilloscope.

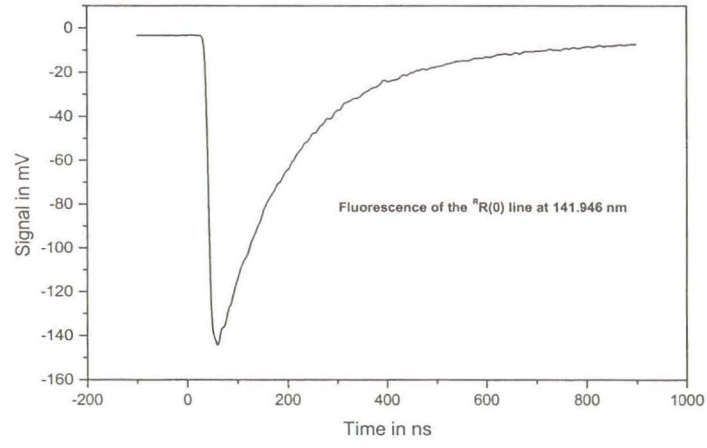

Figure 5-27: The vacuum ultraviolet fluorescence of the ^{R}R(0) triplet state of CO as observed on the oscilloscope.

Chapter 6

Conclusions

6.1 Choice of nonlinear medium for vacuum ultraviolet generation

Four-wave frequency mixing (referring to sum-frequency generation) in a gaseous nonlinear medium is described in this thesis as a method to obtain frequency tunable, small bandwidth, coherent radiation in the vacuum ultraviolet region. No laser that provides tunable, small bandwidth vacuum ultraviolet radiation is available yet, and in the vacuum ultraviolet spectral region the nonlinear crystals used to extend the range of tunable lasers in the infrared and visible regions become opaque, leaving gaseous nonlinear media as the only known solution.

Gaseous optical media have the following advantages:

- high transparency even in the vacuum ultraviolet region,
- good optical quality and homogeneity over large path lengths,
- that these media do not suffer permanent damage at high input power like crystals,
- and can be described well by basic quantum mechanics, facilitating the theoretical calculation of susceptibilities and other parameters.

The absolute conversion efficiency in gaseous nonlinear media is much smaller than in nonlinear crystals, but due to the small bandwidth and divergence of the generated radiation the

spectral brightness is sufficient for use in laser spectroscopy. An additional advantage of vacuum ultraviolet generation by sum-frequency mixing is that the problem of calibrating the vacuum ultraviolet wavelength is shifted to the visible region [47].

Four-wave frequency mixing has been obtained in metal vapours, noble gases and other atomic and molecular systems, but in the region of wavelengths longer than 105 nm (where transparent window material is available) metal vapours are favourable due to the large third order susceptibility and the option of phase matching by the addition of a noble gas. The specific metal vapour used is selected for its optical properties, a sufficiently high third order nonlinear susceptibility for the sum-frequency process and low absorption cross-sections at the incident and generated frequencies, as well as practical considerations - for example that the metal should have a sufficiently high vapour pressure at temperatures that are readily attainable. Magnesium vapour has a sufficiently high vapour pressure, a suitable two-photon resonance at 431 nm that enhances the third order susceptibility for sum-frequency generation of vacuum ultraviolet wavelengths in the region 140 to 160 nm significantly, as well as low absorption losses in this wavelength region.

A sufficiently large third order susceptibility is the microscopic requirement for sum-frequency generation, but the important consideration in a practical source is the macroscopic conversion efficiency: the ratio of the intensity of the sum-frequency wave to the intensity of the incident wave. This conversion efficiency is essentially determined by:

- the degree of constructive interference of all the contributions to the sum-frequency wave generated in different volume elements of the medium and
- competing optical processes in the medium.

Constructive interference of the sum-frequency contributions occur if the wave vector mismatch $\overrightarrow{\triangle k}_{sum} = \overrightarrow{k}_{sum} - (\overrightarrow{k}_1 + \overrightarrow{k}_2 + \overrightarrow{k}_3)$ is close to zero throughout the medium. This is called the phase matching condition. In a magnesium vapour medium, with a colinear beam alignment, the phase matching condition can be met by adding krypton gas and by fine-tuning the krypton magnesium pressure ratio. Magnesium vapour has the advantage over other metals that it can be phase matched with krypton at a rather low pressure ratio of about 12 : 1, facilitating work at a low total pressure that reduces pressure broadening of the resonances. The

phase matching condition requires a high homogeneity of the medium and therefore a stable temperature. A crossed concentric heat pipe oven can provide these conditions by relying on the characteristics of liquid phase equilibria without any active electronic control. The pressure ratio for phase matching and the conversion efficiency at phase matching are influenced by the mode structure and focussing of the incident beams as well as the optical depth of the medium, making it necessary to optimise these conditions.

The intensity of the generated vacuum ultraviolet is directly proportional to the square of the number density N and length L of the medium and the cube of the intensity of the incident beam (see equation 3.10), but competing optical processes set upper limits to the values of the medium density NL and incident intensity beyond which no significant increase in the intensity of the generated vacuum ultraviolet is gained - typical saturation behaviour. The competing processes that have to be considered depend on the intensity regime. In the small signal limit, where $I_{incident}$ is small so that $I_{sum} \ll I_{incident}$, the most important competing processes are the one-photon absorption of the incident and sum-frequencies. The experimental rule of thumb - that the optical depth of the medium $\tau_i = NL\sigma^{(1)}(\omega_i)$, where $\sigma^{(1)}$ is the one-photon absorption cross-section, for all frequencies ω_i involved in the nonlinear process must be of the order of one [38] - limits the medium density that can be used. Magnesium vapour has favourably small one-photon absorption cross-sections $\sigma^{(1)}(\omega_i)$ for the incident frequencies at about 430 nm, as well as for the vacuum ultraviolet frequencies (140 to 160 nm). The latter property is due to the lack of auto-ionisation levels in its ionisation continuum in this energy range [21]. At higher incident intensities, the onset of saturation is caused by field dependent changes of the index of refraction destroying the phase matching condition in the medium [32]. In systems where two-photon resonance is used to enhance the nonlinear susceptibility, two-photon absorption of the resonant incident frequency is the main cause for the onset of saturation due to the population changes it causes [31]. The onset of saturation is characterised in such a system thereby that the optimal conversion does not occur at resonance any more, but slightly off resonance on both sides of it. Magnesium vapour has the advantage above strontium that its smaller two-photon absorption cross-section delays the onset of saturation [21]. The intensity region near the onset of saturation is recommended [47] for optimal conversion, since at higher energies competing higher order nonlinear processes become significant, perturbing the behaviour of the system,

and not much is gained. It was discussed in section 3.7 how circular polarisation of the incident beams can be used to reduce the competition of third-harmonic generation when sum-frequency generation is wanted.

In summary the suitability of magnesium vapour for the generation of vacuum ultraviolet in the region 140 to 160 nm is due to:

- a high third order susceptibility for sum-frequency generation,
- a suitable two-photon resonance to be used for resonance enhancement of the sum-frequency generation process,
- phase matching with krypton gas at a low pressure ratio and
- low one- and two-photon absorption losses of the generated vacuum ultraviolet radiation allowing a higher medium density.

6.2 Performance of the magnesium krypton heat pipe oven

The crossed concentric heat pipe oven produces a magnesium krypton medium that meets the stringent phase matching requirements of homogeneity and thermal stability without relying on electronic control, heat baffles or stabilised heating power. The important experimental parameters namely the temperature, magnesium vapour pressure and partial pressure of the krypton in the medium are physically well defined by the vapour pressure curves of the working materials. The magnesium vapour pressure and the partial krypton pressure can be adjusted accurately and independently by adjusting the externally regulated argon and krypton gas pressures. This facilitates the fine tuning of the pressure ratio for phase matching. The buffer gas confining the metal vapour eliminates the problem of metal vapour being deposited on the windows. The most sensitive test for the heat pipe oven system is the sum-frequency generation process itself. The suitability of the heat pipe oven system is proved by its reliable operation as part of the vacuum ultraviolet source and the repeatable results obtained for sum-frequency generation.

6.3 Conclusions from experimental results with the vacuum ultraviolet laser source

The experimental results obtained in Garching, as discussed in section 5.4, show how the polarisation of the incident beams can be used to select sum-frequency generation among the possible third order nonlinear processes. The experimental phase matching curve obtained with the magnesium krypton medium in the heat pipe oven shows a good agreement with the theory describing the phase matching curve in the parallel beam limit. This facilitates the calculation of an experimental value for the optical depth of the medium and the two-photon absorption cross-section of magnesium vapour. The results show that the wavelength of the generated vacuum ultraviolet can easily be tuned over a wide range. With a medium length of 30 cm the phase matching peak is narrow and the pressure ratio must be adjusted to maintain phase matching as the wavelength is tuned. The laser induced fluorescence results, showing the fine structure splitting of rotational levels of CO, confirm the suitability of the generated sum-frequency laser beam for application in laser spectroscopy.

The experimental work done in Stellenbosch, discussed in section 5.2, shows that the development of such a laser source by sum-frequency generation in a magnesium krypton medium is technically simple and that the wavelength for two-photon resonance and conditions for optimal phase matching are easily determined by experiment. The fine-tuning of the optical system (the dye laser beam quality, the incident laser intensity, focussing conditions and the reduction of pulse to pulse intensity variation) however, requires further optimisation in order to obtain optimal vacuum ultraviolet output or to obtain results that are comparable to theory. It is, for example, clear that in order to characterise the magnesium krypton medium quantitatively (to determine the optical depth and density gradients) by comparison to theoretical calculations the focussing of the incident beam has to be adjusted to approach the parallel beam limit. To obtain the best conversion efficiency however, some tighter focussing will be needed, but the exact focussing condition has to be determined experimentally. The two-photon resonant third harmonic generation process was shown to be very sensitive to the quality of the dye laser beam.

6.4 Proposed future work

The final setup for sum-frequency generation that is planned in the laser laboratory, Physics Department, University of Stellenbosch, is described in section 5.1. It would be advisable to gain some more practical experience with the simple setup for third-harmonic generation, in order to eliminate some practical problems of the setup and to determine the optimal focussing condition of the incident laser beam before modifying the experimental setup for sum-frequency generation by the addition of a second dye laser beam as illustrated in figure 5-3.

The final setup can be applied as source in spectroscopic or analytic work where vacuum ultraviolet radiation is needed or has advantages over visible photons. If this is combined with the linear time of flight mass spectrometer, that is already incorporated into the apparatus, a double selectivity is obtained: the state selectivity of laser spectroscopy as well as mass selectivity provided by the mass spectrometer.

Chapter 7

Appendices

7.0.1 Appendix A: Why is third-harmonic generation (four-wave frequency mixing) in gaseous media used?

Since second harmonic generation (the degenerate case of three-wave mixing) is the lowest order nonlinear process it is expected to be the dominating nonlinear process. In birefringent crystals as nonlinear medium second harmonic generation is the dominating nonlinear phenomenon - and it was one of the first nonlinear phenomena to be observed by Franken and coworkers in a birefringent quartz crystal shortly after the first successful laser operation in 1960. Birefringent crystals are now used in many applications as frequency doublers. Birefringent crystals have the restriction that they become opaque (absorbing) in the ultraviolet or vacuum ultraviolet region. Therefore there is always a lower limit for the wavelengths that can be produced by second harmonic generation in birefringent crystals. To produce shorter wavelengths by sum-frequency mixing a gaseous nonlinear medium that remains transparent in the ultraviolet and vacuum ultraviolet spectral regions must be used.

Gaseous nonlinear media have the advantages of high transparency, that the preparation of a volume of medium with good optical quality over large dimensions is easy and high radiation density does not cause irreversible damage to the medium as to a crystal. The properties of gaseous media that reduce their efficiency is the low particle density and the fact that second order nonlinear processes such as second harmonic generation cannot be used any more: the susceptibility for second harmonic generation vanishes for centrosymmetric media like liquids,

gases or crystals with cubic symmetry.

This can be demonstrated classically by considering the general expression for the nonlinear polarisation term $\widehat{P}_{2\omega}^{(NL)}$ responsible for the generation of a second harmonic wave with frequency 2ω in the presence of high intensity radiation at the fundamental frequency ω:

$$\widehat{P}_{2\omega}^{(NL)} = N\chi^{(2)}(-2\omega;\omega,\omega)\left(\widehat{E}_{\omega}(z)\right)\left(\widehat{E}_{\omega}(z)\right)$$

The nonlinear polarisation $\widehat{P}_{2\omega}^{(NL)}$ is proportional to the square of the amplitude of the electric field $\widehat{E}_{\omega}(z)$ of the fundamental (incident) radiation as well as to the number density N of the medium. The proportionality constant is the second order nonlinear susceptibility $\chi^{(2)}(-2\omega;\omega,\omega)$. In a medium that is centrosymmetric (where the optical properties of the medium are the same in all directions) it can be expected that reversal of the electric fields will cause the polarisation generated by them to be reversed too. If this is true

$$-\widehat{P}_{2\omega}^{(NL)} = N\chi^{(2)}(-2\omega;\omega,\omega)\left(-\widehat{E}_{\omega}(z)\right)\left(-\widehat{E}_{\omega}(z)\right)$$

but then

$$-\widehat{P}_{2\omega}^{(NL)} = (-1)^2 N\chi^{(2)}(-2\omega;\omega,\omega)\left(\widehat{E}_{\omega}(z)\right)\left(\widehat{E}_{\omega}(z)\right) = \widehat{P}_{2\omega}^{(NL)}$$

meaning that $\widehat{P}_{2\omega}^{(NL)} = 0$. Evidently second harmonic generation (three wave frequency mixing) and all other even order processes[1], cannot occur in centrosymmetric media.

The quantum mechanical expression for the even order susceptibilities provides a fundamental reason for their vanishing in some media. All the second order susceptibilities have a form similar to the expression for $\chi^{(2)}(-2\omega;\omega,\omega)$ given here [27, equation 17.14.3]:

$$\chi^{(2)}(-2\omega;\omega,\omega) = \frac{1}{\hbar^2}\sum_{n,m}\mu_{gn}\mu_{nm}\mu_{mg}A_{gnm}(\omega)$$

$A_{gnm}(\omega)$ is the ω dependent factor, the form of which is not very important in this discussion. μ_{nm} represents the electric dipole moment for a transition between the electron states labeled

[1] The nonlinear susceptibility $\chi^{(n)}(-\omega_s;\omega_1,\omega_2,...\omega_n)$ is the n^{th} order nonlinear susceptibility describing n^{th} order nonlinear processes such as n^{th} harmonic generation, but it is mathematically a tensor of rank $(n+1)$ connecting the $(n+1)$ interacting electromagnetic waves with frequencies $\omega_1,\omega_2,...,\omega_n,\omega_s$ and therefore the general term for this process is $(n+1)$-wave frequency mixing.

n and m. The transition electric dipole moments μ_{nm} obey the selection rule for electric dipole transitions stating that for a transition $m \rightarrow n$ the states m and n must have opposite parity for μ_{nm} to be non-zero. With this selection rule it is easy to see that $\chi^{(2)}(-2\omega;\omega,\omega)$ must be zero in an atomic gas: for μ_{gn} to be non-zero, n and g must have opposite parity; for μ_{nm} to be non-zero n and m must have opposite parity meaning that m and g must have the same parity. But that inevitably implies that $\mu_{mg} = 0$, therefore $\chi^{(2)}(-2\omega;\omega,\omega) = 0$. In general it follows that the even order susceptibilities vanish in any medium where the atoms or molecules have states of definite parity. The electron states of centrosymmetric media like atomic gases and cubic crystals exhibit definite parity. In noncubic crystals, the unsymmetrical local fields of neighbouring atoms modify the wave function destroying the parity so that the even order susceptibilities are non-zero and second harmonic generation is the lowest order and most important nonlinear phenomenon in these media.

The lowest order nonlinear process in centrosymmetric optical media like vapours and crystals with a centre of symmetry is therefore four-wave frequency mixing, or third-harmonic generation in the degenerate case. If the centrosymmetric symmetry in such a medium is disturbed by for example an external electric or magnetic field, the second order nonlinear processes will become observable.

7.0.2 Appendix B: Phase and group velocity

The existence of a perfectly monochromatic wave is purely theoretical. In any practical situation of radiation propagating through a medium there are always a certain spread of frequencies present. Such a superposition of harmonic waves gives rise to wave groups carrying energy. In the (theoretical) case of only two frequencies, ω and $\omega + \delta\omega$, propagating together the resultant wave can (in one dimension) be described by

$$\Psi(x,t) = 2A\cos\frac{1}{2}(\delta\omega t - \delta k x)\cos(\omega t - kx)$$

This expression can be interpreted as a high frequency (ω) wave of which the amplitude is modulated by an envelope with a much smaller frequency $\delta\omega$ therefore varying slower in time. Both are propagating: the propagation of the high frequency wave is determined by its wave

number k and the associated phase velocity $v = \omega/k$, and the propagation of the modulation by wave number δk and the group velocity[2] $v_g = \delta\omega/\delta k = \frac{d\omega}{dk}$ in the limit of small intervals. v_g is the velocity of energy transport by the wave group. In a dispersive medium v_g is related to the phase velocity v. This relation can be derived [3, p. 387-391] as follows: From the definitions of phase velocity

$$v = \frac{\omega}{k} = \frac{c}{n}$$

and group velocity

$$v_g = \frac{d\omega}{dk},$$

follows

$$\begin{aligned}
\frac{1}{v_g} &= \frac{dk}{d\omega} = \frac{d}{d\omega}\left(\frac{\omega}{v}\right) = \frac{1}{v} - \frac{\omega}{v^2}\frac{dv}{d\omega} \\
&= \frac{1}{v} - \frac{\omega n^2}{c^2}\frac{d}{d\omega}\left(\frac{c}{n}\right) \\
&= \frac{1}{v} - \frac{\omega n^2}{c}\frac{d}{dn}\left(\frac{1}{n}\right)\frac{dn}{d\omega} \\
&= \frac{1}{v} - \frac{\omega n^2}{c}\left(-\frac{1}{n^2}\right)\frac{dn}{d\omega} \\
&= \frac{1}{v} + \frac{\omega}{c}\frac{dn}{d\omega}
\end{aligned}$$

giving

$$\frac{c}{v_g} = \frac{c}{v} + \omega\frac{dn}{d\omega} = n + \omega\frac{dn}{d\omega}. \tag{7.1}$$

It can be seen from figure 2-4 that except for the region of the absorption line itself $\frac{dn}{d\omega}$ is positive. The form of the variation of $n(\omega)$ with ω ensures that $\frac{c}{v_g}$ remains greater than unity even in regions where n is less than unity. In the region of absorption other considerations dominate the rate of energy transfer [20, p. 475].

[2] To find the velocity of the wave described by $\cos(\omega' t - k' x)$ the movement of a constant value of the amplitude (for example the wave crest) must be followed. At the wave crest, $(\omega' t - k' x) = 0$ so that $\cos(\omega' t - k' x) = 1$. To maintain $(\omega' t - k' x) = 0$ when t increases by δt, x must increase with δx so that the increment $(\omega' \delta t - k' \delta x) = 0$. This gives $v' = \delta x/\delta t = \omega'/k'$.

7.0.3 Appendix C: The physical interpretation of the complex linear susceptibility

Where the effect of absorption is discussed first on page 14 it was stated that when absorption is taken into account (i) the linear susceptibility becomes complex due to the fact that the electric field and induced polarisation are not in phase and (ii) the wave vector of the electric field k becomes a complex quantity related to complex linear susceptibility by the equation

$$\begin{aligned}(k_\omega)^2 &= \frac{\omega^2}{c^2}\left(1+4\pi N\chi^{(1)}(\omega)\right)\\ &= \frac{\omega^2}{c^2}\left(1+4\pi N\overline{\chi}^{(1)}(\omega)+i4\pi N\widetilde{\chi}^{(1)}(\omega)\right)\end{aligned} \tag{7.2}$$

where $\overline{\chi}^{(1)}(\omega)$ and $\widetilde{\chi}^{(1)}(\omega)$ represent the real and imaginary parts of the linear susceptibility at frequency ω respectively. In analogy with equation 2.11 the complex wave vector defines a complex index of refraction $n(\omega)$ by

$$k_\omega = \frac{\omega}{c}n(\omega)$$

giving

$$n^2(\omega) = 1+4\pi N\chi^{(1)}(\omega). \tag{7.3}$$

A complex wave vector has the physical meaning that the amplitude of the electromagnetic wave is attenuated as it propagates through the medium. In order to show this mathematically the complex wave vector has to be separated into its real and imaginary parts. Let k_ω be given by

$$k_\omega = \overline{k}_\omega + i\widetilde{k}_\omega \tag{7.4}$$

where $\overline{k}_\omega$ and $\widetilde{k}_\omega$ represent the real and imaginary parts of the wave vector respectively. Then a plane wave of which the amplitude is constant in time propagating in the z-direction through the medium has the form

$$\begin{aligned}\mathbf{E}(z,t) &= \widehat{\varepsilon}\left[\widehat{E}\exp\left(-i\omega t+i(\overline{k}_\omega+i\widetilde{k}_\omega)z\right)+cc\right]\\ &= \widehat{\varepsilon}\left[\widehat{E}\exp\left(-i\omega t+i\overline{k}_\omega z-\widetilde{k}_\omega z\right)+cc\right]\end{aligned}$$

$$= \widehat{\varepsilon}\left[\widehat{E}\exp\left(-i\omega t + i\overline{k}_\omega z\right)\exp\left(-\widetilde{k}_\omega z\right) + cc\right] \tag{7.5}$$

$$= \widehat{\varepsilon}\left[\widehat{E}\exp\left(-i\omega t + i\overline{k}_\omega z\right) + cc\right]\exp\left(-\widetilde{k}_\omega z\right) \tag{7.6}$$

or

$$\mathbf{E}(z,t) = \widehat{\varepsilon}\left[\widehat{E}(z)\exp\left(-i\omega t + i\overline{k}_\omega z\right) + cc\right]$$

where $\widehat{E}(z) = \widehat{E}\exp\left(-\widetilde{k}_\omega z\right)$ gives the z-dependent amplitude of the wave. Physically the $\exp\left(i\overline{k}_\omega z\right)$ factor determining the phase velocity υ of the wave in the medium is related to the (real) index of refraction, $\upsilon = c/\overline{n}(\omega) = \omega/\overline{k}_\omega$, and the $\exp\left(-\widetilde{k}_\omega z\right)$ factor contains the exponential decay of the electric field amplitude due to the absorption of the field in the medium as quantified by the absorption coefficient $\widetilde{\kappa}_\omega \propto \widetilde{k}_\omega$. Such an exponential decay of the electric field amplitude is the well known result of Beer's law for absorption

$$\begin{aligned} \frac{d\widehat{E}(z)}{dz} &= -\widetilde{k}\widehat{E}(z) \\ \int_{\widehat{E}(0)}^{\widehat{E}(z)} \frac{1}{\widehat{E}} d\widehat{E} &= -\widetilde{k}\int_0^z dz \end{aligned} \tag{7.7}$$

with the solution

$$\widehat{E}(z) = \widehat{E}(0)\exp\left(-\widetilde{k}_\omega z\right)$$

The question that is not satisfactorily explained in any of the cited texts is how the real and imaginary parts of the wave vector (in other words the index of refraction and the absorption coefficient) are related to the linear susceptibility and what approximations are made to arrive at the relations that are generally used. It became clear that the approximations made in the derivation of these relations can be made in different ways of which two are discussed here. The first one that is discussed below serves as derivation of the expressions used in the derivation of the fundamental equation of nonlinear optics in section 2.3.1; the second is the method found in the literature as in [27] and [8, p. 64].

The first derivation starts out from equation 7.4, from which follows that

$$(k_\omega)^2 = (\overline{k}_\omega)^2 - (\widetilde{k}_\omega)^2 + 2i\overline{k}_\omega\widetilde{k}_\omega \tag{7.8}$$

When the imaginary part of the wave vector (i.e. the damping of the electric field amplitude) is small, as it usually is in transparent optical media like vapours, it can be assumed that $(\widetilde{k}_\omega)^2 \ll (\overline{k}_\omega)^2$ and equation 7.8 can be approximated by

$$(k_\omega)^2 = (\overline{k}_\omega)^2 + 2i\overline{k}_\omega\widetilde{k}_\omega. \tag{7.9}$$

When equation 7.9 is compared with equation 7.2, the real parts yield

$$(\overline{k}_\omega)^2 = \frac{\omega^2}{c^2}\overline{n}^2(\omega) = \frac{\omega^2}{c^2}\left(1 + 4\pi N\overline{\chi}^{(1)}(\omega)\right), \tag{7.10}$$

giving

$$\overline{k}_\omega = \frac{\omega}{c}\overline{n}(\omega) = \frac{\omega}{c}\left(1 + 4\pi N\overline{\chi}^{(1)}(\omega)\right)^{1/2}. \tag{7.11}$$

In the case when $4\pi N\overline{\chi}^{(1)}(\omega) \ll 1$, meaning that the index of refraction of the medium must be near to unity which holds for a gaseous medium in the visible region, the first two terms of the series expansion[3] of the square root $(1+x)^{1/2} = 1+\frac{1}{2}x+\frac{1}{2}(\frac{1}{2}-1)\frac{x^2}{2}+...$ (with $x = 4\pi N\overline{\chi}^{(1)}(\omega)$, a real number) can be used as an approximation, giving

$$\overline{k}_\omega = \frac{\omega}{c}\overline{n}(\omega) \approx \frac{\omega}{c}\left(1 + 2\pi N\overline{\chi}^{(1)}(\omega)\right) \tag{7.12}$$

Equation 7.12 agrees exactly with the definitions used for the real wave vector k_j in equation 2.74 (section 2.3.1) and the definitions for index of refraction $\overline{n}(\omega)$ in equations 2.13 (section 2.2.1.1) and 2.20 (section 2.2.1.2) and $\overline{n}_j$ in equation 2.66 (section 2.3.1).

Comparison of the imaginary parts of equations 7.2 and 7.9 yields

$$2\overline{k}_\omega\widetilde{k}_\omega = \frac{\omega^2}{c^2}4\pi N\widetilde{\chi}^{(1)}(\omega)$$

giving for the imaginary part of the wave vector

$$\widetilde{k}_\omega = \frac{\omega^2}{c^2}2\pi N\widetilde{\chi}^{(1)}(\omega)\left(\frac{1}{\overline{k}_\omega}\right) = \frac{\omega^2}{c^2}2\pi N\widetilde{\chi}^{(1)}(\omega)\left(\frac{c}{\omega\overline{n}(\omega)}\right)$$

[3] This series expansion in the case when x is real holds for $-1 < x \leq 1$.

$$= \frac{\omega}{c\overline{n}(\omega)} 2\pi N \widetilde{\chi}^{(1)}(\omega), \tag{7.13}$$

for the imaginary part of the index of refraction

$$\widetilde{n}(\omega) = \frac{1}{\overline{n}(\omega)} 2\pi N \widetilde{\chi}^{(1)}(\omega), \tag{7.14}$$

for the absorption coefficient

$$\kappa_\omega = N \frac{4\pi\omega}{c\overline{n}(\omega)} \widetilde{\chi}^{(1)}(\omega) = 2\widetilde{k}(\omega) \tag{7.15}$$

and for the absorption cross-section

$$\sigma_\omega^{(1)} = \frac{4\pi\omega}{c\overline{n}(\omega)} \widetilde{\chi}^{(1)}(\omega) = 2\widetilde{k}(\omega)/N. \tag{7.16}$$

The factor 2 is added in the definitions of κ_ω and $\sigma_\omega^{(1)}$ to make a transformation from an amplitude damping constant $\widetilde{k}(\omega)$ to intensity damping constants κ_ω and $\sigma_\omega^{(1)}$. These equations 7.15 and 7.16, showing the dependence of the absorption coefficient and cross-section on the real index of refraction as well as the imaginary part of the linear susceptibility, are the relations used to derive the fundamental equation of nonlinear optics in section 2.3.1 in a consistent way. In the process of deriving the fundamental equation a second order differential equation containing the second order differentials of the electric field both in time and space is transformed to a first order differential equation - an expression for $\frac{d\widehat{E}_q(z)}{dz}$ that contains the typical $-\widetilde{k}\widehat{E}_q(z) \propto -\widetilde{\kappa}\widehat{E}_q(z)$ absorption term as seen in Beer's law, equation 7.7. It is then seen that this absorption term is the result of the one-photon absorption of the electric wave with frequency ω_q.

In the definition of the absorption coefficient and cross-section in the literature, such as the absorption cross-section $\sigma_j^{(1)}$ in [50], the absorption coefficient $\alpha(\omega)$ in [8, p. 65] and $a(\omega)$ in [27, p. 75] the $\frac{1}{\overline{n}(\omega)}$ factor is often neglected - which is acceptable under the assumption that $\overline{n}(\omega) \approx 1$. These definitions are derived in the following way: Under the assumption that $\overline{n}(\omega) \approx 1$ (i.e. $N\overline{\chi}^{(1)}(\omega) \ll 1$) as well as small absorption $N\widetilde{\chi}^{(1)}(\omega) \ll 1$, with the result that $\left|N\chi^{(1)}(\omega)\right| \ll 1$, equation 7.3 is approximated by expanding the square root factor as a power

series[4] and keeping only the first two terms, giving

$$\begin{aligned} n(\omega) &= \left(1 + 4\pi N\chi^{(1)}(\omega)\right)^{1/2} \\ &\approx 1 + 2\pi N\chi^{(1)}(\omega) \\ &= 1 + 2\pi N\overline{\chi}^{(1)}(\omega) + i2\pi N\widetilde{\chi}^{(1)}(\omega) \\ &= \overline{n}(\omega) + i\widetilde{n}(\omega) \end{aligned}$$

with

$$\overline{n}(\omega) = 1 + 2\pi N\overline{\chi}^{(1)}(\omega) \tag{7.17}$$

corresponding to equation 7.12, and

$$\widetilde{n}(\omega) = 2\pi N\widetilde{\chi}^{(1)}(\omega) \tag{7.18}$$

corresponding to equation 7.14 under the condition that $\overline{n}(\omega) = 1$. In a gaseous medium at low pressure this approximation is sufficiently accurate for most purposes [8]. In sections 2.2.1.1 and 2.2.1.2 this approximation is used to derive the expressions 2.14, 2.16, 2.18 and 2.20.

The approximations - of small absorption and that the index of refraction is near to unity - made in the two methods are essentially the same, but the results differ slightly due to different ways of applying the approximations with the effect that the explicit dependence of the absorption coefficient on the real index of refraction vanishes in the second derivation.

[4] Note that the variable $x = 4\pi N\chi^{(1)}(\omega)$ in this expansion is a complex number as opposed to the real series expansion used in the approximation method discussed first. The complex expansion holds for $|x| < 1$.

Bibliography

[1] J.A. Armstrong, N. Bloembergen, J. Ducuing and P.S. Pershan (1962). "Interactions between Light Waves in a Nonlinear Dielectric", *Phys. Rev.* **127**, no. 6, p. 1918-1939.

[2] S.H. Ashworth and J.M. Brown (1991). "*An Atlas of Optogalvanic Transitions in Neon*", Science and Engineering Research Council, report RAL-91-069, Chilton, Didcot, Oxon OX11 0QX.

[3] N.K. Bajaj (1984). "*The Physics of waves and oscillations*", Chapter 9, p. 386-391. Tata McBraw-Hill Publishing Company, New Delhi.

[4] J. Bohdansky and H.E. Schins (1965). "New method for vapor-pressure measurements at high temperature and high pressure," *J. Appl. Phys.* **36**, p. 3683.

[5] D.M. Bloom, J.T. Yardley, J.F. Young, S.E. Harris (1974). *Appl. Phys. Lett.* **24**, p. 427.

[6] R.W. Boyd and J.G. Dodd (1980). "Analysis of the pressure, density and velocity distributions in a spectroscopic heat-pipe oven and the resulting limitations on device performance", *J. Appl. Phys.* **51**, p. 6058.

[7] N.B. Delone and V.P. Krainov (1988). *"Fundamental of Nonlinear Optics of Atomic Gases"*, Chapters 1 and 3. John Wiley and Sons, New York.

[8] W. Demtröder (1996). "*Laser Spectroscopy*", Second Enlarged Edition, Chapter 3, p. 57-66, 661-667. Springer Verlag, Berlin.

[9] A.R. Edmonds (1957). "*Angular momentum in Quantum Mechanics*", p. 75. Princeton University Press, Princeton, New Jersey.

[10] A. Faghri (1995). *"Heat pipe science and technology"*, Chapter 1. Taylor and Francis, New York.

[11] J.E. Goldsmith and J.E. Lawler (1981). "Optogalvanic Spectroscopy", *Contemp. Phys.* **22**, no. 2, p. 235.

[12] R.B. Green, R.A. Keller, G.G. Luther, P.K. Schenck and J.X. Travis (1976). *IEEE J. Quantum Electron* **QE-13**, p.63.

[13] G. Grover, T. Cotter and G. Erickson (1964). "Structure of very high thermal conductance," *J. Appl. Phys.* **35**, p. 1990.

[14] G. Grover (1966). "Evaporation-condensation heat transfer device," U.S. Patent 3229759, Application 2 December 1963, Approved 18 January 1966.

[15] R.D. Guenther (1990). *"Modern Optics"*, Chapter 15. John Wiley and Sons, New York.

[16] D.C. Hanna, M.A. Yuratich and D. Cotter (1979). *"Nonlinear Optics of Free Atoms and Molecules"*, Chapters 2-4. Springer-Verlag, Heidelberg.

[17] S.E. Harris, R.B. Miles (1971). "Proposed Third-Harmonic Generation in Phase-matched Metal Vapors", *Appl. Phys. Lett.* **19**, p. 385.

[18] M. Hippler and J. Pfab (1993). "Optogalvanic spectroscopy of argon and wavelength calibration in the near-ultraviolet", *Optics Communications* **67**, p. 347.

[19] R.T. Hodgson, P.P. Sorokin, J.J. Wynne (1974). "Tunable coherent vacuum-ultraviolet generation in atomic vapors", *Phys. Rev. Lett.* **32**, p. 343.

[20] F.A. Jenkins and H.E. White (1950). "*Fundamentals of Optics*", Second Edition, Chapter 23. McGraw-Hill Book Company, New York.

[21] H. Junginger, H.B.Puell, H.Scheingraber, C.R.Vidal (1980). "Resonant Third-Harmonic Generation in a Low-Loss Medium", *IEEE J. Quantum Electron. Q* **E-16**, no. 10, p. 1132.

[22] J.R. Lalanne, A. Ducasse and S. Kielich (1994). "*Laser-Molecule Interaction*", Preface. John Wiley and Sons, Inc., New York.

[23] K.M. Leung, J.F. Ward, B.J. Orr (1974). "Two-photon resonant, optical third-harmonic generation in cesium vapor", *Phys. Rev. A* **9**, p. 2440.

[24] D.M. Mehs and T.M. Niemczyk (1978). "Measurement of Electron Temperatures in the Hollow Cathode Discharge", *Appl. Spectrosc.* **32**, p. 269.

[25] A. Mellinger and C.R. Vidal (1994). "Laser-reduced fluorescence spectroscopy on predissociated CO triplet states", *J. Chem. Phys.* **101**, p. 104.

[26] A. Mellinger (1995). "Untersuchung hochangeregter Triplettzustände des CO-Moleküls", Doktorarbeit, Technische Universität München und Max Planck Institut für extraterrestrische Physik.

[27] P.W.Milonni and J.H.Eberley (1988). "*Lasers*", Chapters 2.3, 3.1-3.6, 17 and 18. John Wiley and Sons, New York.

[28] C.E. Moore (1949). "Atomic energy levels", *Circular of the Nat. Bur. of Stand.* vol. **1**, no. 467, p. 107.

[29] G.H.C. New, J.F. Ward (1967). "Optical third-harmonic generation in gases", *Phys. Rev. Lett.* **19**, p. 556.

[30] F.M. Phelps III (1982). *"MIT wavelength tables"*, Volume 2. MIT Press.

[31] H. Puell and H. Scheingraber and C.R. Vidal (1980). "Saturation of resonant third-harmonic generation in phase-matched systems", *Phys. Rev.A.* **22**, no. 3, p. 1165.

[32] H. Puell, K. Spanner, W. Falkenstein, W. Kaiser and C.R. Vidal (1976). "Third-harmonic generation of mode-locked Nd:glass laser pulses in phase-matched Rb-Xe mixtures", *Phys. Rev. A.* **14**, p. 2240.

[33] H. Puell and C.R. Vidal (1976). "Nonlinear polarisations and excitations and their time dependence in discrete multilevel systems", *Phys. Rev. A* **14**, p 2225.

[34] W.G. Rado (1967). *Phys. Rev. Lett.* **11**, p. 123.

[35] J.J. Sakurai (1995). "Modern Quantum Mechanics", Chapter 3. Addison-Wesley Publishing Company, Reading, Massachusetts.

[36] H. Scheingraber, H. Puell, C.R. Vidal (1978). "Quantitative analysis of resonant third harmonic generation in strontium", *Phys. Rev. A* **18**, p. 2585.

[37] H. Scheingraber and C.R. Vidal (1981). "Heat pipe oven of well-defined column density", *Rev. Sci. Instrum.* **52** (7), p. 1010.

[38] B. Steffes, X. Li, A. Mellinger and C.R. Vidal (1996). "Heat pipe oven for large column densities with a well-defined optical path length", *Appl. Phys. B* **62**, p.87.

[39] B. Steffes (1999). Private communication on "Construction and operation of a crossed concentric heat pipe oven."

[40] C.M. Steinmann and B. Steffes (1999). "Manual for Construction and Use of the Crossed Concentric Heat Pipe Oven System", document available in the laser laboratory of the Physics Department, University of Stellenbosch.

[41] T. Sykora and C.R. Vidal (1998). "Interaction of a magnetic field with the $a'^3\sum^+ - A^1\Pi$ complex in CO", *J. Chem. Phys.* **108**, p. 6320.

[42] C.R. Vidal and J. Cooper (1969). "Heat-Pipe Oven: A New, Well-Defined Metal Vapor Device for Spectroscopic Measurements", *J. Appl. Phys.* **40** (8), p. 3370.

[43] C.R. Vidal and F.B. Haller (1971). "Heat Pipe Oven Applications. I. Isothermal heater of well defined temperature. II. Production of metal vapor-gas mixtures," *Rev. Sci. Instr.* **42**, no. 12, p1779.

[44] C.R. Vidal and M.M. Hessel (1972). "Heat-Pipe Oven for Homogeneous Mixtures of Saturated and Unsaturated Vapors; Application to NaLi," *J. Appl. Phys.* **43**, no. 6, p. 2776.

[45] C.R. Vidal (1973). "Spectroscopic observations of subsonic and sonic vapor flow inside an open-ended heat pipe," *J.Appl.Phys.* **44**, no.5, p. 2225.

[46] C.R. Vidal (1980). "Coherent VUV sources for high resolution spectroscopy", *Appl. Opt.* **19**, no. 23, p. 3897.

[47] C.R. Vidal (1987). "Four-wave frequency mixing in gases" in "Tunable lasers" (L.F. Mollenauer and J.C. White, eds.), *Topics in Applied Physics* **59**, p. 57-113. Springer Verlag, Heidelberg.

[48] C.R. Vidal (1988). "Vacuum ultraviolet laser spectroscopy of small molecules", *Advances in Atomic and Molecular Physics* **23**, p. 1.

[49] C.R. Vidal (1996). "Vapor cells and heat pipes", *Experimental methods in the Physical Sciences* **29B**, p. 67.

[50] C.R. Vidal (1998). "*Laser spectroscopy of atoms and molecules I*", Max-Planck-Institut für Extraterrestrische Physik, Garching, Germany.

[51] S.C. Wallace and G. Zdasiuk (1976). "High-efficiency four-wave sum mixing in magnesium at 140 nm", *Appl. Phys. Lett.* **28**, no. 8, p. 449.

[52] J.F. Ward and G.H.C. New (1969). "Optical Third Harmonic Generation in Gases by a Focussed Laser Beam", *Phys. Rev.* **185**, no. 1, p 57.

[53] Y.M. Yui, T.J. McIlrath and R. Mahon (1979). "Effects of spatial modes on third-harmonic generation", *Phys. Rev. A* **20**, no. 6, p. 2470.

[54] J.F. Young, G.C. Bjorklund, A.H. Kung, R.B. Miles and S.E. Harris (1971). "Third-Harmonic Generation in Phase-Matched Rb Vapor", *Phys. Rev. Lett.* **27**, p. 1551.